DEVELOPMENT OF A ROBOTIC EXOSKELETON SYSTEM FOR GAIT REHABILITATION

CHEN GONG

(B.Eng., Shanghai Jiao Tong University, China)

A THESIS SUBMITTED

FOR THE DEGREE OF DOCTOR OF PHILOSOPHY
DEPARTMENT OF BIOMEDICAL ENGINEERING
NATIONAL UNIVERSITY OF SINGAPORE

2016

DECLARATION

I hereby declare that this thesis is my original work and it has been written by me in its entirety. I have duly acknowledged all the sources of information, which have been used in the thesis.

This thesis has also not been submitted for any degree in any university previously.

Chen Gong

CHEN Gong

Dec. 2015

ACKNOWLEDGEMENTS

I would like to express my deepest gratitude to my supervisor Dr. Yu Haoyong, who offered me the opportunity to join this project, welcome me as a member of his research group and gave me the chance to study and discover in Singapore. His guidance and immense knowledge helped me in my research, and my research could not be accomplished without his supervision.

I would like to thank the members of Singapore Institute for Neurotechnology (SiNAPSE) and Advanced Robotics Center (ARC) at NUS, Dr. Guo Zhao, Dr. Huang Sunan, Dr. Li Xiang, Dr. Emre Sariyildiz, Dr. Sun Yu, Dr. Qi Peng, Dr. Pan Yongping, Dr. Mun Kyung-Ryoul, Dr. Li Cheng, Mr. Gu Xiaoyi, Mr. Zhang Cheng, Ms. Veena Salim, Ms. Pavithra Thangavel. I would also like to thank my friends Dr. Teng Yanbo, Mr. Sun Bo, Mr. Yang Yumeng. Thanks for their incredible support and encouragements.

I would like to thank the Department of Biomedical Engineering at NUS for the financial support during my pursuit of the PhD. Thanks also goes to SiNAPSE for the wonderful office and lab facilities.

A special thanks to my family. Words cannot express how grateful I am to my father, mother, sister and beloved wife for the sacrifices that they’ve made on my behalf. I would also like to thank all of my friends who supported me in many ways and incented me to strive towards my goal.

CONTENTS

ABSTRACT

In recent years, the rapid advancement of robotics technology has pushed the development of gait rehabilitation robotics to automate gait rehabilitation therapy for stroke patients. This thesis presents a robotic exoskeleton system aiming at providing overground gait rehabilitation training to sub-acute and chronic stroke patients at home and outpatient setting.

The exoskeleton robotic system consists of a knee joint and an ankle joint. It is wearable, compact, lightweight and in modular design. The robotic joint is actuated by a novel series elastic actuator (SEA), which is compliant and force-controllable. The novel SEA is developed as a solution to the limitation of conventional SEA design. By employing one low-stiffness translational spring and one high-stiffness torsion spring in series, the actuator has a high intrinsic compliance while retaining the capacity to provide peak force. The actuation mechanism of the robot and the selection of the actuator spring stiffness are optimized based on the biomechanics of human gait, so that the exoskeleton can provide full assistance during overground walking, and remain compliant for most period of a gait cycle.

A human-robot interaction controller is implemented in the robot, which can accurately and stably control the interactive torque between the robot and human joints. The controller design is based on the model of the SEA, and mainly consists of human joint motion compensation and friction compensation, and is enhanced with a disturbance observer. Such a control scheme enables the robot to achieve low output impedance when operating in the human-in-charge mode and achieve accurate force tracking when operating in the assistive mode.

Based on the human-robot interaction controller, an upper-level control strategy is implemented for overground gait training. In this control strategy, a novel synchronization method is developed to synchronize a normal reference trajectory to the actual human gait. To be specific, an adaptive oscillator is utilized to estimate the strider percentage of human gait based on the gait event information, which is detected in real time with a hidden Markov model (HMM). Synchronous reference trajectories for the robot are then generated with the estimated stride percentage according to a lookup table. An impedance-control-based strategy is implemented in the robot to provide assistive torque according to the synchronous reference gait trajectory.

To validate the design and evaluate the performance of the robotic exoskeleton system, experiments of overground walking have been conducted on healthy subjects. Experimental results demonstrate that this robot can provide synchronous and effective assistance to the human joints during overground walking, which can improve the gait pattern when it is abnormal. The exoskeleton system will be further tested with stroke patients, and has the potential of clinical applications in the future.

LIST OF TABLES

LIST OF FIGURES

NOMENCLATURE

AAN	Assist-As-Needed
ADL	Activities of Daily Living
ANOVA	Analysis of Variance
ASH	walking with High Assistance
ASL	walking with Low Assistance
BWS	Body Weight Support
CAD	Computer-Aided Design
CGA	Clinical Gait Analysis
CFRP	Carbon Fiber-Reinforced Plastic
CoP	Center of Pressure
DC	Direct Current
DoF	Degree of Freedom
EEG	Electroencephalography
EMG	Electromyography
FA	Feet Adjacent
FES	Functional Electrical Simulation
FPGA	Field-Programmable Gate Array
FW	Free Walking
GL	Gastrocnemius Lateralis
HMM	Hidden Markov Model
HR	Heel Rise
IC	Initial Contact
IMU	Inertia Measurement Unit
IRB	Institutional Review Board
ISw	Initial Swing
LR	Loading Response
LUT	Look-Up Table
MSt	Mid-Stance

MSw	Mid-Swing
OI	Opposite Initial contact
OT	Opposite Toe off
PAM	Pneumatic Artificial Muscle
PD	Proportional-Derivative
PID	Proportional-Integral-Derivative
PSw	Pre-Swing
RF	Rectus Femoris
RMS	Root Mean Square
ROM	Range of Motion
SAW	Simulated Abnormal Walking
SEA	Series Elastic Actuator
SM	Semitendinosus
TA	Tibialis Anterior
TO	Toe Off
TSt	Terminal Stance
TSw	Terminal Swing
TV	Tibia Vertical
UUB	Ultimately Uniformly Bounded
ZA	Zero-Assistive walking

Chapter 1

Introduction

Stroke has become the leading cause of permanent adult disability. Since loss of walking ability is a major problem for stroke survivors, recovery of walking is a priority goal after stroke. However, conventional manual gait training is expensive, labor-intensive and less consistent. Robotic device is then introduced to automate the gait rehabilitation training. Robotic device offers a wide range of advantages. For example, robot does not get tired so that it can provide intensive training in good repeatability. Robot can also record and assess the rehabilitation progress consistently. However, most of current robotic devices integrate with fixed treadmills. They are bulky and expensive, which limits their availability to the patients. Yet a significant portion of patients have residual gait impairment. There is a great need for a home-based wearable robotic system for gait training. Motivated by this need, we develop a robotic knee-ankle-foot exoskeleton system for gait training. The background, motivation, objectives and contributions of this thesis is introduced in this chapter.

1. Introduction

In this section, the background is introduced about stroke and the following gait disorder, conventional manual gait therapy and robotic rehabilitation gait therapy.

1.1 Stroke and gait disorder

Stroke is a leading cause of serious long-term disability and also the fourth most frequent cause of death in the industrialized countries [1, 2]. In the United States an estimated 6.6 million adults have had a stroke; and projections show that by 2030, an additional 3.4 million people will have had a stroke [1]. Between 2012 and 2030, total direct medical stroke-related costs are projected to triple, from $71.6 billion to $184.1 billion in US [1].

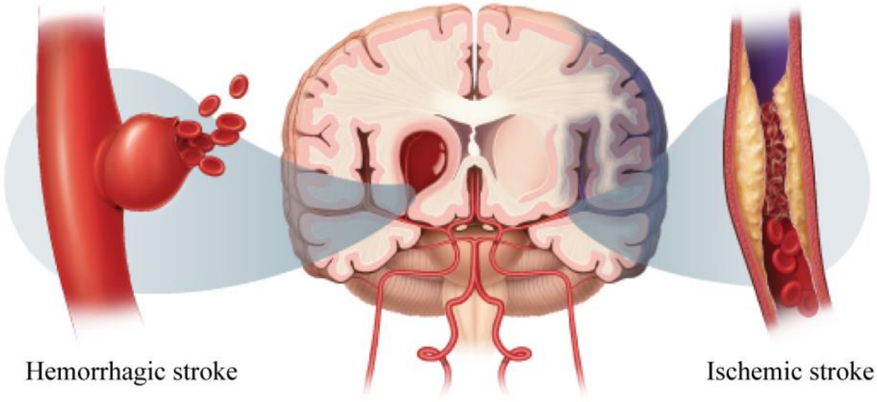

Figure 1-1. Types of stroke; hemorrhagic stroke (left) and ischemic stroke (right) (reprinted from http://fescenter.org/wp-content/uploads/2013/11/What-is-a-stroke.jpg).

Stroke is caused by the interruption of the blood supply to the brain, generally due to a burst blood vessel (ischemic stroke) or lodged clot (hemorrhagic stroke) as shown in Figure 1-1 [3]. About 70% of people survive the stroke, but most of them suffer from hemiparesis, i.e. partial paralysis of one side of the body, impaired vocational capacity and sensory loss [4].

As the most basic form of human locomotion, gait is an extremely complex endeavor with neuromuscular activity and dynamic interactions of internal and external forces. Most stroke survivors are left with walking difficulties throughout the sub-acute and chronic stages of stroke [5, 6]. Abnormal gait patterns can be characterized by significantly reduced gait speed, shortened step length, an inability to maintain balance, and gait asymmetry; these are observed in the majority of individuals with post-stroke hemiplegia [5-8]. In addition, this loss of mobility greatly affects patients as they lose their sense of independence and this adversely impacts their social lifestyle [9].

1.2 Conventional manual gait rehabilitation therapy

Despite the defective motor functions caused by stroke, brain has an amazing characteristic called neuroplasticity. Neuroplasticity refers to the brain’s ability to reorganize itself by forming new neural pathways, which allows the brain to adapt to the changes in behavior, environment, and neural processes. Based on this concept, the impaired gait function can be restored through intensive, repetitive and persistent training [10, 11].

A proper gait rehabilitation regimen that includes balance training, weight bearing exercises, strength training, and the use of electrical stimulation has been established to improve and restore the gait patterns [12, 13]. Clinical trials also show that chronic, non-ambulatory hemiparetic patients improved their gait ability through the conventional rehabilitation process [14, 15].

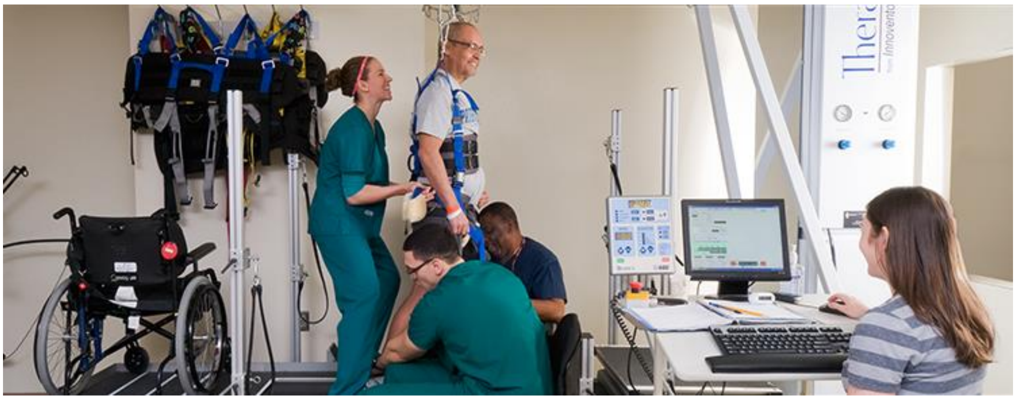

Figure 1-2. Gait rehabilitation training on the treadmill with the help of three therapists. (reprinted from http://helenhayeshospital.org/wp-content/uploads/2014/12/BODY-WEIGHT-SUPPORTED-GAIT-TRAINING-banner.png).

However, conventional rehabilitation is labor-intensive and limited in terms of availability, duration, and training session frequency due to a lack of trained therapists and hospital recourses. In a typical gait training (Figure 1-2), the patient's leg movements need to be assisted by at least two therapists; and in certain cases, a third therapist is needed to maintain balance and assist the pelvic motion. The duration of each training session is always limited due to the fatigue of the therapists. The quantification of gait performance and the assessment of rehabilitation progress are not consistent because training sessions are largely subjective and depend on therapists' individual experiences. Besides, therapists often have to lift up the body-weight of patients, or work in ergonomically unfavorable postures, there is the possibility that the therapist will suffer from back injury [16-18]. The condition even deteriorates with the increasing number of stroke patients and increasing physiotherapy costs, which leaves the patients with lifelong walking difficulties. In this regard, there is a strong need to reduce the excessive labor of therapists and to increase the quality of the gait rehabilitation process.

1.3 Robotic gait rehabilitation therapy

Due to the difficulties in the manual gait therapy, robotic devices are suitable to serve as a solution to automate the gait rehabilitation training [19]. Robotic devices can take over the strenuous and repetitive task, allowing more intensive movements, delivering therapy at a reasonable cost, and quantitatively assessing the recovery level by measuring gait kinematics and physiological signal (Figure 1-3) [20]. The therapists are then able to focus on more meaningful tasks such as interacting with patients, supervising the training session and assessing the outcome of the therapy. One therapist can even manage several robotic devices simultaneously, which greatly increases the efficiency of the personnel.

Various gait rehabilitation robots have been developed [21, 22] and evaluated with clinical experiments [23-25]. Most of the clinical trials indicated that robotic gait training alone or the combination of robotic gait training and conventional manual therapy is superior to conventional manual therapy alone in terms of gait function recovery [25-28]. Some trials reported roughly equal improvement, while the robotic gait training requiring less input from therapist [16, 25, 29, 30]. Although a few trials reported less improvement with robotic gait training in terms of gait speed and endurance [31]; there is no doubt that robotic devices have the potential in expanding its usage in gait rehabilitation after stroke.

Figure 1-3. Robot-aided gait rehabilitation training with a therapist supervising the training session. (reprinted from http://ptjournal.apta.org/content/85/1/52/F1.large.jpg).

2. Motivations

Notwithstanding the aforementioned benefits, the application of robotic gait rehabilitation is limited. For the existing gait rehabilitation robots, most of them are integrated with fixed treadmills. They are bulky, heavy, and patients are constrained on a treadmill, which hinders the walking independence of patients. The rehabilitation control strategy is also less efficient to achieve good rehabilitation progress. Besides, only a few major hospitals or rehabilitation centers can afford a robotic device and it takes about 2.36 years to break even after purchasing one [32].

On the other hand, a significant portion of stroke patients has residual gait impairment after the therapy in the hospital. Long-term training should be given to the patients to further recover the gait function. However, without therapeutic guidance and training facility, the rehabilitation progress is slow and difficult to track. There is a great need for a home-based wearable robotic system for gait rehabilitation.

A number of researches tried to develop ankle robots which targeted specifically for the ankle joint problem, such as drop foot. Others proposed knee robots to aid the knee joint motion. However, limited research aimed at providing active assistance to both the knee and ankle joints.

The work in this thesis is motivated by the desire to develop a portable gait rehabilitation robotic system and provide robotic gait therapy for better recovery after stroke. Effective rehabilitation robots can offer a wide range of advantages:

- The robots can release the patient from the treadmill and provide real overground walking training in order to increase the walking independence of the patients.
- The robots are lightweight, portable enough for patients to carry out gait training at outpatient or home setting. Patients can receive more frequent training in their daily life.
- There is general agreement that 50%~80% of stroke survivors can walk independently at 3 weeks or at discharge from hospital [6, 33] and by 6 months this figure may be as high as 85% [34]. Hence, body weight support (BWS) system should be excluded in order for a compact and user friendly design.
- Robots do not get tired so that intensive training with good repeatability can be delivered. Kinematics of human limbs and interaction forces can be collected and controlled.

- Robotic system can provide gait therapy based on the condition of the patients and capture patient’s performance data to evaluate the recovery progress.

3. Objectives

The main objective of this thesis is to conceive a new generation of a knee-ankle-foot robotic system aiming for stroke patients with residual knee and ankle function impairments to perform overground gait rehabilitation training. The robot should be compact, lightweight, safe and low-price so that patients can perform gait training with the robot in home setting. The robot should also be capable of providing full support to the patients during walking. Considering that most stroke patients are affected by hemiparesis, we start building our prototype for one leg.

A second objective is to develop a novel actuator of the robot. The actuator should be compliant and backdrivable so that it is safe for human-robot interaction application. The actuator should also be compact and lightweight, while retaining the capability of providing large assistive force. Fast and accurate force tracking performance and adequate bandwidth for rehabilitation robotics application should be achieved.

A third objective is to study the human-robot interactions and control the interactive torque between the robot and the human limbs. It is essential to understand the force control performance of the exoskeleton when human motion is involved. Stability of the human-robot interaction controller has to be guaranteed in order to deliver safe assistance during walking.

A fourth objective is to develop intelligent control strategy of the robot to provide overground gait training. The robot should be able to collect the kinematics information of the human gait and provide assistance to improve the gait pattern when it is abnormal. The assistance should be safe and effective.

More fundamentally, our project aims at helping stroke patient to recover their gait function and improving their life quality. By investigating the performance of different robotic therapy strategies, we can increase our knowledge of neuro-recovery after stroke, and determine which types of therapy or exercises should be applied for optimal rehabilitation progress.

4. Contributions

The contributions of this thesis are summarized as:

First, we present the design and control of a portable knee-ankle-foot robotic exoskeleton system. Following bottom-up approach, we designed the mechanical structure and actuator of the robot to achieve real overground walking; a joint-level force controller is then developed to provide accurate assistance during human-robot interaction; an upper-level rehabilitation control strategy is then implemented, which can provide synchronous assistance during overground gait training.

Second, we present a novel series elastic actuator (SEA) to drive the robotic joint. This SEA is developed as a solution to overcome the major limitation of the conventional SEA design. By employing two springs with vastly different stiffness, the actuator can achieve large output range while maintain a high intrinsic compliance.

The actuator design is also based on the biomechanics of human gait, which makes it suitable for our gait rehabilitation robot.

Third, based on the model of SEA, we developed a human-interaction controller, which can provide accurate assistive torque to human joint during walking. Compared with the previous work presented in [35-37], our work has the following improvements: 1) the assumption in [35] that the modeling error and disturbance are constant is removed; 2) the rigorous mathematical proof is given to show the stability of the closed-loop system.

Fourth, a novel gait-event-based synchronization method for gait rehabilitation robotics via a bio-inspired adaptive oscillator is developed and implemented in our exoskeleton robot. Compared with the previous work, the major superiority of our work includes: 1) this method has a simple structure and is easy to implement; 2) our method is efficient and effective at achieving human-robot synchronization; 3) this method is robust in synchronization with abnormal gait patterns so it is applicable and feasible for gait rehabilitation robotics.

5. Contributed papers

Journal papers:

[1] **Gong Chen**, C. K. Chan, Z. Guo, H. Yu, "A Review of Lower Extremity Assistive Robotic Exoskeletons in Rehabilitation Therapy," *Critical Reviews in Biomedical Engineering*, 41(4-5), 2013.

[2] **Gong Chen**, H. Yu, "A Portable Powered Knee-Ankle-Foot Orthosis," *ASME*

Transactions Journal of Medical Devices, 8(2): 020927, 2014.

[3] **Gong Chen**, Z. Guo, H. Yu, “Gait Rehabilitation Robotics: Next Generation Technology for Stroke Rehabilitation,” *Asia Pacific Biotech News (APBN)*, 19(2), 2015.

[4] **Gong Chen**, P. Qi, Z. Guo, H. Yu, “Mechanical Design and Evaluation of a Compact Portable Knee-Ankle-Foot Robot for Gait Rehabilitation,” *Mechanism and Machine Theory*, 103: 51-64, 2016.

[5] **Gong Chen**, P. Qi, Z. Guo, H. Yu, “Gait-Event-Based Synchronization Method for Gait Rehabilitation Robots via a Bio-Inspired Adaptive Oscillator,” *IEEE Transactions on Biomedical Engineering* (accepted).

[6] H. Yu, S. Huang, **Gong Chen**, N. Thakor, “Control Design of a Novel Compliant Actuator for Rehabilitation Robots,” *Mechatronics*, 23(8): 1072-1083, 2013.

[7] H. Yu, **Gong Chen**, Z. Guo, “Design of a Novel Portable Knee Ankle Orthotics,” *IEEE Life Sciences eNewsletter*, Jan. 2014.

[8] H. Yu, S. Huang, **Gong Chen**, Y. Pan, Z. Guo, “Human-Robot Interaction Control of Rehabilitation Robots with Series Elastic Actuators,” *IEEE Transactions on Robotics*, 31(5): 1089-1100, 2015.

[9] E. Sariyildiz, **Gong Chen**, H. Yu, “An Acceleration-Based Robust Motion Controller Design for a Novel Series Elastic Actuator,” *IEEE Transactions on Industrial Electronics*, 63(3): 1900-11910, 2016.

[10] X. Li, Y. Pan, **Gong Chen**, H. Yu, “Adaptive Human-Robot Interaction Control for Robots Driven by Series Elastic Actuators,” *IEEE Transactions on Robotics*,

2015 (conditional accepted).

[11] X. Li, Y. Pan, **Gong Chen**, H. Yu, “Continuous Tracking Control for a Compliant Actuator with Two-Stage Stiffness,” *IEEE Transactions on Automation Science and Engineering*, 2016 (accepted).

[12] E. Sariyildiz, **Gong Chen**, H. Yu, “Robust Vibration Control of Multi-Mass Resonant Systems via Disturbance Observer in State Space,” *IEEE Transactions on Industrial Electronics*, 2015 (revised manuscript Submitted).

[13] E. Sariyildiz, **Gong Chen**, H. Yu, "A Unified Robust Motion Controller Design for Series Elastic Actuators." *IEEE/ASME Transactions on Mechatronics*, 2015 (revised manuscript Submitted).

[14] X. Li, Y. Pan, **Gong Chen**, H. Yu, “Multi-Modal Control Scheme for Rehabilitation Robotic Exoskeletons,” *International Journal of Robotics Research*, 2016 (conditional accepted).

Conference papers:

[1] **Gong Chen**, Z. Guo, H. Yu, “Design and Evaluation of a Portable Knee-Ankle-Foot Robot for Gait Rehabilitation,” *ASME 2015 International Design Engineering Technical Conferences & Computers and Information in Engineering Conference (IDETC/CIE)* 2015.

[2] **Gong Chen**, V. Salim, H. Yu, “A Novel Gait Phase-Based Control Strategy for a Portable Knee-Ankle-Foot Robot,” *IEEE International Conference on Rehabilitation Robotics (ICORR)*, pp. 571-576, 2015.

[3] **Gong Chen**, Z. Guo, H. Yu, “Gait Event-Based Human-Robot Synchrony for

Gait Rehabilitation Using Adaptive Oscillator," *IEEE International Conference on Robotics and Biomimetics (ROBIO)*, pp. 138-143, 2015.

[4] H. Yu, S. Huang, **Gong Chen**, S. L. Toh, et al., "Design and Analysis of a Novel Compact Compliant Actuator with Variable Impedance," *IEEE International Conference on Robotics and Biomimetics (ROBIO)*, pp. 1188-1193, 2012.

[5] H. Yu, S. Huang, **Gong Chen**, S. L. Toh, Y. Ghorbel, et al., "A Novel Compact Compliant Actuator Design for Rehabilitation Robots," *IEEE International Conference on Rehabilitation Robotics (ICORR)*, pp. 1-6, 2013.

[6] H. Yu, M. Cruz, **Gong Chen**, S. Huang, et al., "Mechanical Design of a Portable Knee-Ankle-Foot Robot," *IEEE International Conference on Robotics and Automation (ICRA)*, pp. 2175-2180, 2013.

[7] O. B. Farah, Z. Guo, **Gong Chen**, C. Zhu, H. Yu, "Power Analysis of a Series Elastic Actuator for Ankle Joint Gait Rehabilitation," *IEEE International Conference on Robotics and Automation (ICRA)*, pp. 2754-2760, 2015.

[8] X. Gu, Z. Guo, Y. Peng, **Gong Chen**, H. Yu, "Effects of compliant and flexible trunks on peak-power of a lizard-inspired robot," *IEEE International Conference on Robotics and Biomimetics (ROBIO)*, pp. 493-498, 2015.

[9] E. Sariyildiz, **Gong Chen**, H. Yu, "Robust Position Control of a Novel Series Elastic Actuator via Disturbance Observer," *IEEE/RSJ International Conference on Intelligent Robots and Systems (IROS)*, pp. 5423-5428, 2015.

[10] X. Li, **Gong Chen**, Y. Pan, H. Yu, "Region Control for Robots Driven by Series Elastic Actuators," *IEEE International Conference on Robotics and Automation (ICRA)*, pp. 1102-1107, 2016.

[11] J. Li, **Gong Chen**, P. Thangavel, H. Yu, N. Thakor, A. Bezerianos, Y. Sun, “A Robotic Knee Exoskeleton for Walking Assistance and Connectivity Topology Exploration in EEG signal,” *IEEE RAS/EMBS International Conference on Biomedical Robotics and Biomechatronics (BioRob),* pp. 1068-1073, 2016.

[12] E. Sariyildiz, **Gong Chen**, H. Yu, “An Active Disturbance Rejection Controller Design for the Robust Position Control of Series Elastic Actuators,” *IEEE/RSJ International Conference on Intelligent Robots and Systems (IROS)*, 2016 (accepted).

6. Thesis Overview

A flowchart is shown in Figure 1-4 to illustrate the structure of this thesis.

Chapter 2 introduces the existing robotic systems for gait rehabilitation. Three aspects: mechanical design, actuation system and control strategy are discussed.

Chapter 3 presents the mechanical design of a portable knee-ankle-foot exoskeleton robot. A novel compliant SEA is also presented as the actuator of the robotic joints. The structure of the robot and actuator is optimized based on the human gait biomechanics. The modeling and controller of the actuator is developed to achieve force control. The robot is also evaluated by providing assistance during overground walking experiment with healthy subjects.

Chapter 4 presents a human-robot interaction controller, which is developed for controlling the interactive torque between the robot and human joints. It consists mainly of human interaction compensation, friction compensation, and is enhanced with a disturbance observer. Theoretical analysis for the proposed controller has proven that it can guarantee the stability of the human-robot interaction. Experiment is conducted on the ankle joint of the robot.

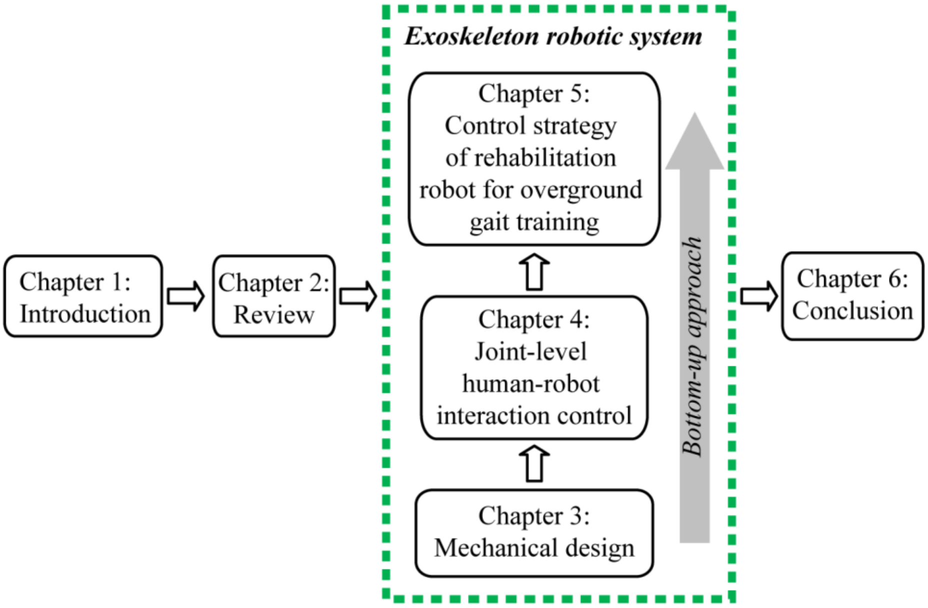

Figure 1-4. Structure of the thesis.

Chapter 5 presents a novel human-robot synchronization method for gait rehabilitation robotics. Inspired by the phenomenon of the synchronous flashing of fireflies, we develop a synchronization method using gait events since gait events are pulse-like signal. The gait events are detected in real time during overground walking based on hidden Markov model (HMM). A bio-inspired adaptive oscillator is employed to estimate the stride percentage of the human gait based on the detect gait events. Reference trajectories synchronous to the human gait are then generated according to the estimated phase. An impedance-based control strategy is implemented to provide assistive gait rehabilitation training. Experiments on healthy subjects have been conducted to evaluate the performance of this control strategy.

Finally, Chapter 6 summarizes the contributions of this work and discusses the further work in gait rehabilitation robotics.

Chapter 2

Gait Rehabilitation Robotic Systems: Review and Outlook

In recent years, the rapid advancement of robotics technology has pushed the development of gait rehabilitation robotics to automate gait rehabilitation therapy for stroke patients. Robots are capable of providing intensive gait training, better quantitative feedback and improved functional outcomes compared to the conventional manual therapy. This chapter provides an introduction to the existing gait rehabilitation robotic systems and discusses future prospects for innovation. Three aspects: mechanical design, actuation system and control strategy are included. Special emphasis is placed on the exoskeleton-based robotic systems for rehabilitation. The review also discusses the limitations of current exoskeletons and technical challenges faced in exoskeleton development in order to reveal the directions to more effective exoskeleton robotic systems.

1. *Mechanical design*

In this section, the mechanical design of existing gait robotic systems is introduced. We first illustrate different types of robotic systems. A special focus is then given to the exoskeleton-based robotic systems.

1.1 Overview of gait rehabilitation robots

Robots can be designed to rehabilitate certain parts of the lower limbs with different functions and purposes. Mechanical design also affects the implementation of rehabilitation strategies. On the whole, the device can be classified into two groups: non-mobile robots (Figure 2-1(a)-(d)) and overground rehabilitation robots (Figure 2-1(e)-(h)).

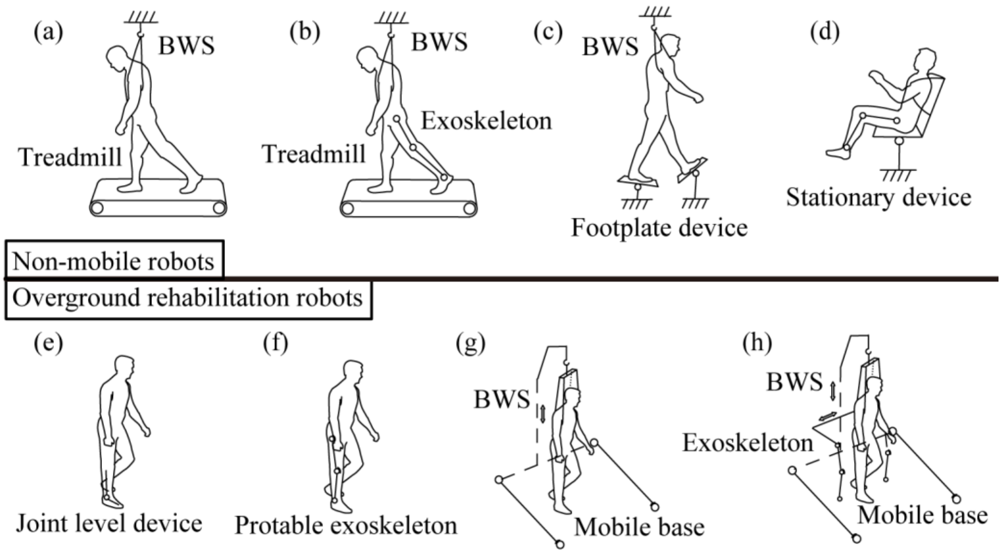

Figure 2-1. (a) treadmill-based BWS system, (b) treadmill-based exoskeleton, (c) footplate device, (d) stationary device, (e) joint level device, (f) portable exoskeleton, (g) mobile robotic trainer, (h) exoskeleton with mobile platform.

In the first group, immobile robots are devices that enable the users to receive gait training in a fixed and confined area which include treadmill-based body weight support (BWS) system (Figure 2-1(a)), treadmill-based exoskeleton (Figure 2-1(b)), BWS foot plate device (Figure 2-1(c)) and stationary device (Figure 2-1(d)).

Robotic gait rehabilitation trainer (RGR) is an example of treadmill-based BWS system (Figure 2-1(a)), which offers the patient with the assistance of a BWS system and gait training on a treadmill [38].

In treadmill-based exoskeleton systems (Figure 2-1(b)), exoskeleton employs the treadmill-based mechanism with the assistance of BWS system while the user is walking on the treadmill. In this design, the BWS system is employed to maintain the balance while the exoskeleton is used to provide assistance to the lower-limb joints. This design is widely adopted and has been implemented in Lokomat [39], ReoAmbulator [40], ALEX (active leg exoskeleton) [41], LOPES (LOwer-extremity Powered ExoSkeleton) [42], University of Auckland system [43], POGO and PAM [44] and et al.

The design in Figure 2-1(c) is known as the BWS footplate device. In this design, the footplate is considered as the end effector of the robot instead of a wearable exoskeleton. This BWS footplate mechanism, which is implemented in Gait Trainer GTI [45], LokoHelp [46] , has the same objective in providing the controlled movements to the patient’s feet besides giving assistance via BWS.

The fourth device in Figure 2-1(d), which is called the stationary device, provides guided movements in lower-limb joint to obtain the effective muscle strengthening and endurance, instead of providing focus to the gait function. ERIGO [47], Motion

Maker [48], Lambda [49], and stationary hip-knee-ankle-foot system [50] are the devices that utilized this stationary device.

In the second group of gait rehabilitation device, overground rehabilitation robots are designed to allow the subjects to walk overground and increase the independence of gait training. In this overground rehabilitation robot, the mobility of the patient is improved tremendously as the patient is not confined in the walking area or restricted to the sagittal plane movement. Examples types of robot are joint level device (Figure 2-1(e)), portable exoskeleton (Figure 2-1(f)), mobile robotic trainer (Figure 2-1(g)), and exoskeleton with mobile platform Figure 2-1(h)).

Joint level device as shown in Figure 2-1(e), is designed for single joint rehabilitation, for example MIT ankle robot [51, 52], Ankle-Foot Orthosis [53] and SUkorpion AR [54].

Portable exoskeleton as shown in Figure 2-1(f), comprises robotic orthosis for multiple lower-limb joints. Various devices can be found such as ReWalk [55], Ekso [56], KAFO [57], HAL [58], PGO [59], Vanderbilt lower limb exoskeleton [60] and et al. It provides assistive force to individual’s lower-limb joints of both legs. Besides gait training device, it is also an assistive tool for walking or stair climbing in daily life.

Mobile robotic trainer as shown in Figure 2-1(g), provides both BWS and overground motion. The existing device that applies this concept is ANDAGO [61], KineAssist [62] and NUS walker [63].

The last type of design in Figure 2-1(h) is exoskeleton with mobile platform, which is an exoskeleton system combining robotic mobile platform, a BWS system and a lower-limb exoskeleton for overground training. WalkTrainer [64], SUABR [65], SJTU mobile system [66] and NaTUre-gaits [67] are several examples of exoskeletons with such mechanisms.

Systems that are associated with the robotic exoskeleton are capable of providing assistance and guidance to the joints of the human lower limbs. These exoskeleton systems are known for their flexibility in control strategies implementation and effectiveness in guiding the movements of the joints; hence, attracted strong interest in the research community in recent years [22]. To ease the understanding of the exoskeleton system, an in-depth explanation is provided for the three types of exoskeleton-based gait rehabilitation systems: treadmill-based exoskeleton, exoskeleton with mobile platform and portable exoskeleton.

1.2 Treadmill-based exoskeleton

Treadmill-based exoskeleton usually composed of a BWS system, a pair of powered leg exoskeleton and a treadmill. The patient can perform gait training on a treadmill with the body weight support and the assistive torque on the lower-limb joints. Various designs have been developed based on this concept, such as ReoAmbulator, which commercialized by Motorika Ltd. (marketed in USA as the “AutoAmbulator”) (Figure 2-2(a)) [68]; Lokomat, which is a commercially available device and also the most widely adopted rehabilitation robot around the world (Figure 2-2(b)) [17]; ALEX, which is designed in University of Delaware (Figure 2-2(c)) [69] and its updated version ALEX II [70] and ALEX III [71]; and LOPES from University of Twente (Figure 2-2(d)) [42].

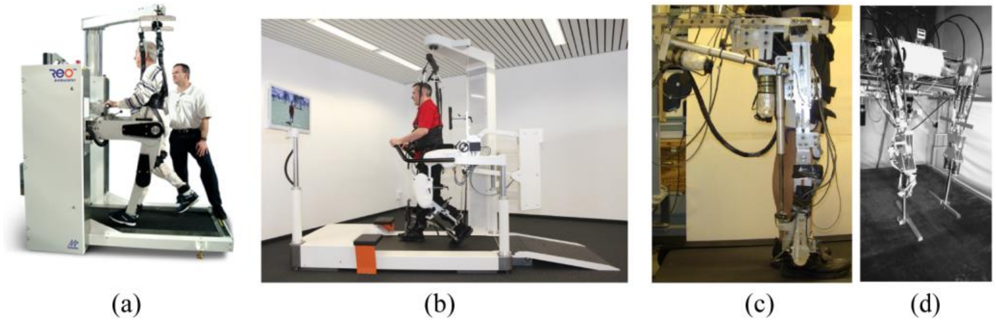

Figure 2-2. (a) ReoAmbulator [40]. (b) Lokomat (Picture: Hocoma, Switzerland). (c) ALEX [41]. (d) LOPES [42].

Exoskeleton of treadmill-based is considered as the conventional method of rehabilitation exoskeleton robot design and has been proven to be effective in clinical application [23]. Notwithstanding, by employing this design, patients are only allowed to move on the treadmill, in which the leg motion will be substantially limited to the sagittal plane. Essential gait movements in pelvic, like rotating, inclining and moving horizontally are also inhibited. These restrictions may result in an abnormal gait pattern, leading to altered muscle activity and eventually the rehabilitation progress is inferior to overground gait training [72, 73]. Besides, the existing designs are bulky, heavy, expensive and only available in a limited number of hospitals or rehabilitation centers. The cost is also high, which limits them from wider application.

1.3 Exoskeleton with mobile platform

To provide real overground walking, exoskeleton system is implemented on a mobile platform instead of a treadmill. The system often comes with a BWS so that the system can provide balance support and body weight unloading. Examples that utilize such systems are WalkTrainer, which was developed at the Ecole Polytechnique Federale de Lausanne (EPFL, Figure 2-3(a)) [64]; EXPOS (exoskeleton for patients and the old) from Sogang University [65] and its updated version SUBAR (Sogang University biomedical assistive robot) in Figure 2-3(b) [74]; NaTUre-gaits (Natural and TUnable rehabilitation gait system) from Nanyang Technological University (Figure 2-3(c)) [75]; and a mobile robot from Shanghai Jiao Tong University (Figure 2-3(d)) [66].

These devices are designed to enable realistic overground walking. However, the major drawback of these systems is the restrictions on the pelvic motions. Some degrees of freedom (DoF) are constrained or left unactuated. The WalkTrainer and NaTUre-gait facilitate active support in six DoFs of pelvic motion; however, it leads to complicated mechanical structure and inefficiency in sensor fusion and control implementation. Besides, the other conventional physical training, such as stairs and slope climbing are limited.

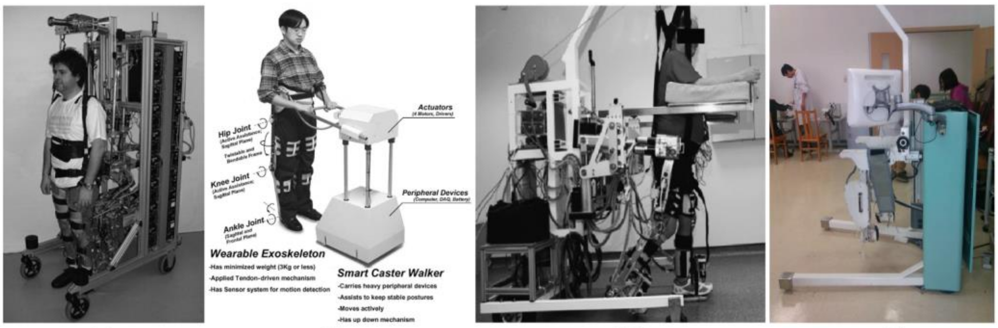

(a) (b) (c) (d)

Figure 2-3. (a) WalkTrainer [64]. (b)SUBAR [65]. (c) NaTUre-gaits [75]. (d) SJTU mobile robot [66].

1.4 Portable exoskeletons

In order to increase the mobility of the treated patients, various portable exoskeleton systems have been developed, such as ReWalk (Figure 2-4(a), Argo Medical Technologies Ltd.) [55, 76]; Ekso (Exoskeleton Lower Extremity Gait System) from Ekso Bionics (Figure 2-4(b)) [56]; Vanderbilt lower limb exoskeleton (Figure 2-4(c)) [60]; and MINDWALKER (Figure 2-4(d)) [77] and et al.

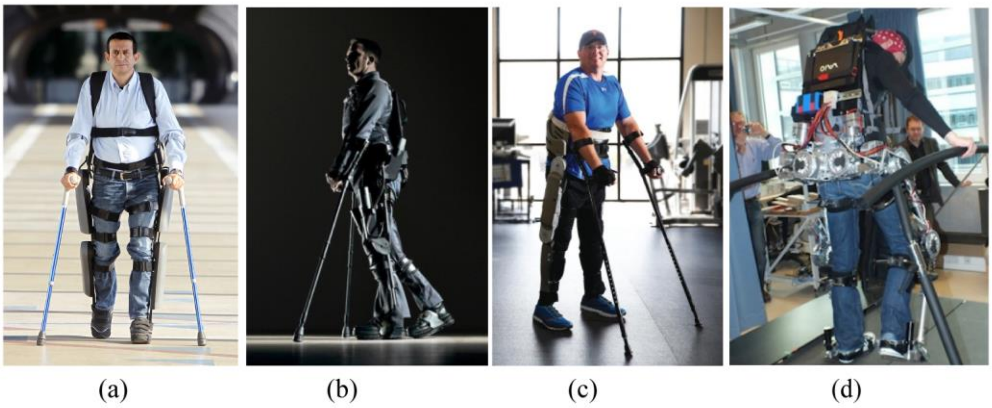

Figure 2-4. (a) ReWalk [55]. (b) Ekso [56]. (c) Vanderbilt lower limb exoskeleton [60]. (d) MINDWALKER [77].

The portable exoskeleton provides more freedom in motion, such as sit-to-stand, stand-to-sit, overground walking, turning and stairs climbing. There is general agreement that 50%~80% of stroke survivors can walk independently at 3 weeks or at discharge from hospital [6, 33] and by 6 months this figure may be as high as 85% [34]. Hence, BWS system is excluded to achieve a compact design, which can be extended to daily assistive use besides gait training. Targeted therapy can also be designed for patients with specific function impairment. More importantly, they are portable, compact and can be treated as rehabilitation tools and assistive robots in patient’s daily activities.

2. Actuation system

The design of the actuation system is crucial for robots as it determines the capability and control performance of the system. In this section, we first introduce the power source that has been employed in gait rehabilitation robotics. Then we discuss the actuators with different actuation modes, including rigid actuator and compliant actuator, especially series elastic actuator (SEA).

2.1 Power source

In terms of power source, three types of actuators have been utilized in exoskeleton systems: hydraulic, pneumatic actuator and electric motor. Hydraulic system, which was adopted by Ekso, has the advantage of providing large output, but requires an additional energy supply system [78, 79]. Pneumatic artificial muscle (PAM) is known for its lightweight and high compliance (due to the fact that air is compressible [80]). It can be found in KAFO [57], system from University of Auckland [43]. However, the nonlinear characteristic makes the pneumatically powered exoskeleton difficult to be controlled. Besides, it is known that the hydraulic and pneumatic exoskeletons are not portable as the actuators are usually bulky; and accessories, such as pump and tank are needed. Electric motor is the mostly widely used power source and has been adopted in many existing designs. The usage of electric motor produces the desired and controllable output with fast and good response.

2.2 Actuation mode

It must be borne in mind that the rehabilitation robots possess direct interaction with humans physically. Therefore, safety is a critical concern for human-robot interaction. Conventional industrial robot requires rigid actuators to achieve precise position control performance, and is not inherently safe due to its high output impedance and non-backdrivibility. Conversely, compliant actuator seems to provide a better solution. Many innovative compliant actuators have been designed for use in rehabilitation robots [81-83]. The most well-known compliant actuator is the SEA [84, 85].

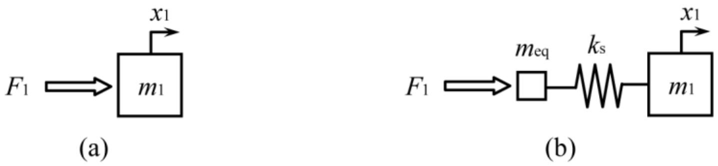

Figure 2-5. Actuator mode: (a) rigid actuator; (b) SEA with soft spring. F_1 is the motor output force; m_1 represents the robot; x_1 is the position of the robot; m_{eq} is the equivalent mass of the motor; k_s is the spring stiffness.

Different from conventional rigid actuator (Figure 2-5(a)), in which the motor drives the load directly, SEA is a kind of actuator, in which an elastic component is placed between the power source and load (Figure 2-5(b)). In 1995, J. Pratt and Williamson first introduced a complete SEA design [84]. The basic components of SEAs included a motor, a gear transmission, a set of linear springs, and a sensor measuring the deflection of the spring [84]. The force output was derived from the spring based on Hooke’s law. A control loop then controlled the actuator to the desired output force. Later, Robinson conducted a deep study on the modeling and control analysis of the SEA in his PhD research [86, 87]. By introducing an elastic element between the load and the geared motor, the inertia and non-linear frictions of the motor and the transmission are decoupled from the load and external impacts and shocks are isolated from the gear transmission. It also makes the force sensing and control problem into a position sensing and control problem [84, 88]. Force/torque sensor thus is not needed, which simplifies the robot structure and improves the controller stability [89]. This is beneficial in rehabilitation robotics since it is more important to control the interaction force instead of the position of the robot [90].

Therefore, in human friendly robotics applications, SEAs are known to offer a range of advantages over stiff actuators, which include high force/torque controllability and fidelity, low output impedance, back-drivability, tolerance to shock and impacts [91]. Various SEA designs have been developed for rehabilitation robot, including linear SEAs [86, 92, 93], where a linear spring is adopted, and rotary SEAs [35, 94, 95], where a torsion spring is used to transmit the output force.

3. Control strategy

In this section, a review of the control strategies of the gait rehabilitation robots is given. The control strategies are classified into two groups: human intention-based control strategies and trajectory-based control strategies.

3.1 Human intention-based control strategies

Ideally, the patients should fully control the robot to have it synchronized with their intentions. The most direct way is to implement a mechanical switch, with which patients can select a desired mode for assistance. This is also the most commonly used method in the existing commercialized systems.

To automate the robots, various researches have been conducted to estimate the human intention through physiological signals. For example, electromyography (EMG) is the electrical activity produced by skeletal muscles. A large number of EMG-based controllers have been developed for rehabilitation robots [25]. They are employed by HAL [58], KAFO [57] and NEUROExos [96, 97] and so on. However, it is plausible that noises in EMG signals increase the intricacy of muscle activity evaluation. Furthermore, EMG signals are very sensitive to the electrode placement. Disturbance from the neighboring muscles and skin conditions (e.g. sweat on the skin) will further make the detection unreliable.

In recent years, there is growing interest in developing the electroencephalograph (EEG) based control strategies for gait rehabilitation robots [98-100]. EEG is an electrophysiological monitoring method to record electrical activity of the brain. However, the usage of EEG in providing human intention will be a challenge as the algorithm of the controller and the mapping limitation during locomotion sources are no located in the brain cortex [101] and the relatively slow speed for real time application [102]. Besides, in some applications, electrodes have to be implanted into the brain for a clear signal, which is highly invasive.

Besides the physiological signals, human intention can be estimated from other information. Referring to Indego, changes of the center of pressure (CoP) on the ground are tracked to predict human movements, such as sit-to-stand or stand-to-sit [103]. EXPO and SJTU system employ an air bladder on the legs to detect human intention through the change of the air pressure [65, 104].

Conclusively, many researches have been proposed, which actively explore the feasibility of the intention-based control strategies for robotic gait rehabilitation. However, they have some drawbacks, mainly related to the signal acquisition and user-specific calibration. A lot of sensors have to be implemented and a lot of work has to be done for signal processing. Besides, deciding how much assistance to be provided is also difficult. The application of intention-based control strategies is still limited.

3.2 Trajectory-based control strategy

In the early stage of robotic gait rehabilitation, exoskeletons move the patient’s limbs passively to follow a predefined normal gait trajectory. However, the efficacy of this passive training is low due to the lack of human initiative participation; and the decrease in physical effort of patients even brings negative impact on the function rehabilitation [105, 106]. Physiological and psychological participation of the patients has to be encouraged to facilitate the rehabilitation progress. Thus, a commonly stated rehabilitation rationale in gait exercise is to provide assistance-as-needed (AAN), which means that the robotic devices will only supply as much effort as a patient needs to accomplish training tasks or maintain a normal gait pattern [25]. Based on this, impedance control is developed in order to engage human voluntary work in the rehabilitation treatment.

The concept of impedance control was firstly proposed by Hogan [107]. In this case, the controller provides assistive force when human limb deviates from a reference gait trajectory and the restoring force is proportional to the deviation [17, 25, 42, 108]. By changing the virtual impedance, different levels of assistance can be achieved flexibly. To be specific, when the impedance is set to be zero, the robot will follow the human movement and try to minimize the interaction force, which refers to the “human-in-charge” mode; and on the contrary, when the impedance is set to be very high, the robot behaves like in position control and follows the reference trajectory, which refers to the “robot-in-charge” mode; and when the impedance is selected to be low, assistive force can be provided and the robot works in assistive mode [42].

Recent controllers have implemented more sophisticated forms of impedance. For instance, ALEX employed a force fields controller, which exerts both tangential and normal forces at the ankle with respect to the speed of the reference trajectories. [108]. LOPES group proposed Virtual Mode Control whereby the selection of different gait functions is allowed [109]. Alexander et al. developed a path control strategy, in which the motion of the patient’s leg is constrained in a virtual tunnel with stiff walls [110]. Clinical study on the impedance control-based strategies also affirmed its effectiveness in gait function rehabilitation [24].

4. Discussion

Although research has been done extensively, the technology of robotic exoskeleton is still evolving rapidly to achieve better effectiveness. It is predicted that the portable exoskeleton has relatively high potential in expanding its usage as it helps to increase the mobility of the patients, such as to perform overground walking, sit-to-stand, stand-to-sit and stairs climbing postures. Notwithstanding the benefits mentioned above, the weight remains to be the main challenge in the portable exoskeleton design. Compactness and capability should be also considered in exoskeleton design. Motivated by this, we have developed a portable, compact, modular knee-ankle-foot exoskeleton robot, which will be presented in Chapter 3.

The review on the actuation systems reveals that SEA offers a wide range of advantages over rigid actuators, which makes it appropriate for rehabilitation robotics application. It is characterized by its intrinsic compliancy for safe human-interaction and high force controllability and fidelity. However, most of the existing SEA designs are bulky, heavy and stiff. Motivated by this, we develop a novel SEA, which will be presented in Chapter 3.

Through this study of the control strategies, it broadly reflects that the impedance control-based strategies are desired in the next technological shift of robotic gait rehabilitation. Patient’s initiative can be greatly encouraged to achieve optimal rehabilitation therapy. The major concern of this strategy is that human-robot synchronization is required to deliver safe and effective assistance. If the robotic assistance is not synchronous with the human gait, the robot may resist the human walking, and may even cause injury [111, 112]. Motivated by the need, we have developed a novel bio-inspired synchronization method, which will be illustrated in Chapter 5.

Conclusively, an insight review has been conducted in this chapter, including on the mechanical designs, actuation systems and control strategies that are currently utilized in robotic systems for gait rehabilitation.

Chapter 3

Mechanical Design of a Portable Knee-Ankle-Foot Exoskeleton Robot

This chapter presents the mechanical design and evaluation of a knee-ankle-foot robot, which is compact, modular and portable for stroke patients to carry out overground gait training at outpatient and home settings. A novel SEA is developed for safe human-robot interactions. As a solution to the limitation of conventional SEA designs, one low-stiffness translational spring and a high-stiffness torsion spring are placed in series for force transmission. The springs are selected based on gait biomechanics to maintain a high intrinsic compliance for most period of a gait cycle, while retaining the capacity to provide the peak force. To achieve portability, the robotic joint mechanism is optimized based on gait biomechanics, and the mechanical structure is built with lightweight materials. This robot demonstrates stable and accurate force control in experiments conducted on healthy subjects with overground walking. The activation level of the major leg muscles of subjects is reduced as indicated by the EMG signals and the normal gait pattern is maintained during the test, which demonstrates that the robot can provide effective assistive force to the subjects during overground walking.

1. Introduction

The incidence of stroke keeps growing rapidly with the increase of the aging population [2]. Stroke survivors suffer from muscle weakness, paralysis, gait disorder and pain and are affected in their ability to perform activities of daily living (ADL) [113]. As the main therapy for stroke patients, physical exercise aims to evoke brain plasticity to improve locomotive functions [19, 114]. However, conventional manually assisted gait training is expensive, labor intensive and physically demanding for therapists [17]. Rehabilitation robotics was then successfully introduced into the earlier phases of recovery after stroke to overcome the major limitations of traditional manual therapy [23]. The robots can deliver high-quality rehabilitation therapies, and evaluate the recovery progress as well.

Over the years, various gait rehabilitation robotic devices have been developed based on different concepts [21, 22]. However, most of existing robotic gait training systems are integrated with fixed platforms and treadmills. They are bulky, expensive and only available in a limited number of rehabilitation centers or big hospitals. There is a great need for portable exoskeleton systems for overground gait rehabilitation. The portable exoskeleton can provide more freedom in motion. More importantly, they are portable, compact and can deliver gait training at home or outpatient setting.

(A) Challenge in portable exoskeleton design

Notwithstanding the benefits mentioned above, the weight remains to be the main challenge in the portable exoskeleton design. For example, the ankle robot developed at MIT [52] weighs 3.1 kg for just the ankle joint. The commercialized knee assistive device developed by Tibion [115] weighs more than 4.5 kg for just the knee joint. Toyota unveiled a knee assistive robot called Independent Walk Assist robot, which weighs 3.5 kg [116]. A quasi-passive compliant stance control orthosis (CSCO) for knee joint assistance recently developed by Shamaei et al. weighs 3kg [117]. Lightweight exoskeletons are to be developed to achieve free locomotion. Compactness, battery and capability should be also considered in exoskeleton design.

Besides, it is known that the ankle joint plays an important role in biomechanics during walking [118]. However, ankle joint is usually left unactuated in the existing designs, which may leads to an unnatural gait pattern. Portable devices aimed at providing active assistive torque to both the knee and ankle joints are also very rare due to ineffective and bulky actuation design. The key solution is to develop an efficient, capable but lightweight actuation system, which will be further explained in the following sub-section.

(B) Challenge in SEA design

As discussed in Chapter 2, SEA is suitable for rehabilitation robotics application. SEA is safe for human-robot interaction due to its intrinsic compliance; and has high force fidelity and controllability.

However, the performance of the SEAs largely depends on the spring constant and SEA faces a dilemma of compliance and force range, for which, a tradeoff has to be made [87]. A low-stiffness spring produces high fidelity of force control and low output impedance, but it also limits the output force range and control bandwidth due to the limitation of the deflection length (Figure 3-1(a)). On the other hand, a high stiffness spring increases the output force range, but reduces the force control fidelity (Figure 3-1(b)). To achieve both high compliance and large output force range, a very long soft spring has to be employed (Figure 3-1(c)), which leads to a bulky robot design.

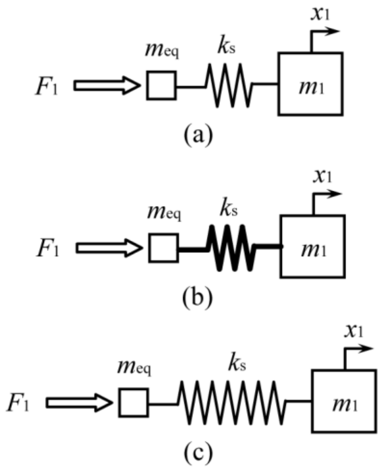

Figure 3-1. SEA design: (a) SEA with soft spring; (b) SEA with stiff spring; (c) SEA with soft but long spring. F_1 is the motor output force; m_1 represents the robot; x_1 is the position of the robot; m_{eq} is the equivalent mass of the motor; k_s is the spring stiffness.

In order to achieve the high force transmission, most current SEAs adopted high stiffness springs, which lead to the compromised force control performance, intrinsic compliance and back-drivability. Additionally, the existing SEA designs are relatively bulky and heavy.

In this chapter, we present a compact and modular knee-ankle-foot robot aiming for sub-acute and chronic stroke patients to conduct gait rehabilitation at outpatient rehabilitation centers or at private homes. Considering that most stroke survivors suffer hemiparetic deficits, we start building our prototype for one leg. The system can be easily reconfigured into either a knee robot or an ankle robot to suit different symptoms, such as knee hyperextension and drop foot. In order for the device to be able to provide large assistance while remain compliant, we developed a novel compact SEA [89]. Corresponding linkage mechanism is optimized based on the study of human gait biomechanics to achieve portable and capable design. Controller is designed and implemented for the actuator to achieve good force tracking performance. Overground walking experiments have also been conducted on two healthy subjects to verify the effectiveness of the robot.

The rest of this chapter is organized as follows. Section 2 introduces methods of developing the exoskeleton robot system. Section 3 presents the modeling, control and force control performance of the compliant actuator. Section 4 presents the experimental evaluation of the robot with overground walking tests.

2. Design of the robotic exoskeleton system

2.1 Design specifications based on gait biomechanics

Since the primary goal of the device is to facilitate the subject overground walking and provide assistance, the design specification of the proposed robot is determined by analyzing the biomechanics of human gait. Clinical Gait Analysis (CGA) data are utilized to guide the design of the exoskeleton and actuator, which are collected from the CGA normative gait database [119]. Figure 3-2 illustrates the biomechanics in terms of torque, joint angle and power of the knee flexion/extension and ankle dorsiflexion/plantarflexion when a healthy subject (70kg, 0.9m leg-length) walking at

1.0m/s. The biomechanical data is normalized into gait cycle percent (1~100%), which starts from the heel strike of the right leg and ends with the next heel strike of the right leg.

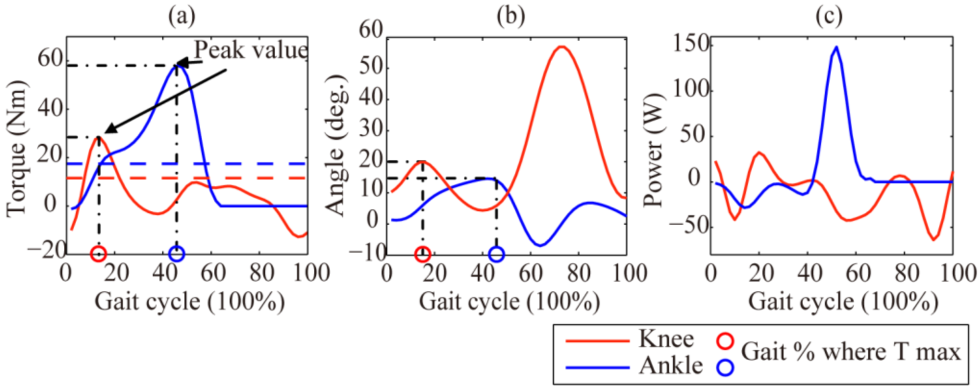

Figure 3-2. Biomechanics of human ankle and knee joints for a 70kg healthy subject during normal gait cycle with 1.0m/s speed, including (a) joint angle, (b) joint torque and (c) joint power. Red and blue lines represent knee and ankle joints respectively. Blue and red circle is the gait percentage where joint torque reaches its maximum. Dot dash line illustrates the joint angles and torques where joint torque is maximum. Dashed line is 30% of peak torque that covers the most part of a gait cycle.

Normally, the walking knee flexion is limited to about 60 °. The peak knee torque reaches 30N ·m during stance phase (18% gait cycle, red circle in Figure 3-2(a)) when knee angle is about 20 ° (Figure 3-2(a)). It is worth noting that knee torque remains under 10 Nm (30% of peak torque) for most of a gait cycle, and goes beyond this value in a small period only (red dashed line in Figure 3-2(a)). Correspondingly, the walking ankle angle ranges from -10 °~15 °, and the peak torque is 60 Nm when the angle is close to 15 ° (42% gait cycle, blue circle in Figure 3-2(a)) during stance phase (Figure 3-2(b)). Similarly, ankle torque stays below 20 Nm (30% of peak torque) for more than half of the gait cycle (blue dashed line in Figure 3-2(a)). It is worthy to note that this character is a driving factor for our novel SEA design to be discussed in Section 2.3. On the other hand, the power requirement of each joint is a driving factor for the motor selection. Thus, an average mechanical power between 100W and 150W is required for the knee and ankle joints (Figure 3-2(c)). These biomechanical data will also be utilized for the mechanical optimization of the following robot and the compliant SEA design.

2.2 Mechanical structure design of the robot

Figure 3-3 shows the overall design of the knee-ankle-foot robot. Ball bearings are employed as the knee and ankle joint of the robot, which align with the knee and ankle joint of human (Figure 3-3(a)). Rotatory potentiometers are installed inside the bearing to determine the joint angles (Figure 3-3(c)). The modular design of a knee module and an ankle module (Figure 3-3(b)) satisfies the requirements of patients under different conditions, which can also be implemented separately. When using both modules together as a whole for the current prototype, a connecting linkage is employed to adjust the length of shank from 40cm to 47cm adapting to a range of different user heights. The actuation mechanism for both the knee and ankle joints in this design is particular, which is a novel compact linear SEA through a four-bar linkage (Figure 3-3(d)). More details of the actuator and actuation mechanism will be discussed in Section 2.3 and Section 2.4. Figure 3-3(e) shows a prototype of the robot. The anthropomorphic structure is built with lightweight carbon fiber reinforced plastic (CFRP) composite material. The robot is easy to don and doff. The total mechanical weight of the prototype weighs about 3.5kg, which makes it portable.

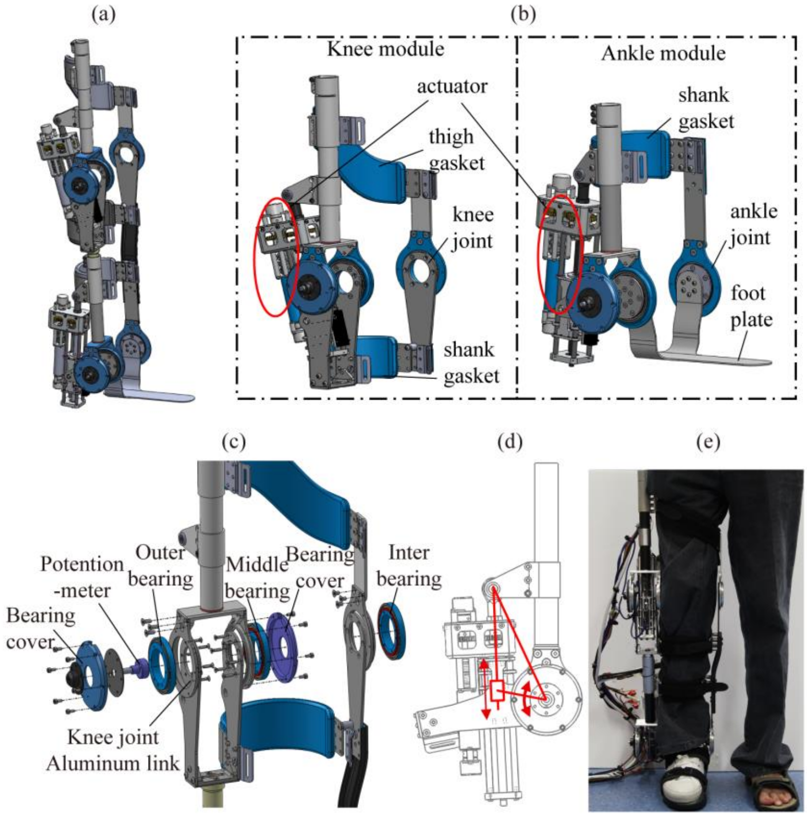

Figure 3-3. (a) CAD model of the knee-ankle-foot robot; (a) CAD models of the knee module and ankle-foot module; (c) explosive views of the robotic joint; (d) slider-crank linkage as the actuation mechanism; (e) front view of a prototype of the robotic system wore by a subject.

Furthermore, it is noted that most powered lower-limb exoskeleton robots adopt a unilateral structure to implement a mechanical joint, such as ReWalk [76], HAL [58] et al. However, this approach generates torques in undesired directions and brings damage to the mechanical structure of the robot (Figure 3-4(a)). Besides, very tight straps have to be used in unilateral designs to prevent the slippage between human limbs and robot, which leads to pain, discomfort, and even skin injuries. To overcome these limitations, bilateral structure is adopted in our design to improve ergonomics of the robot. The force diagram on a bilateral joint is illustrated in Figure 3-4(a). The excess torques in undesired directions can be eliminated, which can improve the safety and comfort of the device.

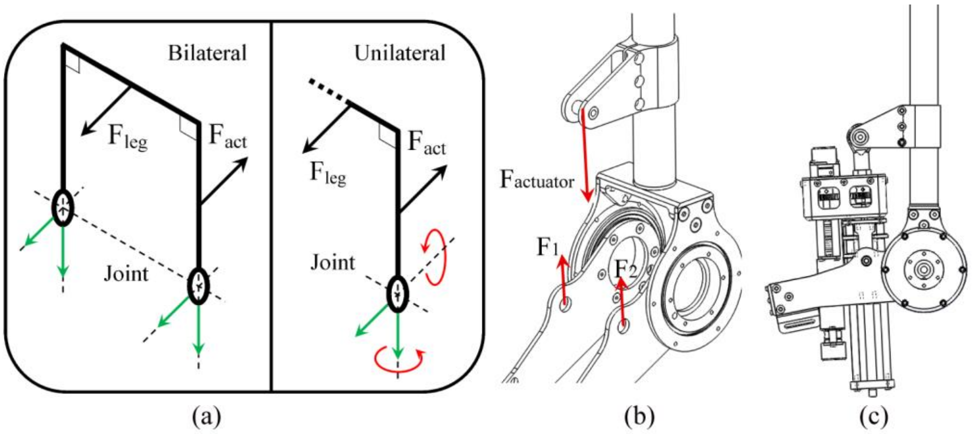

Figure 3-4. (a) Force and torque loaded on robot joint with bilateral and unilateral structures. Green arrow indicates the force in desired direction; red arrow shows the torque in undesired direction. F_{act} is the actuation force and F_{leg} is the interaction force from human leg. (b) Fact, F_1, F_2 are the forces loaded on the actuator. (c) The assembly of the robotic joint.

As shown in Figure 3-4(b), the actuator on the robotic joint is assembled in a symmetric way, which protects the actuator from being damaged by the unbalanced load. The output pin of the actuator is placed in the middle of the actuator body instead of the extreme end, thus the length of the actuator is reduced and achieves compactness and steady force transmission. The actuator can also be fitted into the space between the output frames when the robotic joint bends (Figure 3-4(c)). The compactness of the joint design and the portability of the robot are thus achieved.

2.3 Novel SEA design

The previous study on gait biomechanics (as shown in Figure 3-2) indicates that the average joint torque in human lower-limb joints during normal gait is much lower than the peak value (as described in Section 2.1). It implies that the actuator for gait assistive robots only needs to provide a relatively small torque for most periods of a gait cycle, and this can be handled by a soft spring. As for the higher peak torque, a stiffer spring is then required. On the basis of the above analysis, we develop a novel SEA design, which overcomes the limitations of the conventional SEA designs and makes it more suitable for the gait rehabilitation robot application.

(A) Working principle of the novel SEA

The novelty of this actuator design is the utilization of two springs in series with vastly different stiffness values to handle different force ranges. A soft translational spring handles low-force range, which enables the actuator to achieve the high force fidelity, low output impedance and high intrinsic compliance. A torsion spring with high effective stiffness, handles high-force operation when the soft spring is fully compressed. The torsion spring extends the output force into a larger range and improves the control bandwidth of the actuation system.

Figure 3-5 illustrates the composition of the proposed compliant actuator. The actuator consists of an electrical motor that drives a ball screw through two sets of spring assemblies. Two unidirectional torsion springs are fitted into a custom-made coupler, which becomes a bidirectional torsion spring. Two rotary encoders are located at both sides of the motor and the difference of the two encoder readings will be used to determine the deflection of the torsion spring. A pair of spur gears with 1:1 transmission ratio transfers the force to another parallel shaft of the ball screw, which helps reduce the total length of the actuator. Then, two linear springs are placed within an output carriage and pushed by the ball screw nut. Besides, a linear potentiometer is installed to measure the deflection of the linear spring, thus deriving the output force of the actuator based on Hooke’s law. Figure 3-5(c) further illustrates the design of the actuator in an exploded view. And the directions of the motion transmission are indicated as well.

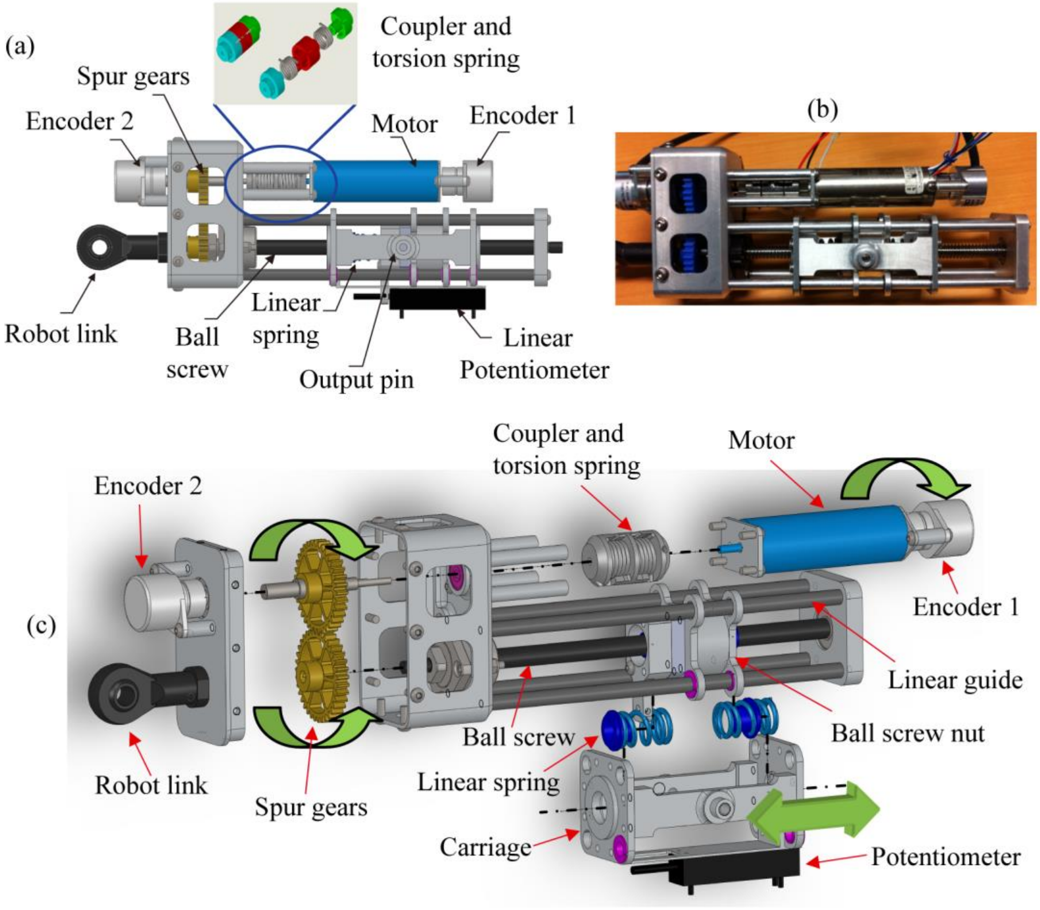

Figure 3-5. (a) CAD model and (b) the prototype of the compliant force controllable SEA and (c) exploded views of the actuator and directions of motion transmission.

A prototype of the actuator is shown in Figure 3-5(b). A Maxon DC brushless motor (EC-4pole 120W, 36V) is adopted as the power source. A linear potentiometer from ETI is applied as the linear spring deflection sensor. Two incremental encoders with 1024tics/rev are used to measure the deflection of the torsion spring. The ball screw is chosen to be 140mm in length with 2mm/rev. The stroke of the actuator is 60mm. The total weight of the SEA prototype is 0.85kg.

(B) Selection of spring stiffness

The selection of the two springs' stiffness is based on the biomechanical analysis of gait, which aims to achieve biomechanical efficiency. The soft linear spring is implemented to increase the intrinsic compliance of the actuator, and keeps the actuator working within the low-force range for most of a gait cycle. The torsion spring is used to extend the range of the output force, and thus should be rigid enough to cover the peak force.

The required output force of the actuator depends on the optimization of the actuation mechanism, which will be given in the following section. According to the optimized results, the required peak force of the actuator along a gait cycle is around 800N. Based on the gait biomechanics in Section 2.1, the required force is lower than 30% of peak force for most periods of a gait cycle; hence, the low-force range (the output force range of the soft spring) is chosen to be 240N. Two linear springs with working stroke of 10mm and the stiffness of 24N/mm are placed at both sides of the ball screw nut to achieve the bidirectional force.

The torsion spring integrates the high effective stiffness to achieve the large output force range. However, large stiffness brings bad force resolution due to the limitation of encoders. We chose 0.29N·m/rad torsion springs with 72° deflection range of the coupler. The resultant output force range is 1128N, with a force resolution of 5.6N. The section of key parameters of this actuator is summarized in Table 3-1.

Table 3-1. Parameters of the actuator prototype.

Variable	Value
Geometry size	230mm×78mm×43mm
Motor power	120W
Output force	±1128N
Low-force range	±240N
Linear spring stiffness	$24x10^3$N/m
Torsion spring stiffness	0.29N·m/rad
Equivalent torsion spring stiffness	2.8622×10^6N/m
Pitch of the ball screw	2mm
Stroke	60mm
Force resolution in low-force range	0.146N
Force resolution in high-force range	5.6N
Total weight	0.85kg

2.4 Design and optimization of the actuation mechanism

The robotic knee and ankle joints are rotated by the SEA through a four-bar linkage, i.e. a slider-crank linkage. The schematic diagram of the mechanism is shown in Figure 3-6. This mechanism is optimized to minimize the required force for the compact SEA design. The geometrical constraints with the physical structure are proposed to provide the adequate and safe range of motion (ROM). The optimization procedure is identical for knee and ankle joints, which follows two steps as shown in Figure 3-6 with the knee joint as an example.

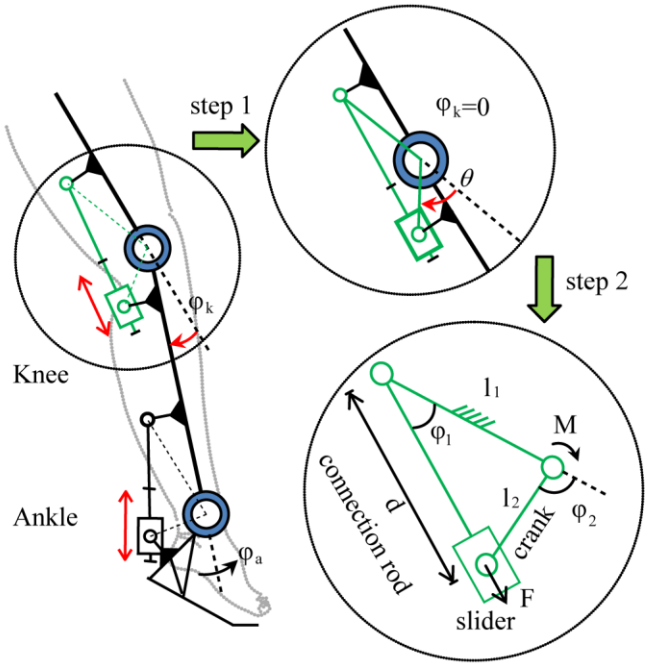

Figure 3-6. Schematic diagram and optimization procedure of the slider-crank mechanism for the robot. φ_k and φ_a denote the knee joint angle and ankle joint angle, respectively. Step 1: selecting the angle θ, where θ is the crank angle when joint angle is zero; Step 2: geometrical parameters optimization, where l_1, l_2 are the lengths of the frame and crank, d is the length of the connection rod, φ_1, φ_2 are the relative angles of each bar, F is the output force of the actuator in the direction of the connection rod, M is the output torque of the robotic joint torque during human gait cycle.

Step 1: selecting the initial crank angle θ when the joint angle φ_k is zero. It satisfies $\theta+\varphi_{Tmax}=90°$, where φ_{Tmax} is the knee joint angle corresponding to the maximum joint torque in a gait cycle (as shown in Figure 3-2). This ensures the crank is vertical to the connection rod when the required torque reaches its peak so that it maximizes the length of the lever-arm to apply the force F (please refer to Figure 3-6). The actual crank angle θ for each joint is illustrated in Table 3-2.

Step 2: optimizing the geometrical parameters of the four-bar linkage to minimize the required peak force of the actuator within a gait cycle. The trajectories of knee joint angle φ_k and joint torque M are derived from CGA data as described in Figure

3-2. Geometric constraints are also considered to ensure the ROM in the normal gait to protect the patient.

Referring to Figure 3-6, the kinematics of the four-bar mechanism can be described as

$$\begin{cases} d\cos\varphi_1 = l_1 + l_2\cos(\varphi_2) \\ d\sin\varphi_1 = l_2\sin(\varphi_2) \end{cases} \tag{3-1}$$

and from which, the crank joint φ_2 can be derived as:

$$\varphi_2 = a\cos((d_{\min}^2 - l_1^2)/(2l_1l_2)) \tag{3-2}$$

And φ_2 also meets

$$\varphi_2 = \varphi_k + \theta \tag{3-3}$$

The robotic joint torque generated by the actuator is given by

$$M = F \cdot l_2\sin(\varphi_2 - \varphi_1) \tag{3-4}$$

The objective function, i.e. the required peak force in a gait cycle, is thus defined as the infinite norm of the actuator force

$$f(X) = \|F\|_\infty = \left\| \frac{M}{l_2\sin(\varphi_2 - \varphi_1)} \right\|_\infty \tag{3-5}$$

The lengths of the frame l_1 and crank l_2 are the parameters to be optimized. The search space is then defined as

$$l = \begin{bmatrix} l_1 & l_2 \end{bmatrix}^T \tag{3-6}$$

The geometrical constraints are given by

$$d_{\max} < l_1 + l_2 \tag{3-7}$$

$$l_1 - l_2 < d_{\min} \tag{3-8}$$

$$l_2 < l_1 \tag{3-9}$$

$$\varphi_{\max req.} < a\cos((d_{\min}^2 - l_1^2)/(2l_1l_2)) - \theta < \varphi_{\max\lim} \tag{3-10}$$

$$\varphi_{\max req.} < a\cos((d_{\min}^2 - l_1^2)/(2l_1l_2)) - \theta < \varphi_{\max\lim} \tag{3-11}$$

where d_{min} , d_{max} are the limiting output displacements of the actuator, of which the range is 125~185mm. $\varphi_{min\ req.}$, $\varphi_{max\ req.}$ represent the required range of joint angles for free human gait. φ_{minlim} , φ_{maxlim} are the limiting joint angles for a safe motion range.

Equations (3-7)-(3-9) ensure the existence of the slider-crank mechanism. Equations (3-10) and (3-11) specify the range of joint motion with the terminal displacements of the actuator. The target ROM of the robotic joint should cover the required range ($\varphi_{min\ req.}$, $\varphi_{max\ req.}$) to allow a normal gait; and is within the limiting joint angles (φ_{minlim} , φ_{maxlim}) to prevent the robot from moving into excessive motion. The values of $\varphi_{min\ req.}$, $\varphi_{max\ req.}$ and φ_{minlim} , φ_{maxlim} are listed in Table 3-2. With these constraints, the ROM of the robotic knee joint is bounded by physical structure and the knee joint movements can be restricted in an adequate and safe range. These equations are subjected to the MATLAB *fmincon* optimization function to minimize the peak force in the feasible workspace.

The required peak force on the actuator with different configurations of l_1, l_2 is drawn on Figure 3-7(a). It is marked as zero if the particular combination does not meet the constraint. In Figure 3-7(a), the green dot denotes the minimum peak force for the actuator, which is taken as optimum. The minimum peak force guiding for spring selection is 687N and 830N on knee and ankle joints, respectively. Figure 3-7(b) presents the trajectories of required actuator output force for both joints during a gait cycle with the optimized configuration. The resulting ROM meets the demands of human walking and is mechanically restricted in the safe range to protect human lower-limb joints. The optimized configurations and resultant ROM of the robotic joints and required peak force of the actuators are summarized in Table 3-2.

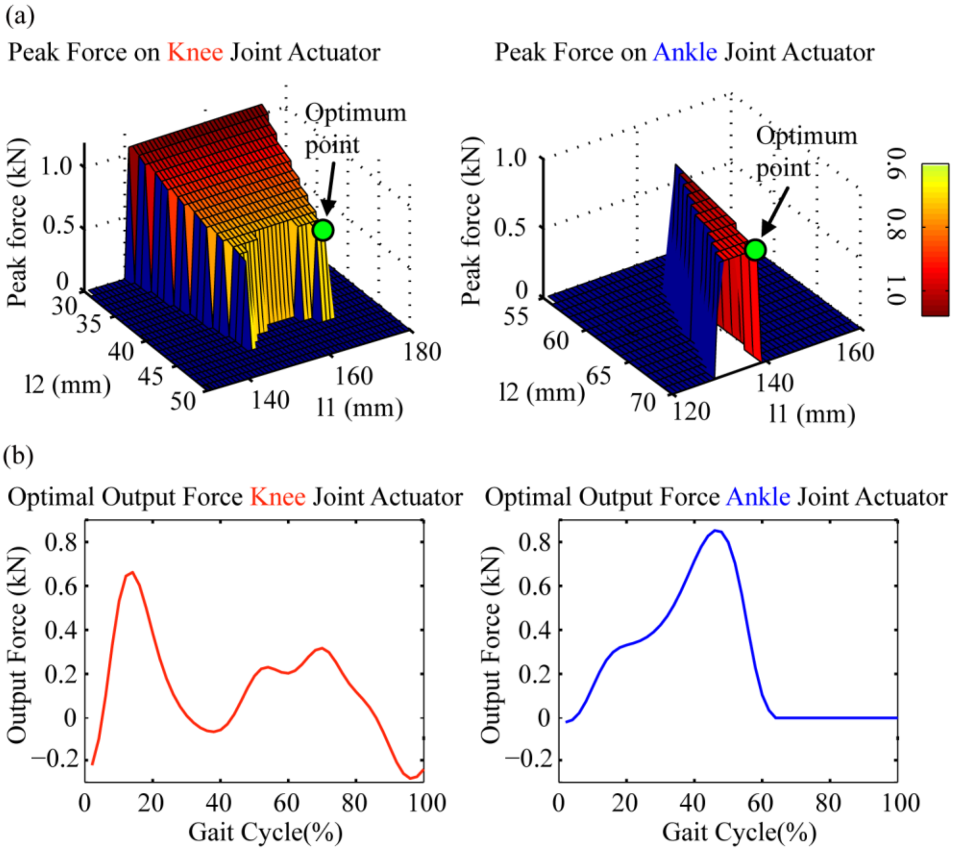

Figure 3-7. the results of the required peak force on both knee joint and ankle joint with different configurations of l_1 and l_2, respectively. The green dot represents the optimum point, where the required peak force is minimum. (b) The output force trajectories of actuators on knee (red) and ankle (blue) joints during a gait cycle with the optimized configuration.

Table 3-2. Optimized parameters of the robotic joints.

Variable	Knee	Ankle
Initial angle θ (°)	70	75
Required range (°) $\varphi_{min\ req.}$~$\varphi_{max\ req.}$	0~70	-10~20
limiting range (°) φ_{minlim}~φ_{maxlim}	0~120	-30~40
l_1 (mm)	168	136
l_2 (mm)	45	70
ROM (°)	0~90.5	-20.8~38
Peak force (N)	687	830

2.5 Robot sensing system

This robot implemented a suit of sensors to monitor human kinematics, muscle activity and interaction force. Encoders and potentiometers are installed on the actuator as described in Section 2.3. Rotatory potentiometers are installed on the robotic joint to determine the angles (Figure 3-3(c)). EMG amplifiers are integrated to record muscle activation patterns. We have also developed an IMU sensing system that can measure kinematics of both legs and human trunk.

3. Modeling and control of the novel SEA

3.1 Modeling of the compliant actuator

In order to analyze the actuator performance at the output end, which produces linear output force, the actuator is modeled as a system consisting of translational elements by converting the rotary elements to equivalent translational elements. The actuator model for the equivalent translational motion is shown in Figure 3-8(a). In this model, F_1 is motor input force, m_1 is equivalent mass of the motor plus the torsional spring coupler and the encoder. J_1 refers to moment of inertia of the motor and the torsional spring coupler and the encoder, p is the pitch of the ball screw, m_2 is equivalent mass of the ball screw and the gears. J_2 refers to moment of inertia for the ball screw and the gears, k_1 is considered as the equivalent translational spring constant of the torsional spring. k_t, and k_2 is spring constant of the translational spring, b_1 and b_2 are the viscous damping for motor and ball screw respectively, and F_2 is output force.

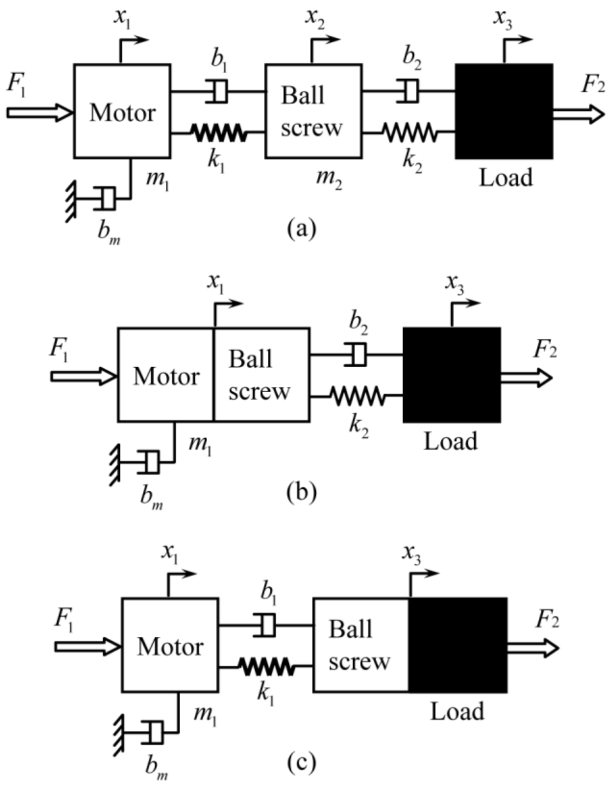

Figure 3-8. Modeling of the series elastic actuator (a) The general case. (b) model for low force range. (c) model for high force range.

The physical parameters of the actuator prototype are listed in Table 3-3, where both the original number and the equivalent translational values are given for the dynamic modeling and analysis purpose. We can see that the spring constant k_1 derived from the torsion spring is 120 times that of k_2, meaning the torsional spring can be considered to be a rigid link when the output force is low and the actuator behaves like a normal SEA with the linear spring only. This can be further justified by the poles of the open loop system. It can be found that there are a pair of poles far away from the imaginary axis; and the system dynamics is dominated by a pair of slower poles, which are contributed by the soft spring [89]. The model of the actuator can then be simplified as shown in Figure 3-8(b). When the output force reaches a level when the linear spring is fully compressed, the actuator will behave like a SEA with only the torsional spring as shown the model in Figure 3-8(c). Because of the simplified model, we can design the actuator controllers following the same methods for the conventional SEAs.

Table 3-3. Parameters of the actuator model.

Values of the hardware parameters for rotational motion	Values of the hardware parameters for equivalent translational motion
J_1=5.517$\times$ 10^{-6} kg.m^2	$m_1 = J_1\left(2\pi / p\right)^2$ =54.4 kg
J_2 =7.406$\times$ 10^{-6} kg.m^2	$m_2 = J_2\left(2\pi / p\right)^2$ =73 kg
Torsional spring k_t =0.29 Nm/rad	$k_1 = k_t\left(2\,\pi\ / p\right)^2$ =2.86$\times$ 10^6 N/m
Linear spring k_2 =24$\times$ 10^3 N/m	k_2 =24$\times$ 10^3 N/m
Pitch of the ball screw (p)=2$\times$ 10^{-3} m	p=2$\times$ 10^{-3} m
Rotary encoder resolution=1024 /rev	Force resolution 5.6 N
Linear potentiometer 25 mm	Force resolution 0.0092 N
Total weight of actuator	0.84 kg

(A) Modeling for the actuator in low-force range

Referring to Figure 3-8(b), the equation of motion according to Newton's second law is given by

$$(m_1+m_2)\ddot{x}_1 = F_1 - k_2(x_1-x_3) - b_2(\dot{x}_1-\dot{x}_3) - b_m\dot{x}_1 \tag{3-12}$$

After Laplace transformation, assuming initial conditions zero, equation (3-12) gives

$$(m_1+m_2)s^2X_1(s) = F_1(s) - k_2(X_1(s)-X_3(s)) - b_2s(X_1(s)-X_3(s)) - b_msX_1(s) \tag{3-13}$$

We can get the system force output by applying the Hooke's law, i.e., $F_2 = k_2(x_1-x_3)$. To investigate the performance of force transmission from the motor to the output, we assuming a fixed load end, x_3=0, and the equation (3-13) can be written as

$$\frac{F_2(s)}{F_1(s)} = \frac{k_2}{(m_1+m_2)s^2+(b_2+b_m)s+k_2} \tag{3-14}$$

From equation (3-14), we can easily derive the natural frequency ω_c of the actuator in low-force range as:

$$\omega_c = \sqrt{\frac{k_2}{m_1+m_2}} \tag{3-15}$$

We can find that the bandwidth of the open loop system depends on the inertia and spring stiffness. Larger inertia or small spring stiffness decrease the natural frequency.

The output impedance Z defined as the transfer function from the x_3 to the output force F_2 is in the uncontrolled case:

$$Z = \frac{F_2(s)}{x_3(s)} = k_2 \frac{-(m_1 + m_2)s^2 - b_m s}{(m_1 + m_2)s^2 + (b_2 + b_m)s + k_2} \tag{3-16}$$

It is observed that at low frequencies the output impedance is ideally equal to zero, and goes to $-k_2$ in the limit at high frequencies. Since the value of k_2 is chosen very small in the design, our actuator can achieve low intrinsic impedance.

(B) Modeling for the actuator in the high-force range

Referring to Figure 3-8(c), we have the following equation for high force case.

$$m_1\ddot{x}_1 = F_1 - k_1(x_1 - x_3) - b_1(\dot{x}_1 - \dot{x}_3) - b_m\dot{x}_1 \tag{3-17}$$

In the case that the load is fixed, using the Hooke's law $F_2 = k_1(x_1 - x_3)$, we have the following model for the output force after Laplace transformation:

$$\frac{F_2(s)}{F_1(s)} = \frac{k_1}{m_1 s^2 + (b_1 + b_m)s + k_1} \tag{3-18}$$

It is found that the natural frequency in high-force range is derived as:

$$\omega_c = \sqrt{\frac{k_1}{m_1}} \tag{3-19}$$

Compared to that in low-force range, the natural frequency in high-force range is hundreds times larger due to the stiffer torsion spring and smaller inertia.

3.2 Controller design of the actuator

(A) Controller of the actuator in low-force range

The model of the actuator in low-force range is second order as shown in Figure 3-8(b), and therefore the force controllers may follow the conventional methods for the normal SEAs. We assume a unity feed-forward signal term and a PD controller with the gains k_p (proportional gain) and k_d (derivative gain). Those gains are to be defined in the control design stage. Figure 3-9 shows the actuator in closed-loop in the low-force range.

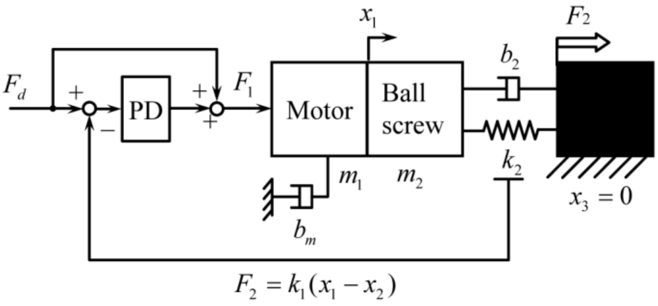

Figure 3-9. Control system of the actuator at low force, where F_d is the desired output force, F_2 is the force reading on the linear spring, as well as the force feedback.

The force control to the motor is given by

$$F_1 = k_p(F_d - F_2) + k_d(\dot{F}_d - \dot{F}_2) + F_d \tag{3-20}$$

where F_d is the desired output force. A stable force control can be achieved by using the proposed PD plus feedforward control.

Taking a Laplace transformation, the closed-loop transfer function for the low force range is given by

$$\frac{F_2(s)}{F_d(s)} = \frac{k_2 k_d s + k_2(k_p + 1)}{(m_1 + m_2)s^2 + (b_2 + b_m + k_2 k_d)s + k_2(k_p + 1)} \tag{3-21}$$

The pole assignment method can be used to design the controller to have the desired poles in such a standard second-order system, as:

$$\frac{Output(s)}{Input(s)} = \frac{\omega_c^2}{s^2 + 2\zeta\omega_c s + \omega_c^2} \tag{3-22}$$

where ζ is the damping ratio of the closed loop.

By combining equations (3-21) and (3-22), the following PD control gains can be produced as:

$$k_p = \frac{\omega_c^2 (m_1 + m_2)}{k_2} - 1 \tag{3-23}$$

$$k_d = \frac{2\zeta_c \omega_c (m_1 + m_2) - (b_2 + b_m)}{k_2} \tag{3-24}$$

Hence, we can design the PD gains to achieve a sufficient large desired bandwidth ω_c comparing to that in open loop control (3-15).

The output impedance of the closed-loop system is defined as the same as the given above, that is

$$Z = \frac{F_2(s)}{x_3(s)} = \frac{-(m_1 + m_2)k_2 s^2 - b_m s}{(m_1 + m_2)s^2 + (b_2 + b_m + k_2 k_d)s + k_2(k_p + 1)} \tag{3-25}$$

where the desired force is zero, i.e., $F_d = 0$. From this equation, the impedance at low frequency is ideally equal to zero but as frequency increases, in the limit the impedance is equal to the spring constant k_2. This property is desired to make the designed actuator insensitive to joint input. With active control, the actuator is backdrivable. For a practical application, the impedance should be as low as possible. This can be done by increasing the control gains or decreasing the spring constant.

(B) Controller of the actuator in high-force range

Similar to the low force range, the high force control is taken as a PD plus feedforward control as shown in Figure 3-10.

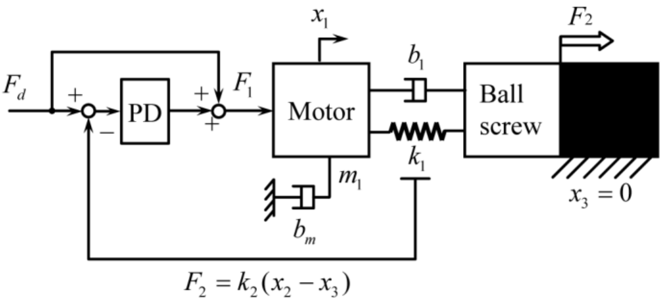

Figure 3-10. Control system of the actuator at high force, F_2 is the force reading on the torsion spring, as well as the force feedback.

The expression of the transfer function for the high force, after Laplace transformation, assuming initial conditions zero at t=0 and a fixed load end, is given by

$$\frac{F_2(s)}{F_d(s)} = \frac{k_1 k_d s + k_1(k_p + 1)}{m_1 s^2 + (b_1 + b_m + k_1 k_d)s + k_1(k_p + 1)} \tag{3-26}$$

The PD gains can be tuned to achieve a sufficient bandwidth.

(C) Controller of the actuator in switching

In a practical application, the desired force profile can vary between the low-force range and high-force range. The controller has to be able to sense the correct force level and switch to the corresponding controller without disturbance or impact. A direct switch strategy is firstly designed as shown in Figure 3-11. The controller switches between the low-force controller and high-force controller depending on the feedback force. To be specific, in low-force range, the force feedback is derived from the linear spring as $F_2 = k_2(x_2 - x_3)$. The control output is from the PD control in the low-force range (3-20) When $F_2 > 240$ N, the feedback force is from the torsion spring as $F_2' = k_1(x_1 - x_2)$, and the control output switches to the PD controller output in the high-force range.

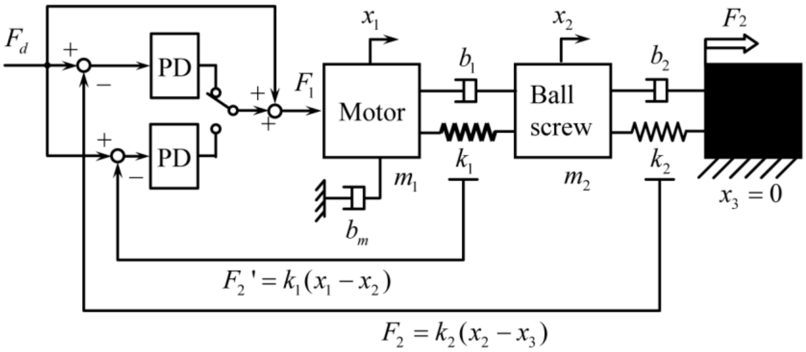

Figure 3-11. Control system of the actuator at direct switching control. F_2 and F_2' are the force readings on the linear spring and torsion spring, respectively.

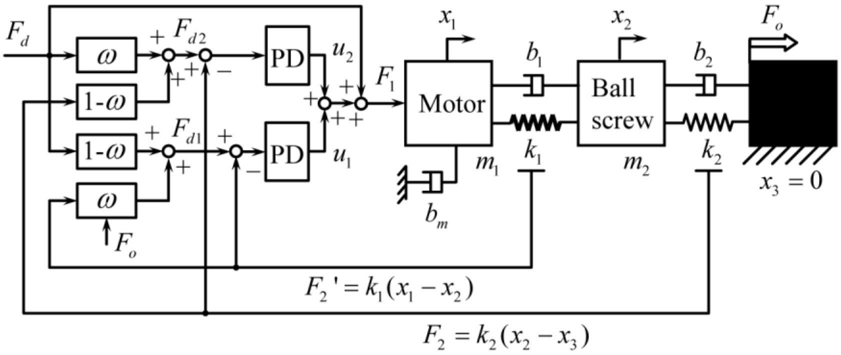

Figure 3-12. Control system of the actuator at switching control. ω is a weight factor, F_o is the output force, F_{d1} and F_{d2} is the desired force for the high-force and low-force controller, respectively.

However, during actual experiment, we found the performance of the direct switching control was unsatisfying. Due to the dynamics of the actuator, the force readings on the two springs are usually different, which leads to a big jump of the force feedback when the controller switches. This difference deteriorates the actuator performance and brings impact to human limb. The performance is even worse with large feedback control gain, which leads to larger force difference on the two springs during switching. Hence, the switching controller is modified and is shown in Figure 3-12.

The force feedback F_o switches between the two springs, i.e. $F_o = F_2$ in the low-force range and $F_o = F_2'$ in the high-force range. A weight factor $\omega(F_o)$ is defined as:

$$\omega = \begin{cases} 1 & , \quad |F_o| < 240 - c \\ \dfrac{240 - |F_o|}{c} & , \quad 240 - c < |F_0| < 240 \\ 0 & , \quad |F_o| > 240 \end{cases} \tag{3-27}$$

where c denotes the width of a band and 240 is the force threshold between the low-force and the high-force range. The weight factor $\omega(F_o)$ is continuous, and is illustrated in Figure 3-13.

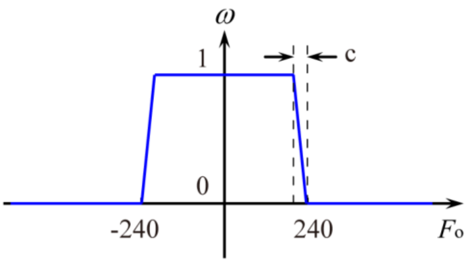

Figure 3-13. An illustration of the weight factor.

Next, two reference variables are specified as:

$$\begin{aligned} F_{d1} &= (1-\omega)F_d + \omega F_2' \\ F_{d2} &= \omega F_d + (1-\omega)F_2 \end{aligned} \tag{3-28}$$

which are reference for the low- and high-force PD controllers, respectively.

The force control to the motor is then given by

$$F_1 = u_1 + u_2 + F_d \tag{3-29}$$

where u_1 and u_2 are control output of the controller in the high-force rang and the low-force range, respectively.

From equations (3-27) and (3-28), when the actuator works in the low-force range, $\omega = 1$. Then the reference in equation (3-28) can be written as: $F_{d1} = F_2'$, $F_{d2} = F_d$. In this condition, the output of the high-force controller $u_1 = 0$, and the actuator works with only the low-force controller, which is the same as equation (3-20). Similarly, when the actuator works in the high-force range, $\omega = 0$ and the actuator works with only the high-force controller. When the actuator works within the band, $0 < \omega < 1$, and the control output is a mix of the control output of both controllers, which ensures a smooth transition between the low-force and the high-force range. The controller is table during the transition of the low-force and the high-force range, which is discussed in our related work [120].

3.3 Experimental results of the actuator control

(A) Experimental setup

The force tracking control scheme was implemented in the SEA as shown in Figure 3-14. The actuator was mounted on a testing jig to fix its output pin. The motor driver is Elmo HAR12/60. The controller is the National Instruments CompactRIO 9074 embedded control and data acquisition system. The force control algorithms are implemented in LabVIEW software platform, which plots the control information on a desktop in realtime. The sampling frequency is 2k Hz.

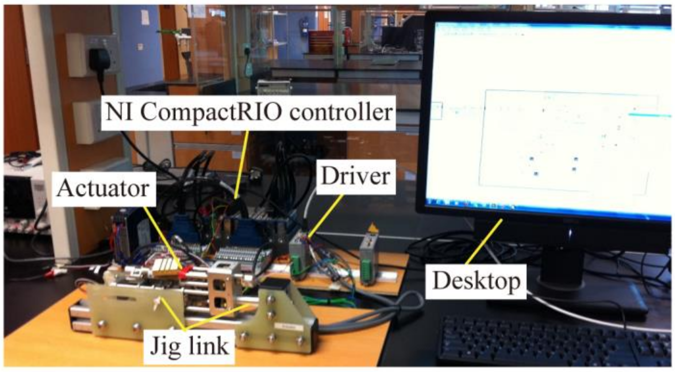

Figure 3-14. Experimental setup.

(B) Experimental results in low-force range

According to our design, the output force was collected from the linear spring in the low-force range. The desired force was sinusoid wave signal. Figure 3-15 shows the force tracking performance of sinusoidal signal at 2 Hz. The tracking error was less than 1%, indicating very high force fidelity.

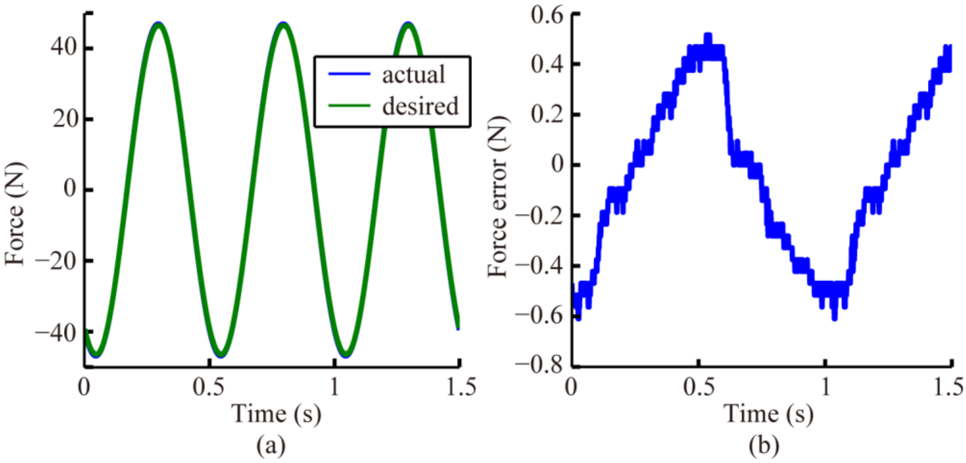

(a)

(b)

Figure 3-15. Low force tracking performance at 2 Hz. (a) force tracking performance, including the actual output force and desired output force. (b) force tracking error.

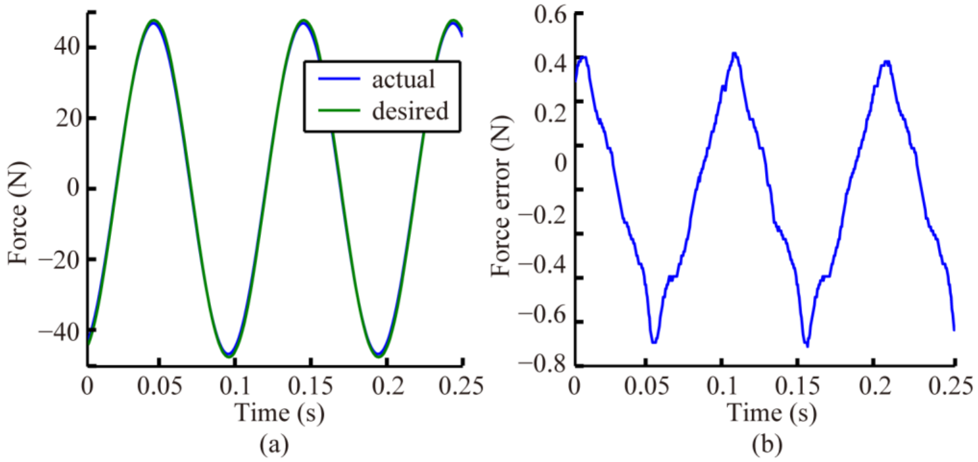

Figure 3-16. Low force tracking performance at 10 Hz. (a) force tracking performance, including the actual output force and desired output force. (b) force tracking error.

For high frequency, the output force tracking performance is illustrated by Figure 3-16, showing the tracking control of a 10 Hz sinusoidal signal. It can be seen that the output tracked input without obvious phase lag and the error was around 3%. This indicates that the closed loop system could achieve at least a 10 Hz bandwidth, which is adequate for rehabilitation robotics.

(C) Experimental results in high-force range

The high force control is based on the measurement of the deflection of the torsional spring. In order to test the force tracking performance at high force range, we first increased the force level above 300 N and superimposed a sinusoidal component to it.

Figure 3-17 shows the force tracking of a 1 Hz signal. Figure 3-18 shows the force tracking of a 30 Hz signal. We can see that the output tracked the input well. However, due to coarse force resolution, the output signal had an error of about 15 N (about three resolution points), which was about 5% of the amplitude. This performance was acceptable considering the high force and high frequency. We believe the performance can be easily improved by employing encoders with higher resolution.

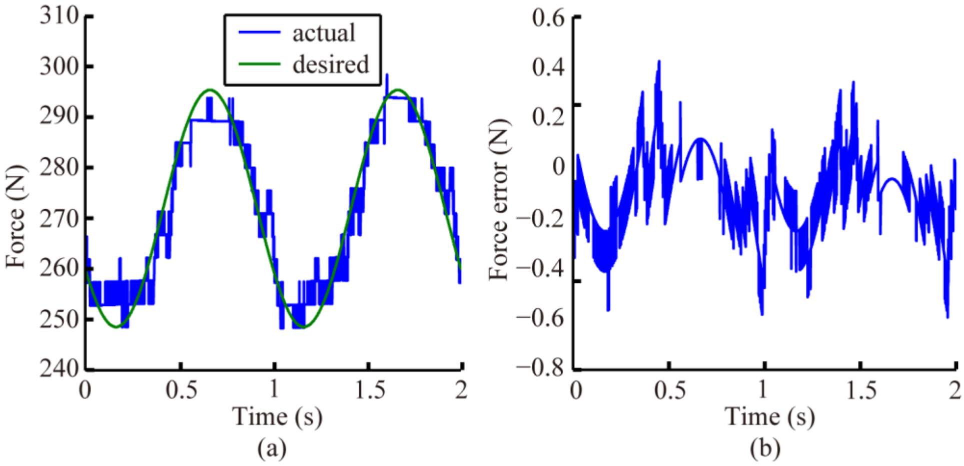

Figure 3-17. High force tracking performance at 1 Hz. (a) force tracking performance, including the actual output force and desired output force. (b) force tracking error.

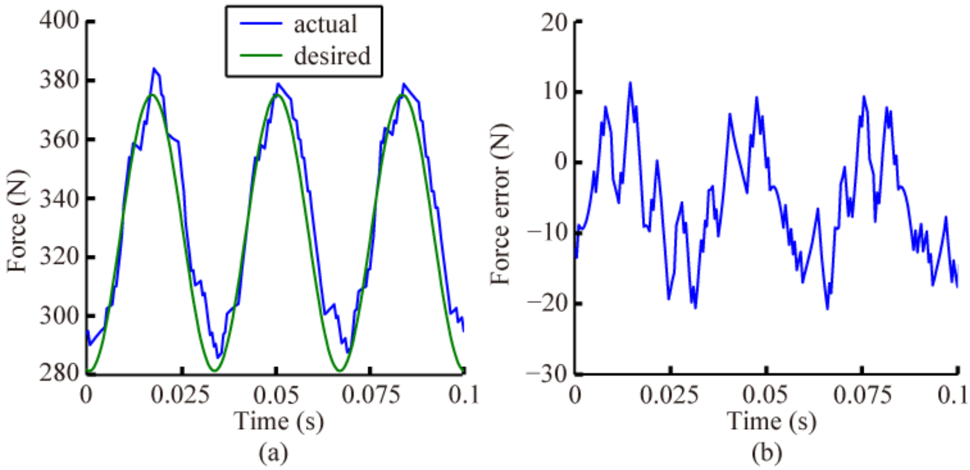

Figure 3-18. High force tracking performance at 30 Hz. (a) force tracking performance, including the actual output force and desired output force. (b) force tracking error.

(D) Experimental results in switching control

For switching control, we employed a sinusoid signal across low-force and high-force range as the desired force trajectory. Figure 3-19 shows a result with direct switching control as described in Figure 3-11. It can be seen that the actuator achieved good force tracking performance in low-force range; however, there was large impact at the switching point. The output force was not smooth and a force error around 200 N was observed. Besides, in this test, we had to decrease the control gain to reduce this impact, however, which deteriorated the performance in both low-force and high-force range.

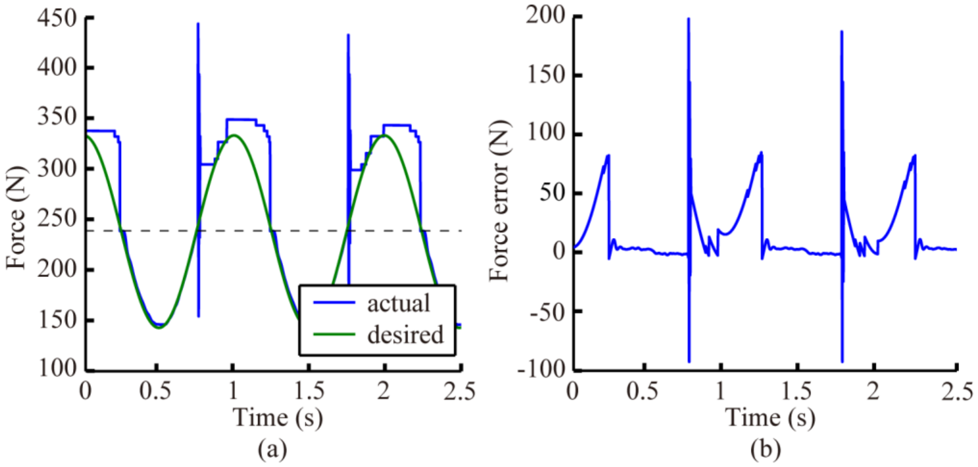

(a) (b)

Figure 3-19. Force control performance with direct switching at 1 Hz. (a) force tracking performance, including the actual output force and desired output force. (b) force tracking error.

Figure 3-20 shows a force tracking result with the modified switching controller as shown in Figure 3-12. The desired trajectory was 1 Hz sinusoid signal and the band c=10 N. It can be seen that the controller sensed and switched at the crossover point without causing any problems. It can also be noted that a low force range the signal was very smooth, but at high force range, the measured signal zigzags. This is because the force resolution at high force range is 5.6 N with the current actuator design. The peak force error was around 15 N, which was less than three resolution points in high-force range. The output force is smooth and the transition is stable.

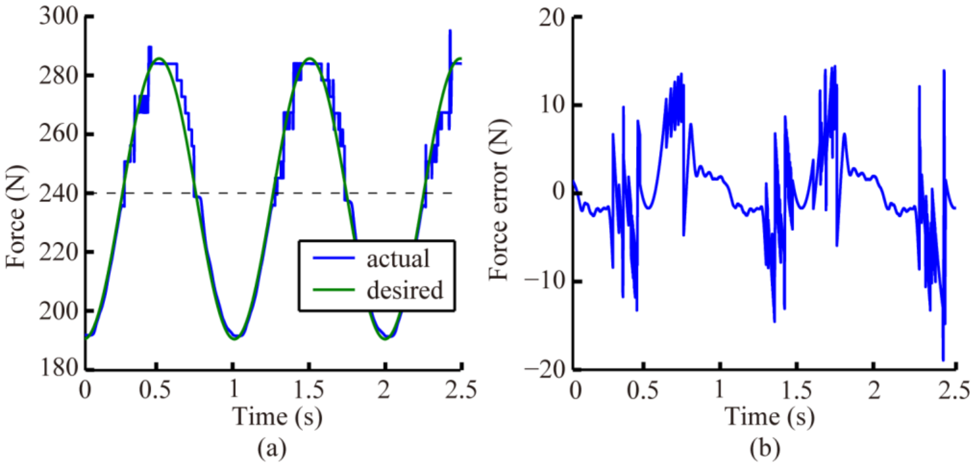

(a)

(b)

Figure 3-20. Force control performance with switching control at 1 Hz. (a) force tracking performance, including the actual output force and desired output force. (b) force tracking error.

4. Experimental evaluation of the robot

A preliminary walking experiment was conducted to evaluate the effectiveness of this rehabilitation robot in terms of force tracking performance and physiological activation of lower-limb muscles. Four healthy subjects participated in the experiment. Their average height was 172.5±7.6 cm (mean ± standard deviation), and weight was 66.3±8.1 kg. Each subject gave informed consent in accordance with the National University of Singapore Institutional Review Board (IRB).

4.1 Experimental protocol

The experiment consisted of walking along a corridor at 0.5 Hz gait with different levels of robotic assistance. Subjects were required to conduct 20 meters uninterrupted gaits in straight line under different conditions. Several trials serve as practice for the subjects to get familiar with the exoskeleton and experiment protocol. In the training sessions, subjects are required to perform the gait as naturally as possible. The experimenter will start collecting data after confirm with the subjects that they can walk naturally with the robotic assistance. Figure 3-21(a)-(d) shows a subject walking with the robot on the right leg. The accessories of the robotic system, including the controller and power supply, are placed on a trolley, which is pushed by an experimenter to follow the subject.

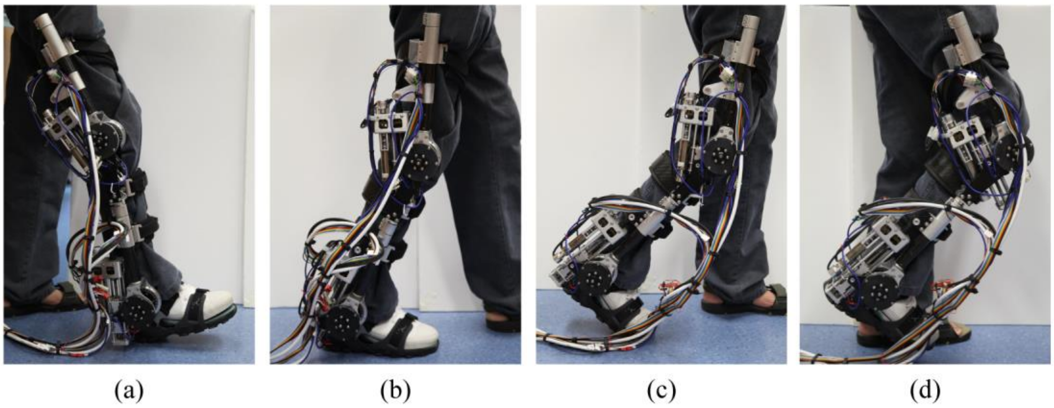

Figure 3-21. (a)–(d) one gait cycle in the overground walking experiment with the subject wearing the robot.

The experimental conditions are listed as:

Without robot: subjects walk without wearing the robot in order to measure the baseline kinematics and muscle activations.

Zero assistive torque: subjects are equipped with the robot on the right leg. Subjects walk in zero-torque mode, in which the desired force is set to be zero. It is intended to be transparent to its user and minimize the interaction between the robot and the wearer.

Force assistance: A certain percentage of the force trajectories (as described in Figure 3-7(b)) is provided by the robot, i.e. *low assistive torque* (knee 10% and ankle 5%) and *high assistive torque* (knee 25% and ankle 10%). The force trajectories are adopted from the CGA data in Section 2.1, but normalized based on the weight of each subject.

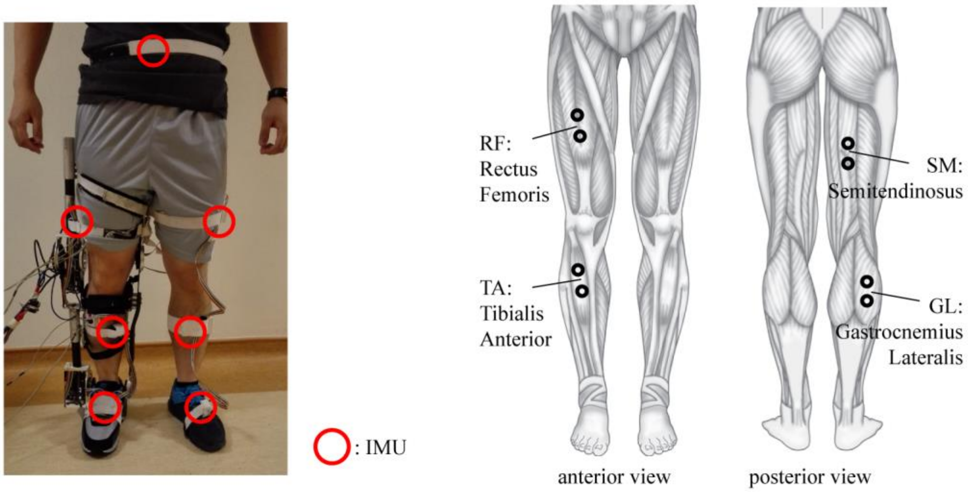

(a) (b)

Figure 3-22. (a) experimental setup of the overground walking test, including the exoskeleton robot, IMU sensors (red circle) and EMG electrodes; (b) the location of the EMG electrodes on the right leg major muscles.

In the tests, EMG activities and joint angles are measured from the assisted right leg. Surface EMG from four major muscles of the leg (Rectus Femoris, RF; Semitendinosus, SM; Tibialis Anterior, TA; Gastrocnemius Lateralis, GL; Figure

3-22) are collected from four bipolar electrodes using ASA-Lab (Advanced Neuro Technology, The Netherlands) [121]. Among these muscles, RF and SM are related to the knee extension and flexion, respectively. TA and GL are related to the ankle dorsiflexion and plantar flexion. The sampling rate is set at 2k Hz. The subject’s joint angular positions are recorded for the right knee (flexion/extension) and ankle (plantarflexion/dorsiflexion) by the potentiometer assembled in the robotic joint.

4.2 Data analysis

Raw EMG data derived from the experiment are processed by a band-passed filter (2nd order Butterworth filter, cutoff frequency of 10-550 Hz) and a band-stopped filter (2nd order Butterworth filter, cutoff frequency of 49-51 Hz). The linear envelope of the processed EMG signals is obtained by applying root mean square (RMS) and filtered by a 4th order Butterworth low pass filter of 5 Hz to achieve a better representation of the EMG signals. To remove the variability among individuals, the EMG signal is normalized with the maximal voluntary isometric contraction (MVIC) method [122]. Thus, the EMG profiles can be represented as a percentage of the MVIC value. The EMG profiles can be compared across the subjects and statistical analysis can be conducted.

All gait data and processed EMG signals obtained from each muscle are segmented and normalized to the percentage of a gait cycle. A total sample of 10 strides is taken for each condition and was interpolated in the same length to compute an average EMG signal.

4.3 Kinematic and force tracking results

Figure 3-23 shows experimental results in the gait assistive tests to illustrate the performance of the robot. Force tracking performance of the robot in knee (red curves) and ankle joints (blue curves) and the joint angles are recorded. Here we only present the results with larger assistance to evaluate our robotic actuation design concept, and the results of two complete cycles are given in this figure. It is noticeable that part of the force trajectory on the knee entered into the high-force range of the actuator (Figure 3-23 middle row, green dashed line). The high-force range performance and the switch between two force ranges are involved in this test. It is

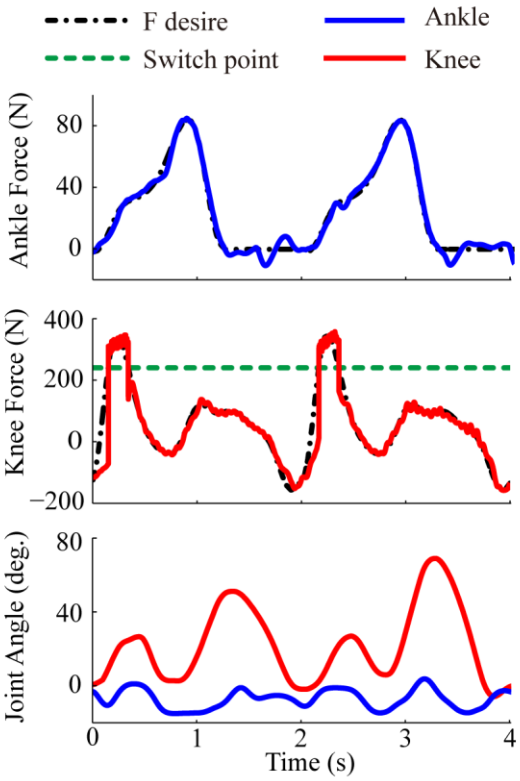

Figure 3-23. An example of force and angle profiles in both knee and ankle joints within two complete gait cycles. The desired force trajectory (black profile) is 10% of the nominal torque on ankle joint, and 25% of that on knee joint. Blue and red profiles represent the results of ankle and knee joints respectively. Green dashed line represents the switch point between low- and high-force ranges.

noted that in high assistive torque trials, a large support was provided only to the knee joint, while the support on ankle joint remained the same as in the low assistive torque scenario so that we could study one joint at a time

As shown in Figure 3-23, the subject walked with a ROM of 5°~60° on the knee joint and -15°~15° on the ankle joint. The error of force control on the ankle joint is less than 4N, which is about 4% of the peak force, and on the knee joint is less than 16.3N, about 5% of the peak force. The maximum force error in low-force range is 15.1N, which is about 4% of the peak force. It also illustrates that the force transition between low- and high-force ranges is stable and fast.

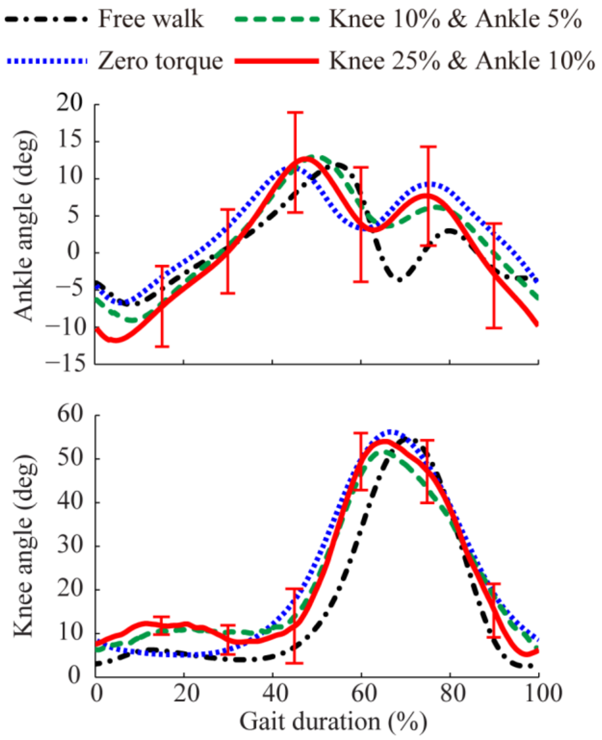

Figure 3-24. Averaged results of the knee and ankle joint angles of four subjects in different conditions: free walk (black curves), zero torque (blue curves), low assistive torque (green curves) and high assistive torque (red curves). The errorbar represents the standard deviation of the angles in the high assistive condition.

Figure 3-24 shows the averaged results of the knee and ankle angles of the four subjects in different experimental conditions. Standard deviation in the high assistive torque condition is also presented with errorbar. In Figure 3-24, it can be seen that the pattern of both the knee and ankle joint angles are similar in different conditions, which indicates that the subjects were able to maintain a natural gait when robotic assistance was provided.

4.4 Muscle activation analysis

Figure 3-25 illustrates experimental results of EMG profiles of four lower-limb muscles in different experimental conditions. The EMG profiles were normalized to the MVIC and averaged in four healthy subjects. The EMG profiles show overall decreasing of muscle activation of the four muscles with the increasing assistive support during the gait cycle. The decreasing is even significant with the high force support. Both assistance modes demonstrate a lower RMS value and peak value for the four muscles. In TA and RF, EMG activations in zero torque and low assistive torque support are larger than that of free modes. This is probably caused by the weight of the robot. Looking at the SM EMG profile, for both force assistance modes, there is approximately a gradual decrease in the peak value.

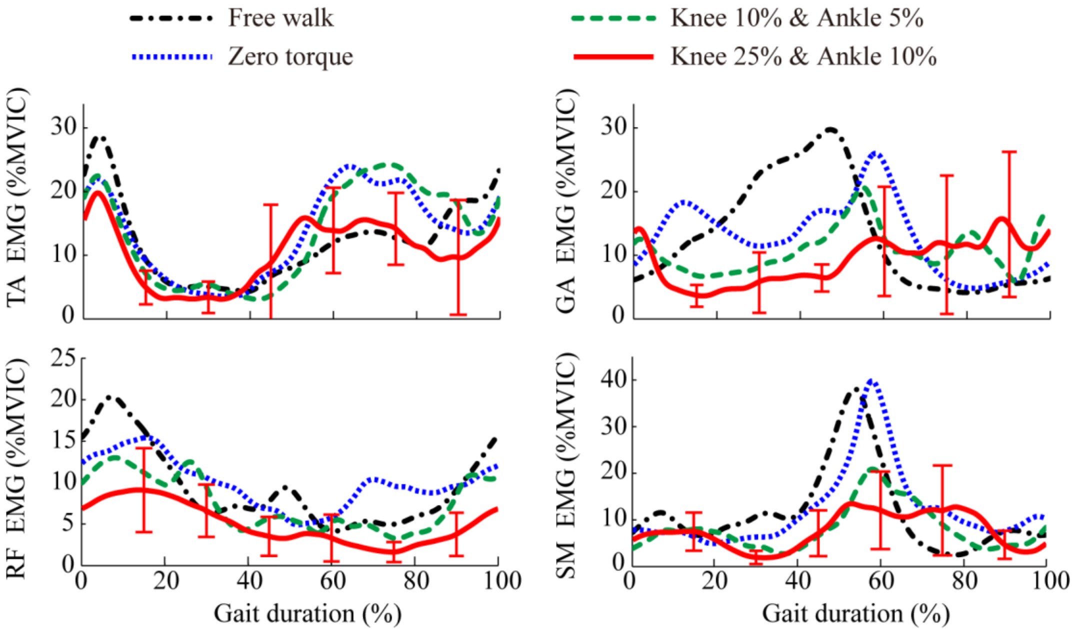

Figure 3-25. Averaged surface EMG profiles of four subjects for each of the four muscles in walking under four different conditions: free walk (black curves), zero torque (blue curves), low assistive torque (green curves) and high assistive torque (red curves). The errorbar represents the standard deviation of the EMG profiles in the high assistive condition.

In conclusion, a significant overall reduction in muscle activity was found in the experiment, which demonstrates that the robot is able to provide stable assistive forces to the two joints during the walking action.

5. Discussion

In Section 3.2, force controllers for the low-force range, high-force range and switching are designed for the actuator. Actually, the switching controller is a general controller that includes all three conditions. When the force reading is outside the band, i.e. $\omega = 1$ or $\omega = 0$, only force controller in the low-force range or high-force range works; and when the force reading is within the band, or $0 < \omega < 1$, the controller can handle switching controller. Hence, this general controller can be implemented for the application.

In Section 4, an overground walking experiment is conducted on two healthy subjects. Experimental results indicate that the robot is effective in delivering assistance, which can reduce the muscle activation of the subjects. However, two major limitations can be found in this test, as:

First, the force tracking performance of the actuator is inferior to that in the actuator tests in Section 3. It is because the output pin of the actuator is fixed in the actuator tests. However, in the walking experiment, the output pin is connected to the exoskeleton, which moves with the human joints. It can be seen that with the human-robot interaction, the force tracking performance deteriorates. Accurate force tracking has to be achieved to accomplish effective assistive walking. Motivated by this, we develop a human-robot interaction controller to provide accurate assistive force during walking, which will be presented in Chapter 4.

Second, in this walking experiment, the robot provides assistance with a fixed force trajectory without considering the status of human gait. The subjects have to catch up the robot and try to synchronize with the robotic assistance. However, it is found that this control strategy is less efficient without human-robot synchronization. The robot may not be able to assist during walking, or even bring resistance. Motivated by this, we develop a human-robot synchronization method to provide synchronous assistance during overground walking, which will be presented in Chapter 5.

6. Summary

In this chapter, we present the mechanical design and experimental evaluation of a compact, portable knee-ankle-foot robot aimed for stroke patients to carry out overground gait training at outpatient and home settings. A novel compliant SEA utilizes two springs in series with different stiffness to achieve back-drivability, large force range and low output impedance for safe human robot interaction. The mechanism for the joint motion was designed and optimized based on gait biomechanics. The actuator modeling and controller design are performed; and an excellent force tracking performance is achieved. Overground walking trials on healthy subjects demonstrated accurate force tracking performance of the robot. Muscle activation represented by EMG signal was reduced gradually with increased levels of assistance, demonstrating that the robot can provide stable and effective assistive forces during gait cycles.

Chapter 4

Human-Robot Interaction Control with Series Elastic Actuators

In the last chapter, an assisted walk test was conducted. However, the force tracking performance is inferior due to the human joint motion. Physical interaction affects the controlled variables and may even cause system instability. Thus, human-robot interaction control design is critical in rehabilitation robotics research. This chapter presents an interaction control strategy for our gait rehabilitation robot driven by SEA. The control design is based on the actuator model with consideration of interaction dynamics. It consists mainly of human joint motion compensation and friction compensation, and is enhanced with a disturbance observer. Such a control scheme enables the robot to achieve low output impedance when operating in human-in-charge mode and achieve accurate force tracking when operating in assistive force control mode. A theoretical proof is provided to show the guaranteed stability of the close-loop system under the proposed controller. The proposed design is verified with an ankle robot in walking experiments.

1. Introduction

Rehabilitation robots must handle intentional physical interaction as well as unexpected interaction forces. Human-robot interaction control is important for two basic operation modes: human-in-charge mode and assistive force control mode, as discussed in Chapter 2. In the human-in-charge mode or zero force control, the robot should be able to follow the human movement with minimal interaction force; this is also characterized as low output impedance or transparency. In the assistive force control mode, the robot should be able to provide accurate force/torque to human limbs as needed; this is also defined as the force tracking performance. In both control modes, it is very important to guarantee the safety of the human-robot interaction; this is also called the stability of the human-robot interaction.

Many control approaches have been proposed for SEAs [84, 86, 87, 90, 93-95, 123-125]. The basic requirement in these controller designs is that the actuator can generate the force as desired. For example, in [87, 93, 95, 123], pure PID control is used to produce a desired output force; in [86], PD plus feedforward control is used to improve the dynamical performance for a class of SEAs. Human-robot interaction control may be achieved by impedance control, which may be referred to as dynamic stiffness control. Low output impedance reduces interaction forces due to disturbance forces and unmodeled dynamics, providing both safety and comfort for the human interacting with the robot. In [90, 124-127], a type of cascaded control is presented to ensure low impedance in human-robot interaction where a PI torque control is used in the outer loop, while a PI velocity control is used in the inner loop. It should be noted in [94] that the impedance control is also implemented by using cascaded control where the outer loop is an impedance control. In [84], a modified PID with feedforward term and human joint compensator is designed to generate desired force and low impedance.

Another requirement for human-robot interaction as stated above is that the control of a robot interacting with human must be stable in the presence of unmodeled human dynamics. Control theory has offered several tools to design stable controllers with the ability to deal with unknown or poorly characterized interference [127]. For example, using a disturbance rejection approach, some uncertain dynamics in the human-robot interaction could be included as disturbance forces; in this case, the disturbance observer can be used to handle the uncertainty. The authors in [35] assumed that the disturbance is constant and designed a disturbance observer to reject the modeling error. In [36], the authors used a feedback plus feedforward force control which was enhanced by a disturbance observer to compensate for plant variations, where feedback and feedforward controls were optimally designed. By using adaptive control theory, the authors in [128] proposed an impedance control scheme to adapt the robotic assistance according to the disability level. However, the stability analysis was not discussed in these papers. In [37], the authors developed a null-space impedance control with a disturbance observer, and stability was discussed in the paper. Unfortunately, the result was based on an n-link robot manipulator and a compliant actuator was not involved in their paper.

In this chapter, we present a human-robot interaction control approach for a rehabilitation robot driven by a SEA. The goal of this controller is to achieve accurate and stable human robot interaction. First, the robot dynamic model with human motion information is established with consideration of nonlinear friction. Second, a controller based on the friction and human motion compensations, which are enhanced by a disturbance observer, is designed, where the acceleration of the assistive robot is required for feedback in the controller. Third, since the acceleration is difficult to obtain in a practical system, the proposed controller is further modified by introducing an auxiliary variable to remove this requirement. A theoretical proof shows that stability of the closed-loop system is guaranteed. Finally, experimental results are provided to verify the effectiveness of the proposed method.

The main contribution of this work is that the proposed control method has the following improvements over those methods presented in [35-37]: 1) the nonlinear friction in the actuation system is compensated for. This can help improve transparency of the assistive robot which interacts with the human; 2) the assumption in [35] that the modeling error and disturbance are constant is removed. This assumption imposes a strict restriction, limiting the scope of applications; 3) the modified disturbance observer does not use acceleration information. As stated in Section 3, requiring the acceleration has some disadvantages; 4) the rigorous mathematical proof is given to show the stability of the closed-loop system, while this issue is not addressed in [35-37].

This chapter is organized as follows: in Section 2, the modeling of the actuator is given. In Section 3, we describe the design of the human-robot interaction controller and stability analysis. Section 4 gives experimental results. A summary is given in Section 5.

2. SEA modeling

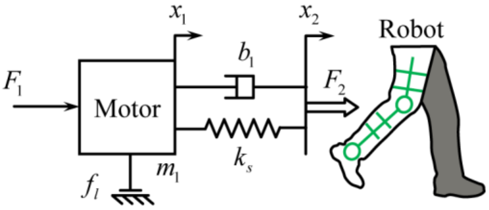

Figure 4-1. Outline of the dynamics of the actuator.

The physical model of the SEA interacting with the human body is as shown in Figure 4-1. To be noted, this research is based on the conventional model of the SEA, which consists of only one spring. This also applicable to our novel SEA design with its simplified model as illustrated in Chapter 3. The output carriage of the actuator is driven by human body motion. Since the actuator outputs linear motion, all the components are transformed into translational elements. The mathematical equation is given by

$$m_1\ddot{x}_1 = F_1 - k_s(x_1 - x_2) - b_1(\dot{x}_1 - \dot{x}_2) - f_l \tag{4-1}$$

where m_1 is equivalent mass of the motor, x_1 is the motor displacement, F_1 is the force input from the motor, x_2 is the human joint displacement, k_s is the spring constant, b_1 is the damping in the mechanism. The parameters of the actuator are listed in Table 4-1. f_l is the friction caused by the motor and ball screw. In general, the friction force f_l is nonlinear and is modeled in the form [129]

$$f_l = \mu_1 \mathrm{sgn}(\dot{x}_1) + f_{s1} e^{-(\dot{x}_1/\dot{x}_s)^2} \mathrm{sgn}(\dot{x}_1) + b\dot{x}_1 \tag{4-2}$$

where μ_1 is the coefficient of the Coulomb friction, f_{s1} is the coefficient of the Stribeck friction, and b is the coefficient of the viscous damping. $\dot{x}_s$ is characteristic velocity of the Stribeck friction [129].

The output force in the spring F_2 , as well as the force feedback, is a function of two variables: the motor displacement x_1 and the joint position x_2. By applying the Hooke's law, i.e., $F_2 = k_s(x_1 - x_2)$, we can describe the actuator as a function of F_2

$$\ddot{F}_2 = \frac{k_s}{m_1}F_1 - \frac{k_s}{m_1}F_2 - \frac{b_1+b}{m_1}\dot{F}_2 - k_s\ddot{x}_2 - \frac{bk_s}{m_1}\dot{x}_2 - \frac{k_s}{m_1}\left(\mu_1 \mathrm{sgn}(\dot{x}_1) + f_{s1} e^{-(\dot{x}_1/\dot{x}_s)^2} \mathrm{sgn}(\dot{x}_1)\right) \tag{4-3}$$

Table 4-1. Parameters of the actuator

Symbol	Quantity	value of the hardware parameters
m_1	equivalent mass of motor	127.4 kg
k_s	spring constant	24×10^3 N/m
p	pitch of the ball screw in the actuator	2 mm
M	total weight of the actuator	0.84 kg

Since the actuator produces linear output force and motion, the rotatory components of the actuator are converted into translational elements, and the parameters in the table are effective parameters in translational direction.

Remark. As indicated in [36, 86], the friction reduction will help enhance the performance of the system by reducing the output impedance. The friction compensation depends on the dynamical model. Existing actuation models use simple friction forms such as viscous friction [36, 86, 87]. Here, we adopt a nonlinear form [129] which includes Coulomb plus viscous friction together with Stribeck friction.

Thus, the present actuation model can reflect the actual actuation behavior more precisely. In addition, the variable $\dot{x}_1$ is the rate of change of the position found by differentiating the position signal, which is obtained from the encoder and filtered with a first-order low pass filter with the cut-off frequency of 50Hz.

3. *Human-robot interaction controller*

In this section, a human-robot interaction controller is proposed based on the modeling of the actuator. The control objectives include: 1) force tracking control, i.e., following the desired force trajectory as closely as possible; 2) ensuring stability and safety when the human motion is involved.

In the force equation (4-3), it should be noted that the human motion is reflected in the term $k_s\ddot{x}_2 + bk_s\dot{x}_2 / m_1$, while the friction force is involved in the term $k_s(\mu_1 \mathrm{sgn}(\dot{x}_1) + f_{s1}e^{-(\dot{x}_1/\dot{x}_s)^2}\mathrm{sgn}(\dot{x}_1)) / m_1$. To design a controller of human-robot interaction, we have to handle these terms. The proposed controller should have the following terms:

$$F_1 = u_h + u_f + u_d + u_{fb} \tag{4-4}$$

where u_h is to compensate for the effect of the human motion, u_f is to compensate for the effect of the friction force, u_d is to remove the disturbance and u_{fb} is to design the feedback control. Substituting the controller (4-4) into (4-3) yields

$$\begin{aligned}\ddot{F}_2 &= \frac{k_s}{m_1}(u_h + u_f + u_d + u_{fb}) - \frac{k_s}{m_1}F_2 - \frac{b_1 + f_m}{m_1}b\dot{F}_2 - k_s\ddot{x}_2 \\ &- \frac{bk_s}{m_1}\dot{x}_2 - \frac{k_s}{m_1}\left(\mu_1 \mathrm{sgn}(\dot{x}_1) + f_{s1}e^{-(\dot{x}_1/\dot{x}_s)^2}\mathrm{sgn}(\dot{x}_1)\right)\end{aligned} \tag{4-5}$$

3.1 Compensation of the human joint motion

Ideally, in order to minimize the resistance force when the human motion is initiated, the control u_h should be designed such that the closed-loop system of the actuator interacting with the human has a zero force, i.e.,

$$\frac{k_s}{m_1}u_h - k_s\ddot{x}_2 - \frac{bk_s}{m_1}\dot{x}_2 = 0 \tag{4-6}$$

From the above analysis, the control u_h should be designed as follows

$$u_h = \frac{m_1}{k_s}\left(k_s\ddot{x}_2 + \frac{bk_s}{m_1}\dot{x}_2\right) \tag{4-7}$$

Unfortunately, the term $\ddot{x}_2$ is obtained from the differentiation of the human joint displacement x_2, which may be very noisy. Following the design of [35], a filter is added into the control. The filter is described in frequency domain as follows:

$$U_h(s) = \frac{1}{(T_N s + 1)^2}\frac{m_1}{k_s}\left(k_s s^2 X_2(s) + \frac{bk_s}{m_1}sX_2(s)\right) \tag{4-8}$$

where s is a complex variable, $U_h(s)$ and $X_2(s)$ are the Laplace transformations of u_h and x_2, respectively, and T_N is a sufficiently small time constant (readers may refer to [35] for the selection of T_N).

3.2 Compensation of the friction force

The friction force increases the impedance of the actuator. Ideally, the designed control u_f should reduce the friction force to achieve low output impedance, i.e.

$$\frac{k_s}{m_1}u_f - \frac{k_s}{m_1}\left(\mu_1 \mathrm{sgn}(\dot{x}_1) + f_{s1}e^{-(\dot{x}_1/\dot{x}_s)^2}\mathrm{sgn}(\dot{x}_1)\right) = 0 \tag{4-9}$$

The compensation term is chosen as

$$u_f = \frac{k_s}{m_1}\left(\mu_1 \mathrm{sgn}(\dot{x}_1) + f_{s1}e^{-(\dot{x}_1/\dot{x}_s)^2}\mathrm{sgn}(\dot{x}_1)\right) \tag{4-10}$$

Considering that $\dot{x}_1$ may contain some noise, the gain should be selected to be small in application.

3.3 Disturbance observer implementation

Since the compensation of the human motion and friction is not perfect, the system has an error, which is regarded as a disturbance after the compensation, i.e.,

$$\ddot{F}_2 = \frac{k_s}{m_1}(u_d + u_{fb}) - \frac{k_s}{m_1}F_2 - \frac{b_1 + b}{m_1}\dot{F}_2 + d \tag{4-11}$$

where d is the system disturbance. To reduce the sensitivity of the control performance to disturbance, a disturbance observer is designed. Figure 4-2 shows the block diagram of the control system, which employs an estimate of the actual disturbance, deduced from a disturbance observer, to handle the disturbance, where $\hat{d}$ represents the estimated disturbance, P is the actual system model, P_n is the nominal model without the disturbance. From equation (4-11), it follows:

$$P_n = \frac{\frac{k_s}{m_1}}{s^2 + \frac{b_1 + b}{m_1} s + \frac{k_s}{m_1}} \tag{4-12}$$

where we use the frequency domain to represent system. The disturbance observer incorporates the inverse of the system model, and thus a low pass filter is necessary to make the observer practically realizable. A filter can take the following form

$$filter = \frac{\alpha_2}{s^2 + \alpha_1 s + \alpha_2} \tag{4-13}$$

where the parameters α_1 and α_2 have to be tuned so that the disturbance suppression characteristics are satisfied. Thus, the disturbance observer is given by

$$u_d = -\frac{\alpha_2}{s^2 + \alpha_1 s + \alpha_2} \hat{d} \tag{4-14}$$

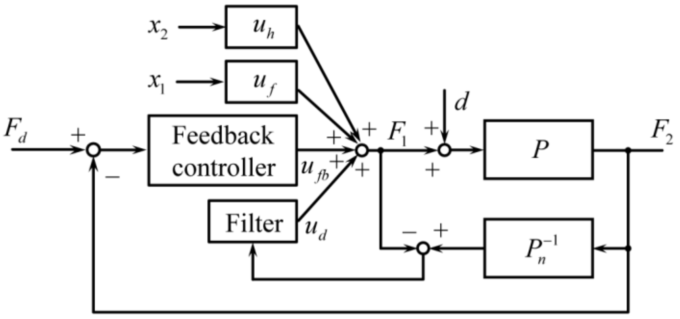

Figure 4-2. Diagram of control system with disturbance observer.

3.4 Force feedback control

For the force feedback control, we have to ensure that the controller can generate accurate output force following the desired force profile.

Define the force error $e = F_d - F_2$. The equation (4-11) is rewritten as

$$\ddot{e} = \ddot{F}_d + \frac{k_s}{m_1}F_d + \frac{b_1+b}{m_1}\dot{F}_d - \frac{k_s}{m_1}u_{fb} - \frac{k_s}{m_1}e - \frac{b_1+b}{m_1}\dot{e} - \frac{k_s}{m_1}u_d - d \tag{4-15}$$

Let $\mathbf{e} := [e, \dot{e}]^T$. The above equation can be written as a compact form

$$\dot{\mathbf{e}} = A\mathbf{e} + B(u_{fb} - F_d - \frac{b_1+b}{k_s}\dot{F}_d - \frac{m_1}{k_s}\ddot{F}_d + \bar{d}) \tag{4-16}$$

$$A = \begin{bmatrix} 0 & 1 \\ -\frac{k_s}{m_1} & -\frac{b_1+b}{m_1} \end{bmatrix}, B = \begin{bmatrix} 0 \\ -\frac{k_s}{m_1} \end{bmatrix} \tag{4-17}$$

where $\bar{d} = u_d + \frac{m_1}{k_s}d$. The following feedback control is given by

$$u_{fb} = F_d + \frac{b_1+b}{k_s}\dot{F}_d + \frac{m_1}{k_s}\ddot{F}_d + K\mathbf{e} \tag{4-18}$$

where K is the feedback gain.

3.5 Modified nonlinear observer interaction control

A disadvantage of the disturbance observer proposed above is that the acceleration must be measured or obtained by differentiating the position measurements. In a practical situation, an accurate accelerometer is not available in many robotic applications. Using a second derivative of the position measurements may bring a large noise into the system. To solve this problem, we define the auxiliary variable [130]

$$z = \hat{d} - w \tag{4-19}$$

where the variable w is determined by

$$\frac{d}{dt}w = L\ddot{F}_1 \tag{4-20}$$

where L is the observer gain. Based on the auxiliary variable, we propose the following nonlinear controller

$$F_1 = u_h + u_f + F_d + \frac{b_1 + b}{k_s}\dot{F}_d + \frac{m_1}{k_s}\ddot{F}_d + K\mathbf{e} - \frac{m_1}{k_s}\hat{d} \tag{4-21}$$

where the terms u_h and u_f are the same as in Sections 3.1 and 3.2.

By introducing the force error e and variable vector $\mathbf{e}$ as in Section 3.4, equation (4-3) can be written as

$$\begin{aligned}\dot{\mathbf{e}} = A\mathbf{e} + B(F_1 + F_d + \frac{b_1 + b}{k_s}\dot{F}_d + \frac{m_1}{k_s}\ddot{F}_d) + d + k_s\ddot{x}_2 \\ + \frac{bk_s}{m_1}\dot{x}_2 + \frac{k_s}{m_1}\left(\mu_1 \mathrm{sgn}(\dot{x}_1) + f_{s1}e^{-(\dot{x}_1/\dot{x}_s)^2}\mathrm{sgn}(\dot{x}_1)\right)\end{aligned} \tag{4-22}$$

where A and B are the same as in (4-17). Substituting the controller (4-21) into the above system yields

$$\dot{\mathbf{e}} = A\mathbf{e} + B(K\mathbf{e} - \frac{m_1}{k_s}\hat{d} + \frac{m_1}{k_s}d) \tag{4-23}$$

where the feedback control gain K is chosen as

$$K = -\gamma^{-1}B^T P \tag{4-24}$$

where γ is a constant and the matrix P is given by the following equation

$$A^T P + PA - \gamma^{-1}PBB^T P + Q = 0 \tag{4-25}$$

where Q should be positive definite matrix which is selected by users. The criterion of the selection is that the larger Q is selected, the smaller the tracking error can be achieved.

The auxiliary variable z is obtained from the following equation

$$\dot{z} = -Lz + L\left(-\frac{k_s}{m_1}u_0 + \frac{k_s}{m_1}F_2 + \frac{b_1+b}{m_1}\dot{F}_2 - w\right) + \frac{m_1}{k_s}\mathbf{e}^T PB \tag{4-26}$$

where $u_0 = F_d + \frac{b_1+b}{k_s}\dot{F}_d + \frac{m_1}{k_s}\ddot{F}_d + K\mathbf{e} - \frac{m_1}{k_s}\hat{d}$.

3.6 Stability analysis

Consider the Lyapunov function

$$V = \mathbf{e}^T P\mathbf{e} + \tilde{d}^2 \tag{4-27}$$

where $\tilde{d} = d - \hat{d}$. Its time derivative is given by

$$\begin{aligned} \dot{V} &= \mathbf{e}^T(A^T P + PA - 2\gamma^{-1}PBB^T P)\mathbf{e} + 2\frac{m_1}{k_s}\mathbf{e}^T PB\tilde{d} + 2\tilde{d}(\dot{d} - \dot{\hat{d}}) \\ &= -\mathbf{e}^T(Q + \gamma^{-1}PBB^T P)\mathbf{e} - 2\frac{m_1}{k_s}\mathbf{e}^T PB\tilde{d} + 2\tilde{d}(\dot{d} - \dot{\hat{d}}) \end{aligned} \tag{4-28}$$

The derivative of the estimated disturbance $\hat{d}$ is given by

$$\begin{aligned} \dot{\hat{d}} &= \dot{z} + \dot{w} \\ &= -Lz + L\left(-\frac{k_s}{m_1}u_0 + \frac{k_s}{m_1}F_2 + \frac{b_1+b}{m_1}\dot{F}_2 - w\right) + \frac{m_1}{k_s}\mathbf{e}^T PB + L\ddot{F}_1 \\ &= -Lz - Lw + Ld + \frac{m_1}{k_s}\mathbf{e}^T PB \\ &= -L\hat{d} + Ld + \frac{m_1}{k_s}\mathbf{e}^T PB = L\tilde{d} + \frac{m_1}{k_s}\mathbf{e}^T PB \end{aligned} \tag{4-29}$$

Substituting the above equation into equation (4-28) produces

$$\begin{aligned} \dot{V} &= -\mathbf{e}^T(Q + \gamma^{-1}PBB^T P)\mathbf{e} + 2\frac{m_1}{k_s}\mathbf{e}^T PB\tilde{d} + 2\tilde{d}\left(\dot{d} - L\tilde{d} - \frac{m_1}{k_s}\mathbf{e}^T PB\right) \\ &= -\mathbf{e}^T(Q + \gamma^{-1}PBB^T P)\mathbf{e} + 2\tilde{d}(\dot{d} - L\tilde{d}) \end{aligned} \tag{4-30}$$

The disturbance is assumed to be slowly varying, i.e., $\left|\dot{d}\right| \le \epsilon$ with ϵ being a constant. Thus, it follows that

$$\begin{aligned} \dot{V} &\le -\mathbf{e}^T(Q+\gamma^{-1}PBB^TP)\mathbf{e} + 2|\tilde{d}|\epsilon - 2L\tilde{d}^2 \\ &\le -\mathbf{e}^T(Q+\gamma^{-1}PBB^TP)\mathbf{e} + L\tilde{d}^2 + L^{-1}\epsilon^2 - 2L\tilde{d}^2 \\ &= -\mathbf{e}^T(Q+\gamma^{-1}PBB^TP)\mathbf{e} - L\tilde{d}^2 + L^{-1}\epsilon^2 \\ &\le -\lambda_{min}(Q+\gamma^{-1}PBB^TP)\|\mathbf{e}\|^2 - L\tilde{d}^2 + L^{-1}\epsilon^2 \end{aligned} \tag{4-31}$$

where we have used the fact that $2|\tilde{d}|\epsilon \le L\tilde{d}^2 + L^{-1}\epsilon^2$.

Equation (4-31) follows $\dot{V} \le -\lambda_{min}(Q+\gamma^{-1}PBB^TP)\|\mathbf{e}\|^2 + L^{-1}\epsilon^2$. Then, $\dot{V} < 0$ as long as

$$\|\mathbf{e}\| > \sqrt{\frac{L^{-1}\epsilon^2}{\lambda_{min}(Q+\gamma^{-1}PBB^TP)}} \tag{4-32}$$

We can also infer from equation (4-31) that $\dot{V} \le -L\tilde{d}^2 + L^{-1}\epsilon^2$, which gives

$$\left|\tilde{d}\right| > \frac{\epsilon}{L} \tag{4-33}$$

Therefore, this demonstrates that the state **e** and $\tilde{d}$ are ultimately uniformly bounded (UUB) [131], which means the state **e** and $\tilde{d}$ will converge to a pre-determined set whose size can be chosen to be small by selecting appropriate parameters Q and L.

Remark 3.1. If the disturbance d is constant, i.e., $\dot{d} = 0$, it is well known from the above analysis that $\dot{V} < 0$. This implies that $\|\mathbf{e}\| \to 0$. This also implies that the tracking error e can converge to zero and the controller can reject the constant disturbance.

Remark 3.2. The state **e** can be made small by selecting a large value of L or control gain K, while the disturbance estimation error $\tilde{d}$ can be made small by selecting a large value of L. By combining the control designs u_h and u_f , the proposed human-robot interaction control can implement the following functions:

$$\frac{k_s}{m_1}u_h - k_s\ddot{x}_3 - \frac{bk_s}{m_1}\dot{x}_3 \approx 0 \tag{4-34}$$

$$\frac{k_s}{m_1}u_f - \frac{k_s}{m_1}\left(\mu_1 \mathrm{sgn}(\dot{x}_1) + f_{s1}e^{-(\dot{x}_1/\dot{x}_s)^2}\mathrm{sgn}(\dot{x}_1)\right) \approx 0 \tag{4-35}$$

which implies that the output impedance of the actuator is very low. In addition, $\tilde{d} \approx 0$ implies that the proposed controller is capable of cancelling the disturbance, and $\mathbf{e} \approx 0$ implies that the proposed controller can generate the desired output force.

4. Experimental results

In this section, the proposed control is applied to the ankle module of the exoskeleton as shown in Figure 4-3. The result can be extended to the knee module without much difficulty. The controller is the NI CompactRIO 9074 programmable automation controller that is an advanced embedded control and data acquisition system. The sampling period chosen for our test is 0.5ms.

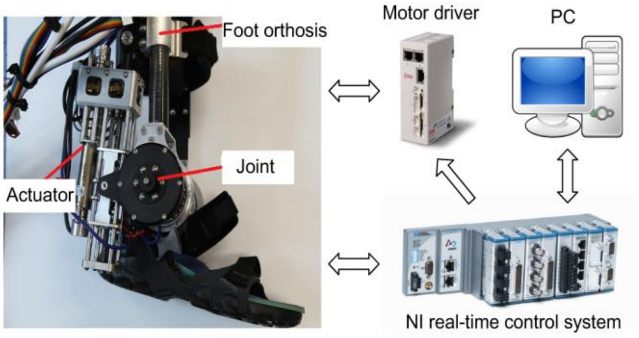

Figure 4-3. Experimental set-up.

4.1 System identification

For the control application, it is necessary to identify the model of the compliant actuator. From the analysis of Section 3, it is known that the model structure is a second-order linear model. Thus, a system identification tool is used to identify parameters of the models [132]. The input signal for the test is a square wave with a frequency of 1Hz (Figure 4-4(a)), which is around the working frequency. The Coulomb friction can be estimated by checking whether the force commences for a given a small amount of input signal; if it does not have, i.e., it is still zero, we have to increase the input signal until the force occurs. It is observed that the output force commences when the input signal is 850. Thus, the coefficient of the Coulomb friction is 850. The Stribeck speed $\dot{x}_s$ depends on lubrication and material properties, and is usually determined empirically. Usually, it ranges from 0.00001 to 0.1 m/s. In our motor, it is 0.1 m/s. The nonlinear model obtained is given by

$$\begin{aligned}\ddot{F}_2 &= -207.21F_2 - 10.80\dot{F}_2 + 195.69u - 850sgn(\dot{x}_1) \\ &\quad -680sgn(\dot{x}_1)e^{-(\frac{\dot{x}_1/20000}{0.1})^2} - 1.5\dot{x}_3 - \ddot{x}_3\end{aligned} \tag{4-36}$$

where the parameters of the frictional model are obtained by using a similar method as shown in [130].

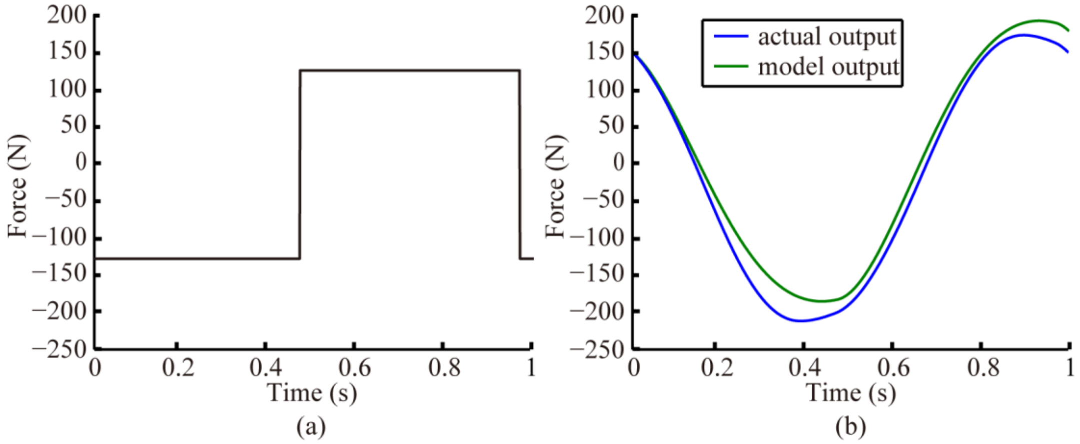

Figure 4-4. Model validation: (a) input signal; (b) blue curve represents actual signal; green curve represents model output.

The comparison of the simulated output and the actual measured output is shown in Figure 4-4(b). One complete cycle is included in the result. As observed, the model output is close to the measured actual output force, and the estimated model is acceptable.

For designing the controller (4-21), the feedback control is determined by computing the equation (4-25) where $Q=diag\{1500,15\}$ and $\gamma=1$. The solution of P is $\begin{bmatrix} 151.9311 & 0.1926 \\ 0.1926 & 0.0198 \end{bmatrix}$. The feedback control gain is $K=\begin{bmatrix} 37.6854 & 3.8751 \end{bmatrix}$. In the auxiliary variable z, the parameter L is taken as 3000.

4.2 Interaction torque and stability test

For the interaction torque and stability test scenario, the joint motion is excited by human. This is to move the joint close to a sine wave and measure the interaction forces at different frequencies while the desired force is set as zero. Concerning human gait, the testing frequency is less than 2 Hz.

Figure 4-5 to Figure 4-7 show the interaction torques and joint motions from slow speed to fast speed. The measured output torques in Figure 4-5 to Figure 4-7 show good performance of the proposed controller. At a low frequency, the interaction torque is near zero with minor peaks of about 0.12 Nm. As the frequency of the excitation is increased, the interaction torque is still oscillating with the height of the peaks below 0.6 Nm. It is observed that at all frequencies the human-robot control system is stable.

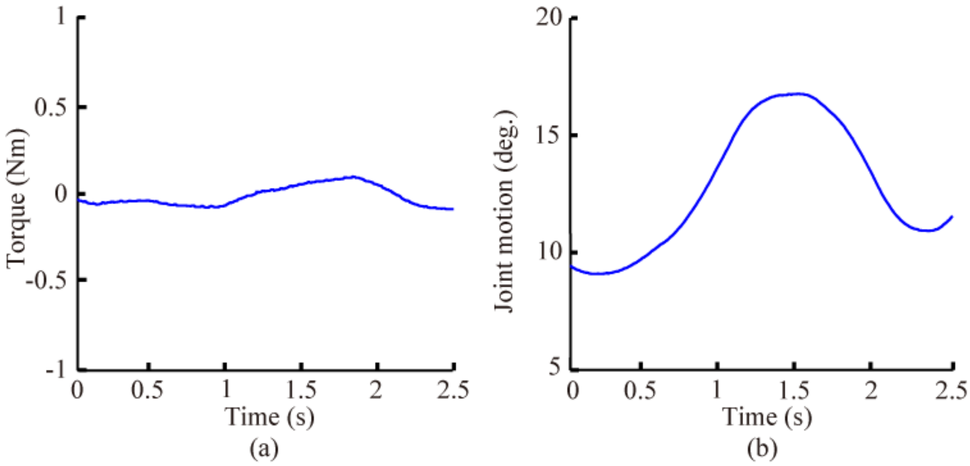

(a)

(b)

Figure 4-5. Stability tests using the proposed controller (frequency is about 0.7Hz). (a) Torque (Nm). (b) Joint motion (deg).

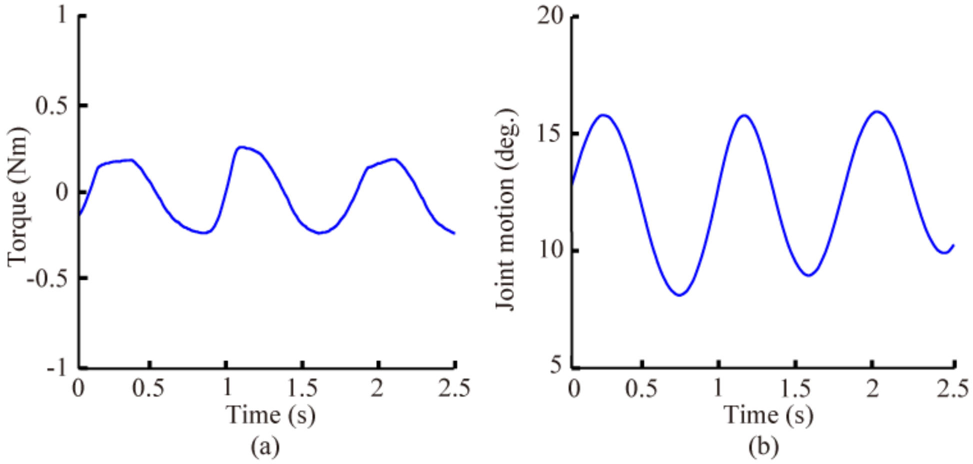

Figure 4-6. Stability tests using the proposed controller (frequency is about 1.2Hz). (a)Torque (Nm). (b) Joint motion (deg).

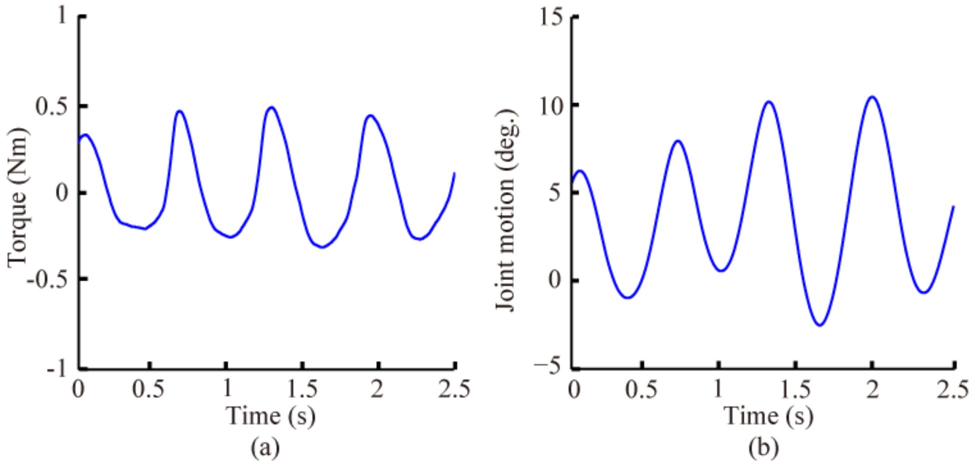

Figure 4-7. Stability tests using the proposed controller (frequency is about 1.6Hz). (a) Torque (Nm). (b) Joint motion (deg).

If we use the same PD controller without the compensation and disturbance observer, the result is shown in Figure 4-8and Figure 4-9. It is observed that at very low frequency the system is stable and the interaction torque is near zero. However, when increasing the frequency the phenomenon of unstable oscillation is observed from the second cycle as shown in Figure 4-9. This demonstrates that the stability issue may arise when applying a traditional PD control to the human-robot interaction environment.

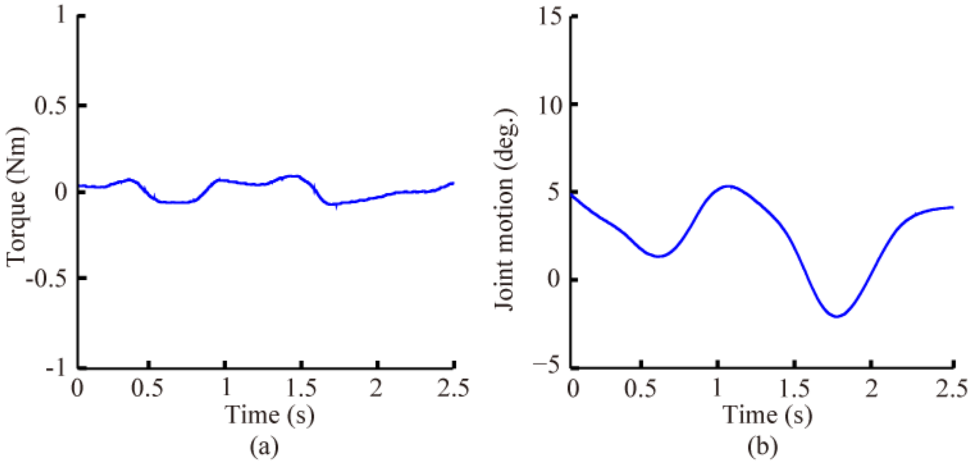

(a)

(b)

Figure 4-8. Tests using pure PD control (frequency is about 0.8Hz). (a) Torque (Nm). (b) Joint motion (deg).

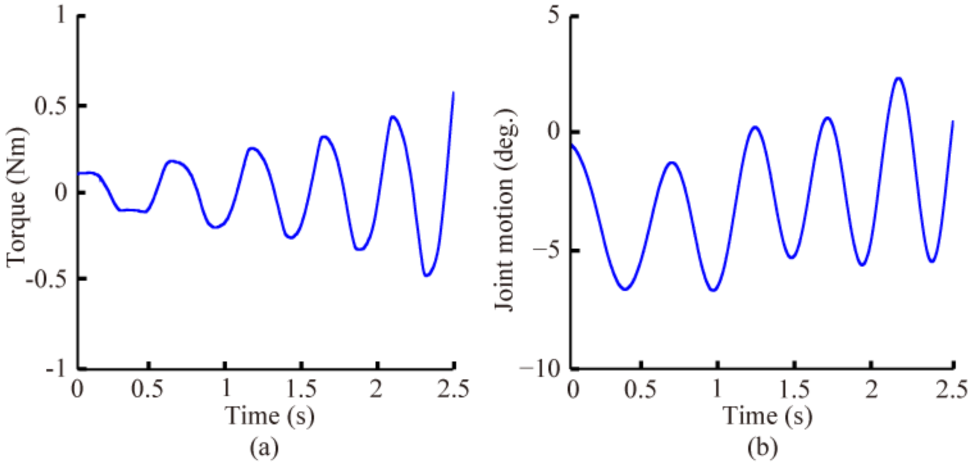

(a)

(b)

Figure 4-9. Tests using pure PD control (frequency is about 1.6Hz). (a) Torque (Nm). (b) Joint motion (deg).

The result with no control, i.e. with motor power off, is shown in Figure 4-10 and Figure 4-11. It demonstrates that the robot is backdrivable even with no power; however, the resistive interaction torque is large compared to the results with control.

At low frequency, the measured interaction torque is about 3 Nm; and at higher frequency, the interaction torque is as larger as 7 Nm. It can be seen that the interaction torque with the proposed controller is less than 1/30 of that with no control. The results indicate that the proposed controller is stable and effective in reducing the output impedance and improving the transparency of the robot.

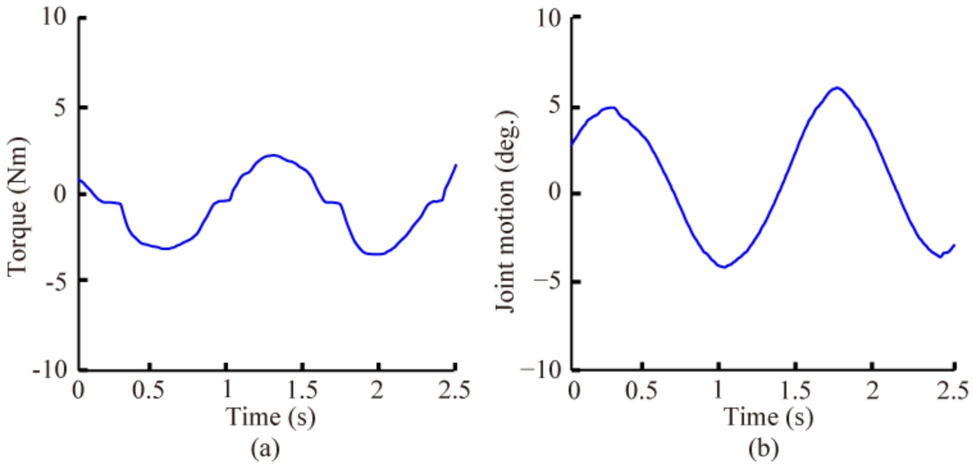

Figure 4-10. Tests with motor turned off (frequency is about 0.7Hz). (a) Torque (Nm). (b) Joint motion (deg).

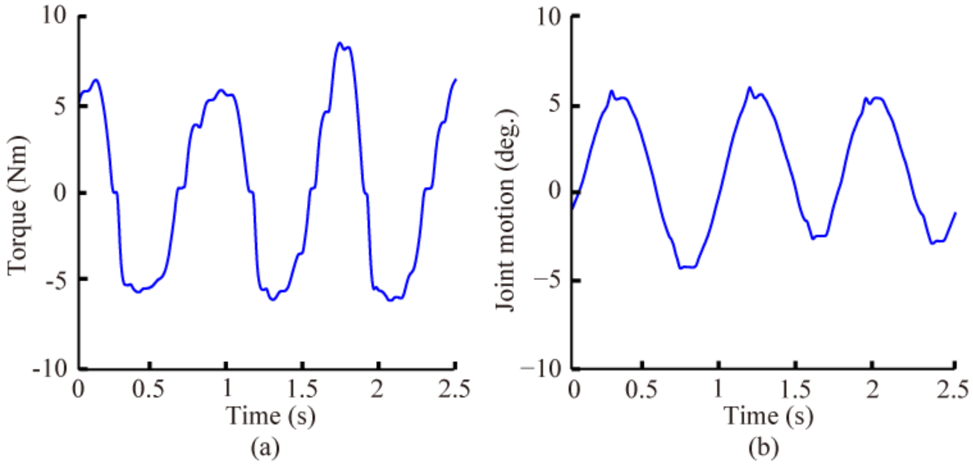

Figure 4-11. Tests with motor turned off (frequency is about 1.2 Hz). (a) Torque (Nm). (b) Joint motion (deg).

Moreover, it is interesting to observe the effect of the friction compensation. In this scenario, only friction compensation is implemented without feedback control. The results can be compared with that when the motor is turned off (results in Figure 4-10 and Figure 4-11). Figure 4-12 shows the result of the simple friction compensation (without Stribeck friction), while Figure 4-13 shows the performance of

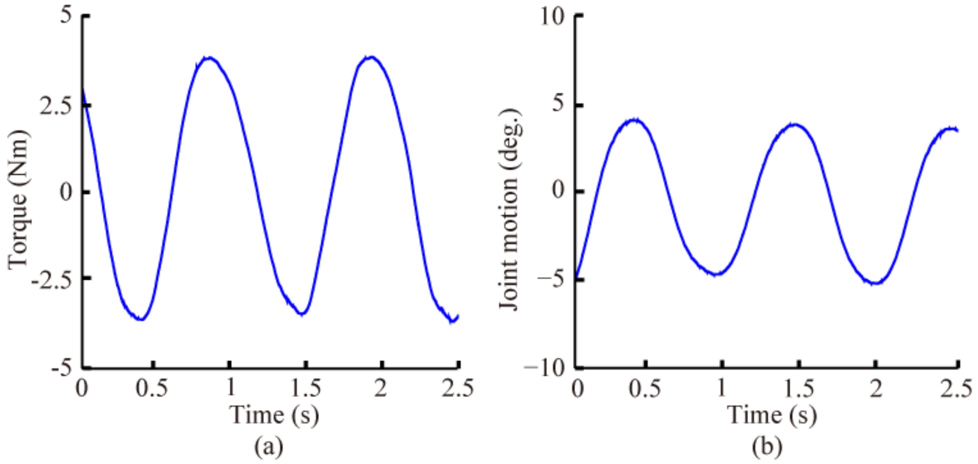

Figure 4-12. Tests with simple friction compensation. (a) Torque (Nm). (b) Joint motion (deg).

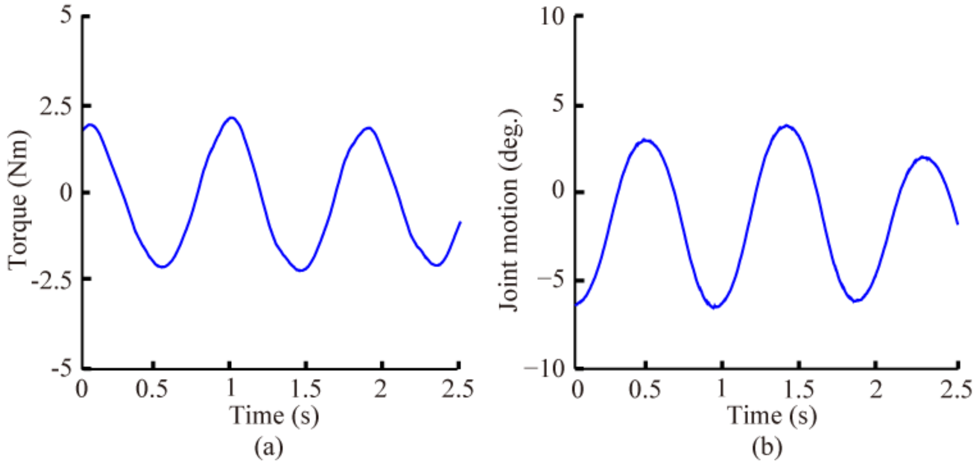

Figure 4-13. Tests with the proposed friction compensation. (a) Torque (Nm). (b) Joint motion (deg).

the proposed friction compensation. With the simple friction compensation, the peak interaction torque was about 4 Nm; while with Stribeck friction model, the peak interaction torque was reduced and was less than 2.5 Nm. It is observed that the friction compensation can improve the performance of the designed exoskeleton, especially in use of our proposed friction compensation with Stribeck model.

4.3 Human walking test

To verify the performance of the proposed controller, the ankle robot was attached to ankle joint of human subjects. During the testing, the movements of the ankle joint may be different in order to demonstrate the effectiveness of the proposed human-robot control.

(A) Human-in-charge control

To test this control mode, healthy subjects wore the exoskeleton and walked in overground gait to measure the zero force control. It is desired that the subject does not feel any resistance from the robot, which means the robot is transparent to the human subject.

This control scheme is tested in three male subjects (personal data is shown in Table 4-2). Figure 4-14 to Figure 4-16 show the control results of the human-in-charge mode. The red circle denotes the start of a gait cycle, which is the initial contact of the right foot. The interaction torques are less than 0.5 Nm during the whole walking motion, which is small that it could not be felt by the subject. The interaction torque peaks at the stance phase. This may be caused by the impact when foot contacts the ground at heel strike, introducing sharp signals during the interaction control. However, it is also observed from the figure that even in this situation the controlled human-robot system is still stable and the gait pattern is normal. This further verifies our theoretical analysis.

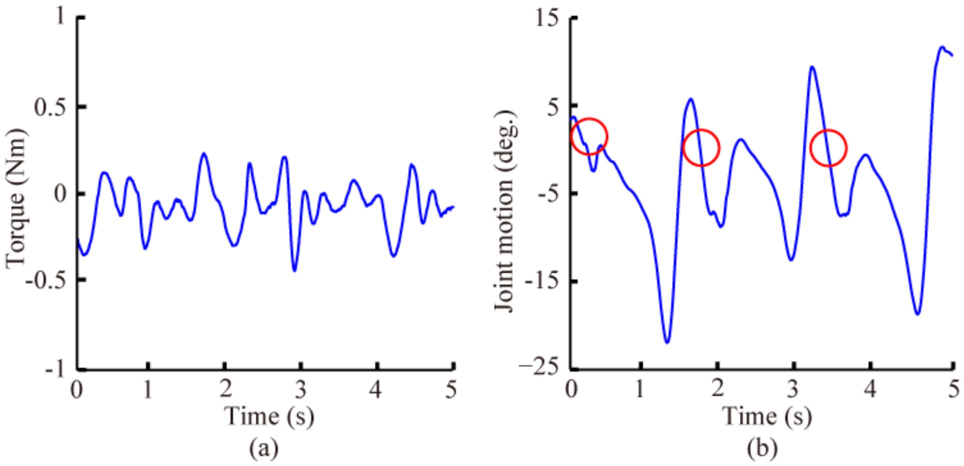

Figure 4-14. Human-in-charge control (subject1). (a) Output torque (Nm). (b) Joint motion (deg). The red circle denotes the start of a gait cycle, which is the initial contact of the right foot.

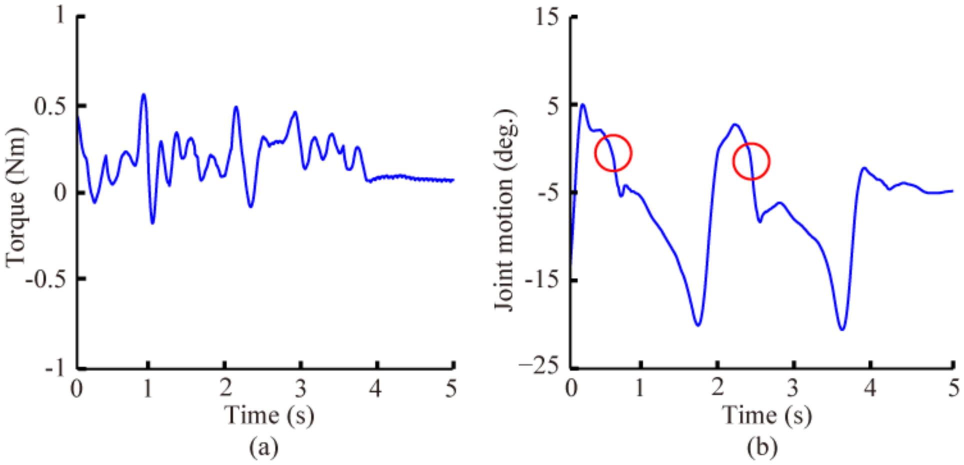

Figure 4-15. Human-in-charge control (subject2). (a) Output torque (Nm). (b) Joint motion (deg). The red circle denotes the start of a gait cycle, which is the initial contact of the right foot.

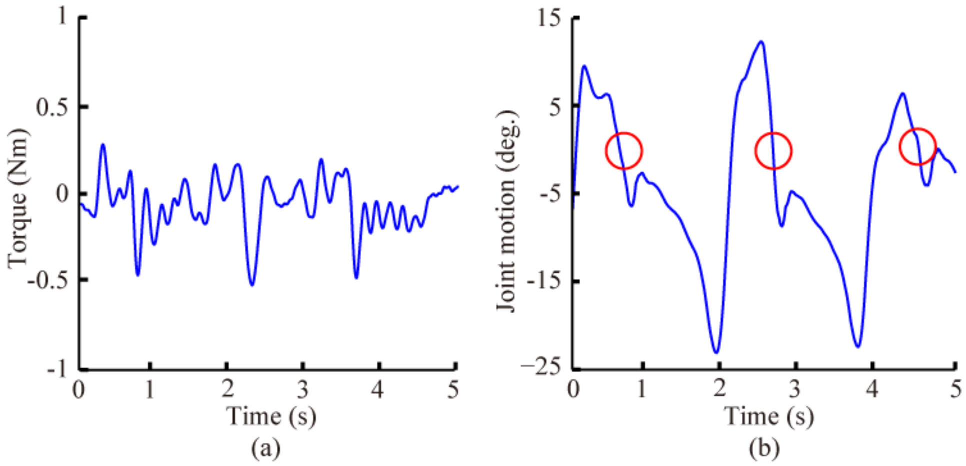

Figure 4-16. Human-in-charge control (subject3). (a) Output torque (Nm). (b) Joint motion (deg). The red circle denotes the start of a gait cycle, which is the initial contact of the right foot.

Table 4-2. Personal data

Parameters	Subject 1	Subject2	Subject3
Height (cm)	167 *cm*	176 *cm*	182 *cm*
Weight (kg)	65 *kg*	73 *kg*	90 *kg*

(B) Assistive force control

In this test scenario, the human-robot interaction enters assistive control mode and the robot provides torque tracking control to the human motions. For the purpose of testing, sinusoidal force signals are used as desired torque trajectories. Advanced control strategies should be implemented to determine the assistive torque in real rehabilitation application.

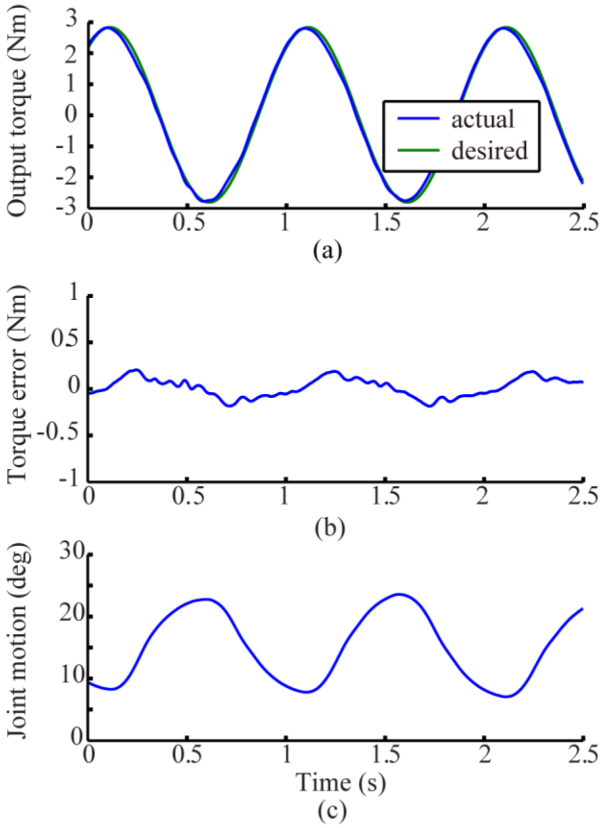

Figure 4-17. Assistive control (Case-1). (a) Output torque (Nm). (b) Torque tracking error (Nm). (c) Joint motion (deg).

Case-1. In this case, the subject was asked to follow the torque generated by the ankle robot to do motions naturally. Using the proposed control law (4-21), we tested the system performance at a frequency of 1 Hz. Figure 4-17 shows the control results, where the top figure is the output torque response, the middle figure is the torque tracking error, and the bottom one is the joint motions. It is observed that the maximum tracking error is $\pm 0.3\,\text{Nm}$.

Case-2. In this case, the subject was asked to stand there and resist the output torque. The control results are shown in Figure 4-18, where the top figure is the output torque, the middle figure is the torque tracking error and the bottom one is the joint angle motions. The maximum tracking error is less than ± 0.2 Nm.

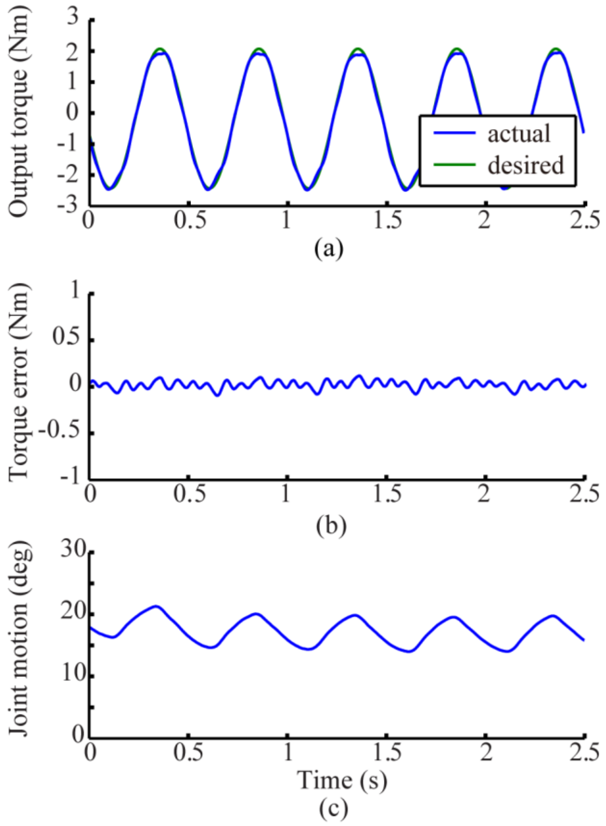

Figure 4-18. Assistive force control (Case-2). (a) Output torque (Nm). (b) Torque tracking error (Nm). (c) Joint motion (deg).

We use two cases to show the performance of the assistive force control: in one the subject follows the robot motions and in the other the subject stands there and blocks the robot motions. The torque tracking performance in the second case is better than that of the first case. The reason is that in the second case the subject interacts less with the robot, thereby introducing less disturbance to the robot control. Both trials demonstrate that our robot is capable of providing an accurate assistive torque to human joint.

5. Summary

We have presented a new controller for human-robot interaction control for a rehabilitation robot with a SEA. By combining joint motion compensation, friction compensation, a disturbance observer and feedback control, our control can implement human-robot interaction control ranging from human-in-charge mode to assistive mode. Theoretical analysis for the proposed controller has proven that it can guarantee the stability of the human-robot interaction. Experimental results have confirmed that the proposed controller can achieve stable force control with good performance in different modes for the rehabilitation ankle robot. Without much difficulty, the proposed controller can also be used in the knee module and any other rehabilitation robot with SEAs.

As discussed in Chapter 3, this controller is developed to provide accurate torque with joint-level motion of human. In the next stage, we will implement the controller in the complete robot for gait training for stroke patients.

Chapter 5

Gait-Event-Based Synchronization Method via an Adaptive Oscillator

In the field of gait rehabilitation robotics, human–robot synchronization is required to provide safe and effective assistance. In this chapter, a novel human–robot synchronization method using gait event information is proposed. This method includes two steps. Firstly, seven gait events in one gait cycle are detected in real time with a HMM; secondly, an adaptive oscillator is utilized to estimate the strider percentage of human gait using any one of the gait events. Synchronous reference trajectories for the robot are then generated with the estimated stride percentage. This adaptive oscillator is a mathematical tool, which was first proposed to explain the phenomenon of synchronous flashing among fireflies. The proposed synchronization method is implemented in a portable knee-ankle-foot robot and tested on 15 healthy subjects. This method has the advantages of simple structure, flexible selection of gait events and fast adaptation. Gait event is the only information needed, and hence the performance of synchronization holds when an abnormal gait pattern is involved. The results of the experiments reveal that our approach is efficient in achieving human–robot synchronization and feasible for rehabilitation robotics application.

1. Introduction

In the field of gait rehabilitation robotics, the synchronization between the motion of the robots and the actual human gait is very important. For example, in impedance-control-based strategies as discussed in Chapter 2, the robotic assistance is specified based on the deviation of the actual position of the lower-limb joints from the reference trajectories of the robots [17, 25, 42, 108]. The common concern in these strategies is that if the robot trajectory is not synchronized with the human gait, the robot may resist the human walking, and may even cause injury [111, 112]. Asynchronous assistance is particularly dangerous in robotic systems without body weight support, which may lead to falling [22]. In strategies that are not based on reference trajectories, synchronization is required to ensure timing accuracy. For example, in gait training aided by functional electrical stimulation (FES, which is a technology to stimulate muscle contraction through electric current applied to the muscles), FES must be triggered at the correct time in order to accomplish a normal gait pattern and safe walking [133, 134].

Motivated by the need for human–robot synchronization, researchers have developed various control strategies. Jezernik *et al.* developed an adaptation algorithm on Lokomat that can synchronize the robot trajectories with the human joints by minimizing the human–machine interaction torque [135]. In this method, the interaction force is responsible for both power transmission and human intention estimation, which may cause resonance between human and robot, and limited applicability for more severe patients [136, 137]. Aoyagi *et al.* developed an algorithm on POGO and PAM that can adjust the replay timing of the reference trajectories according to a state, which is an 18-dimensional vector of position and velocity signals of the robot and human joints [112]. This algorithm is effective in synchronizing the user's gait and their own recorded gait trajectories; however, the applicability for synchronization between normal gait references and subjects or patients with abnormal gait patterns is not ensured [138]. Besides, the position and velocity signals from nine degrees-of-freedom are required, which requires a large amount of sensing and signal processing.

More recently, various adaptive oscillators have been implemented in rehabilitation robotics in order to provide synchronous assistance [137-145]. Adaptive oscillators as a type of mathematical tool can synchronize with an external periodic signal and extract the frequency or/and phase information. Complex sensing or complicated adaptation rules are not required to achieve synchronization. Ronnsse *et al.* implemented an adaptive oscillator in the upper-limb exoskeleton NEUROExos to provide sinusoidal assistance in cyclical elbow flexion/extension movements [138, 139]; and Gams *et al.* employed a different adaptive oscillator in a knee robot to provide sinusoidal support in squatting motions [140]. In order to generate non-sinusoidal trajectories for gait training, several adaptive oscillators need to be implemented [140-142]. The methods have been used in LOPES for walking assistance for hip joints [137], and in ALEX II to provide hip support during treadmill training [145]. To summarize, the existing oscillator-based algorithms are effective in synchronizing the robot with arbitrary periodic input trajectory (human gait trajectory);

however, these methods are limited in the following aspects. Firstly, several oscillators are needed for the generation of a non-sinusoid gait trajectory, which is relatively computationally expensive (as reported in [137], six adaptive oscillators are employed to generate the trajectory for the hip). Secondly, the adaptation to achieve synchronization is relatively slow (for example in [137], it takes around ten cycles to achieve synchronization) and the overall system may diverge if the gain of the input trajectory is set to be large to achieve faster adaptation. Thirdly, the current methods focus on reconstructing the waveform of the input gait trajectories. However, for the purposes of gait rehabilitation, it is more important to provide a normal reference trajectory that is synchronous with the abnormal gait of the patients. For example, the method in [145] employs the aforementioned adaptive oscillator to estimate the frequency of the gait, and estimates the stride percentage collaborating with a foot pressure sensor. Then a reference torque trajectory for the robot is generated using a lookup table (LUT) according to the current stride percentage.

The phenomenon of synchronization can be found in the biological world. For example, a specific species of firefly, *Pteroptyx malaccae*, can achieve both frequency and phase synchronization in flashing, and their synchronization mechanism is modeled by an adaptive oscillator [146]. The oscillator will alter its frequency based on its phase difference from the stimulus (other firefly’s flash) and eventually achieve synchronization. In this chapter, we adopt this adaptive oscillator into gait rehabilitation robotics to achieve human–robot synchronization. The adaptive oscillator represents the estimated gait percentage and the actual gait event during walking is regarded as the external impulsive stimulus. The phase difference of the estimated gait percentage and the detected gait event will drive the frequency adaptation of the oscillator, and eventually the gait percentage can be accurately estimated. In the proposed method, wearable inertia measurement unit (IMU) sensors are utilized to measure the gait pattern and the seven gait events are detected in real time with a hidden Markov model (HMM). The adaptive oscillator is employed to extract the percentage of the human stride based on the gait events. Any one of the seven gait events is adequate for synchronization; and two or more gait events in one gait cycle is beneficial for faster adaptation. The synchronous reference trajectories of the robot are generated with a LUT according to the estimated gait percentage. The oscillator-based synchronization strategy is implemented in a portable knee-ankle-foot robot and an assistive walking protocol is designed. Experiments on 15 healthy subjects are conducted to evaluate the performance of the proposed method.

The rest of this chapter is organized as follows: Section 2 introduces the synchronization method, including gait-event detection, development of the adaptive oscillator, and assistive controller. Section 3 presents the experimental protocol. Section 4 gives the experimental results in different conditions. Section 5 is the discussion and this chapter ends with a summary in section 6.

2. *Methodology*

Gait describes the pattern of human walking. A gait cycle can be subdivided into seven gait phases, including loading response (LR), mid-stance (MSt), terminal stance (TSt), pre-swing (PSw), initial swing (ISw), mid-swing (MSw) and terminal swing

(TSw) (Figure 5-1) [147]. The beginning of each gait phase is denoted as a gait event. Thus, correspondingly, there are seven gait events: initial contact (IC), opposite toe off (OT), heel rise (HR), opposite initial contact (OI), toe off (TO), feet adjacent (FA) and tibia vertical (TV) [147]. This classification is based on the three fundamental gait tasks, which are weight acceptance, single limb support, and swing limb advancement [148]. The sequential occurrences of these gait events represent the transition of the gait phases, which propels the human body forward. Gait events follow a specific sequence and occur at specific periods within a gait cycle during normal overground walking [147, 149, 150].

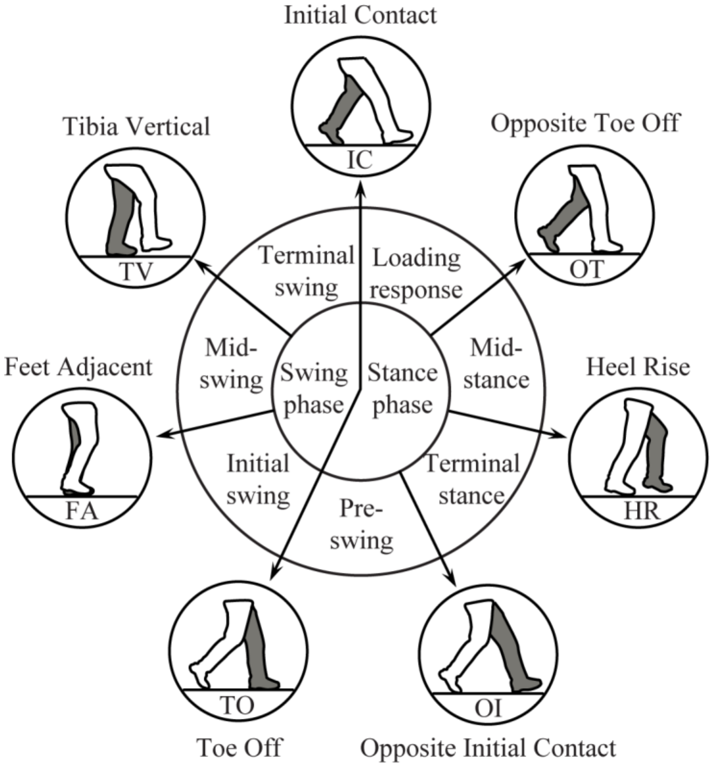

Figure 5-1. Seven gait events and gait phases in one gait cycle.

The process of the gait-event-based synchronization method is illustrated in Figure 5-2. This method aims to generate a synchronous reference trajectory for the robot by estimating the stride percentage of the human gait based on the gait event information. The method can be divided into two steps: gait-event detection with a HMM and stride percentage estimation with an adaptive oscillator for synchronization. Then, a synchronously assistive walking control method is implemented in a rehabilitation robot.

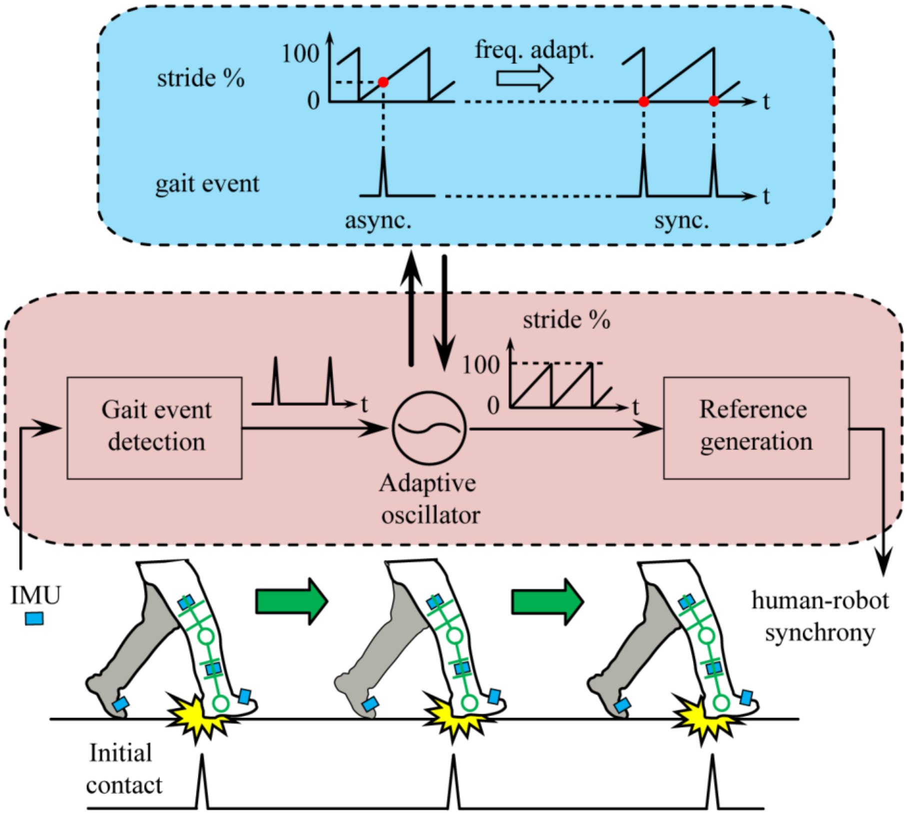

Figure 5-2. Flowchart of the gait-event-based synchronization method using an adaptive oscillator. The gait event of IC as an example is utilized for synchronization, which is described with a pulse signal. Both the frequency and the phase of the adaptive oscillator synchronize with the human gait based on the detected gait event. Synchronous trajectories are then generated for the robot.

2.1 Gait events detection using HMM

In this section, the real-time gait event detection method is introduced. We have developed a HMM-based algorithm to detect the seven gait phases during overground walking; the gait events are then detected with the transitions of the gait phases [151].

IMU sensors, which are electronic devices combining accelerometer, gyroscope and magnetometer, are employed to collect the kinematics of the gait (Figure 5-3). Here it is defined as

$$\mathbf{z}_t = [\omega_R, \alpha_R, \omega_L, \alpha_L, \theta_{Rknee}, \theta_{Rshank}] \tag{5-1}$$

where $\mathbf{z}_t$ is a six-dimensional vector denoting the observation features of the HMM at time t; ω_R, ω_L are the angular rates of both feet and α_R, α_L are their first-order derivatives; and θ_{Rknee} and θ_{Rshank} are the angles of the right knee and the right shank, respectively. These selected features are capable of representing the gait phases.

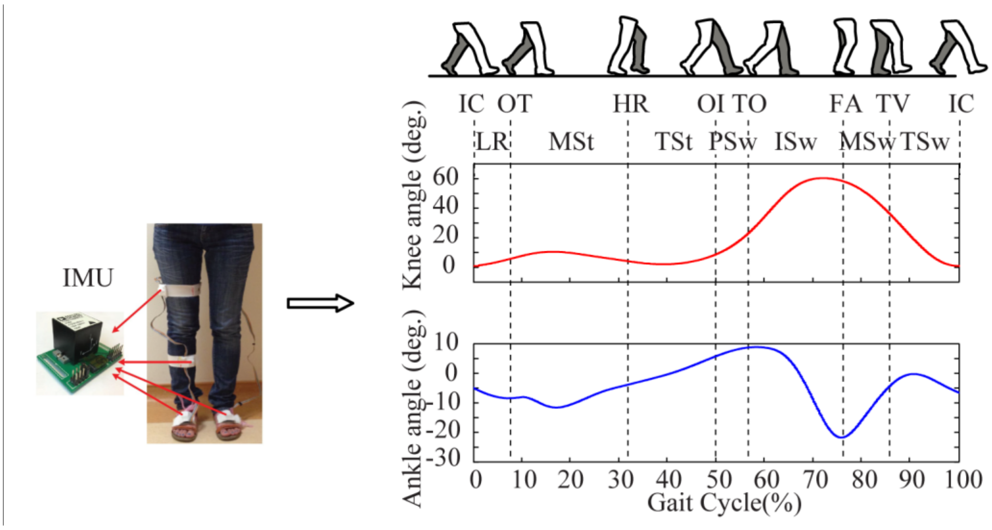

Figure 5-3. IMU sensor system, which is utilized to detect the gait phases and collect kinematics information of knee and ankle joints.

A HMM with seven states corresponding to seven gait phases is built as

$$S=\{LR, MSt, Tst, PSw, ISw, MSw, TSw\} \tag{5-2}$$

To implement the HMM for gait-event detection, three steps need to be carried out consecutively, including initialization, training and decoding. HMM is defined as a statistical Markov model in which its unobservable state sequence $q=q_1q_2...q_T$ can be estimated through an observation sequence $Z=\boldsymbol{z}_1\boldsymbol{z}_2...\boldsymbol{z}_T$, where T is the length of the observation sequence [152]. An HMM can be described by a 5-tuple $(S,\boldsymbol{z}_t,\pi,A,B)$, where $S=\{s_1,s_2,...,s_N\}$ is a set of the N hidden states; π is the prior state probability vector $\pi=\{\pi_i\,|\,\pi_i=P[q_0=s_i], i=1,...,N\}$; A is the state transition probability distribution matrix $A=\{a_{ij}\,|\,a_{ij}=P[q_t=s_i\,|\,q_{t+1}=s_j], i, j=1,...,N\}$; and B is the observation probability distribution matrix $B=\{b_i(\boldsymbol{z}_t)\,|\,b_i(\boldsymbol{z}_t)=P[\boldsymbol{z}_t\,|\,q_t=s_i],$ $i=1,...,N\}$.

For HMM initialization and training, subjects or patients are required to conduct walking trials for the collection of the observation feature data. The benchmark seven phases are firstly annotated based on an adaptive threshold method [151]. With the observation data and gait phases, the parameter set of HMM $\lambda=(\pi,A,B)$ can be initialized. The initialization is based on the statistical results of the duration of each gait phases and the sequence of their transition. The HMM λ is further trained using the Baum–Welch algorithm for better performance [152]. The initialization and training sessions are done using MATLAB and can be completed in a few minutes [151, 152].

With the derived HMM, the most likely gait phase during overground walking is decoded using the Viterbi Algorithm [152]. However, implementation of this method in a conventional way is unsuitable for online application since the instant state has to be detected in real time without the successive observation input. Besides, the Viterbi has to be conducted in every cycle with the observation sequence starting from the beginning. The length of the observation, thus, increases after each cycle, which eventually leads to a huge observation sequence that is slow to process. In our application, an online Viterbi algorithm with a moving window is implemented, which is similar to the method in [153, 154]. The procedure is described with pseudo-code in Table 5-1. Specifically, an observation sequence with 300 observations is employed for decoding, which is a sequence combining the current observation $\boldsymbol{z}_t$ and prior history observations. Considering that the sampling frequency of the IMU system is 100 Hz, this observation window lasts for 3 seconds, which is long enough for detection. The first state of the decoded path is then regarded as the current gait phase. The occurrences of the gait events are then detected in the transitions of the gait phases.

The effectiveness of the HMM-based gait phase detection has been validated with experiments of healthy subjects and dementia patients in our previous work [151]. High accuracy and small time delay in the detection have been achieved for normal and pathological gaits. A general HMM can be established for different subjects; and HMM can be tailored for each individual for better detection. This algorithm has also been tested with robot-aided walking experiments, in which subjects wear our exoskeleton robot on the right leg. Experimental results demonstrate that the seven gait phases can be detected robustly, which is applicable for gait rehabilitation robotics.

Table 5-1. Online state decoding algorithm

Online Viterbi

```
for $i = 1, ..., 7$ do
    $\delta_1(i) = \pi_i \cdot b_{i,z_1}$
end for
for $2 \le n \le 300$ do
    for $1 \le j \le 7$ do
        $\delta_n(j) = \max_{1 \le i \le 7}(\delta_{n-1}(i) \cdot a_{ij}) \cdot b_{j,z_n}$
    end for
end for
return $q = \arg\max_{1 \le i \le 7} \delta_{300}(i)$
```

where i and j is the gait phase, δ is a variable denoting likelihood; q represents the decoded gait phase.

2.2 Adaptive oscillator implementation

As adopted from [146], a self-sustained oscillator is built to estimate the percentage of stride (*stride %*):

$$d\phi / dt = \omega \tag{5-3}$$

where $\phi \in \mathbb{S}^1$ is the phase angle of the oscillator and the set $\mathbb{S}^1$ denotes the *unit circle*, t is time, and $\omega \in \mathbb{R}$ is the time-dependent variable frequency of the oscillator. The phase angle ϕ varies between 0 and 2π, and grows uniformly within one cycle (Figure 5-2). The stride percentage is then derived as

$$stride\ \% = \frac{\phi}{2\pi} \times 100 \tag{5-4}$$

Considering that one of the seven gait events is utilized for synchronization, the occurrence of the gait event can be described with a periodic Dirac delta function $\delta(t/\tau)$, where τ is the period of the gait cycle. In order to achieve synchronization, the oscillator will adapt its frequency based on the incoming gait event as

$$d\omega / dt = \varepsilon(\Omega - \omega) + \delta(t/\tau) \cdot P \cdot G(\omega, \Delta\phi) \tag{5-5}$$

where ε denotes the adaptation rate of the oscillator frequency returning to the human gait frequency, Ω is the frequency of the gait cycle and $\Omega = 2\pi/\tau$, P is a positive value that is related to the amount of the frequency change, $\Delta\phi$ is the phase difference between the adaptive oscillator and the actual gait, $\Delta\phi = (\phi - \Phi)\operatorname{mod}(2\pi)$, where Φ is the predefined phase of the gait event, and $G(\omega, \Delta\phi)$ is employed to vary the frequency according to the detected gait event, which is specified as

$$G(\omega, \Delta\phi) = g^{+}(\Delta\phi)(\omega_{\min} - \omega) + g^{-}(\Delta\phi)(\omega_{\max} - \omega) \tag{5-6}$$

where $\omega_{\min}, \omega_{\max}$ are the allowed minimum and maximum frequencies, and $g^{+}(\Delta\phi)$ and $g^{-}(\Delta\phi)$ are defined as

$$\begin{aligned} g^{+}(\Delta\phi) &= \max\left(\frac{1}{2\pi}\sin(\Delta\phi), 0\right) \\ g^{-}(\Delta\phi) &= -\min\left(\frac{1}{2\pi}\sin(\Delta\phi), 0\right) \end{aligned} \tag{5-7}$$

The phase response curve $G(\omega, \Delta\phi)$ is illustrated with Figure 5-4. In the above model, when $0 < \Delta\phi < \pi$, i.e. the oscillator is leading the gait event, the oscillator frequency will be decreased. Conversely, when $\pi < \Delta\phi < 2\pi$, i.e. the oscillator is lagging behind the gait event, the frequency will be increased.

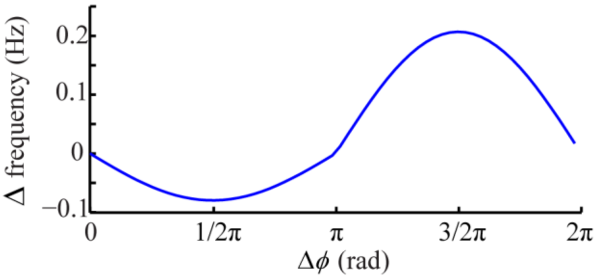

Figure 5-4. Phase response curve (PRC) $G(\omega, \Delta\phi)$, with example of $\omega = 0.7$, $\omega_{\min} = 0.2$, $\omega_{\max} = 2$.

The period of the gait is estimated by using the duration between two successive gait events:

$$\tau = 2\pi / \Omega = t_N - t_{N-1} \tag{5-8}$$

where t_N and t_{N-1} represent the time of the *N*th and (*N*–1)th occurrences of the gait event.

In our application, there are m ($m = 1, 2, ..., 7$) gait events in one gait cycle which can be utilized for faster synchronization. The adaptive oscillator is extended as

$$\begin{aligned} d\phi / dt &= \omega \\ d\omega / dt &= \varepsilon(\Omega - \omega) + \sum_{n=1}^{m} \delta(t_n / \tau) \cdot P \cdot G(\omega, \Delta\phi_n) \end{aligned} \tag{5-9}$$

where $\delta(t_n / \tau)$ is the periodic Dirac delta function denoting the *n*th ($n = 1, 2, ..., m$) gait-event occurrence, and $\Delta\phi_n$ is the phase difference between the adaptive oscillator and the *n*th gait event, $\Delta\phi_n = (\phi - \Phi_n) \bmod (2\pi)$, where Φ_n is the predefined phase of the *n*th gait event. With the modified adaptive oscillator, more gait events in one gait cycle can be used to detect the phase difference between the oscillator and the actual gait, and thus synchronization can be achieved faster.

The period of the gait is estimated by using the duration between two successive gait events:

$$\tau = 2\pi / \Omega = \frac{1}{m}\sum_{n=1}^{m}(t_{n_N} - t_{n_{N-1}}) \tag{5-10}$$

where t_{n_N} and $t_{n_{N-1}}$ represent the time of the *N*th and (*N*–1)th occurrences of the *n*th gait event.

The stability of the adaptive oscillator and the convergence of the phase error have been rigorously proved in [146], which shows that the adaptive oscillator synchronizes to the frequency Ω and with a phase error of $\boldsymbol{O}(\varepsilon)$.

In this method, the value of *P* is related to the velocity of the frequency adaptation. A large *P* leads to a faster convergence of phase error between the oscillator and actual gait and vice versa. However, with a large *P*, the oscillator is more sensitive to the phase difference. The value of ε determines how fast the frequency of the oscillator returns to that of the human gait. With a large ε, the oscillator can finish adaptation in a short period of time, leading to a sharp change of the estimated phase, and vice versa. These two parameters collectively determine the performance of the synchronization method. Fine-tuning of ε and P is required in actual application.

The reference trajectories for the robot are generated using the estimated stride percentage based on a LUT. An example is illustrated in Figure 5-5, where a LUT is shown, corresponding to the robotic knee and ankle joints. The reference trajectories are recorded from a healthy subject during free walking, and are normalized based on the stride percentage [108]. The phase of each gait event is also collected and averaged as the reference phase Φ_n during synchronization. In our paper, we use $\Phi_1 = 0\%$, $\Phi_2 = 7\%$, $\Phi_3 = 48\%$, $\Phi_4 = 50\%$, $\Phi_5 = 60\%$, $\Phi_6 = 77\%$, $\Phi_7 = 86\%$. It is worth mentioning that the trajectories for different robot joints can be easily generated from the same oscillator without implementing other oscillators.

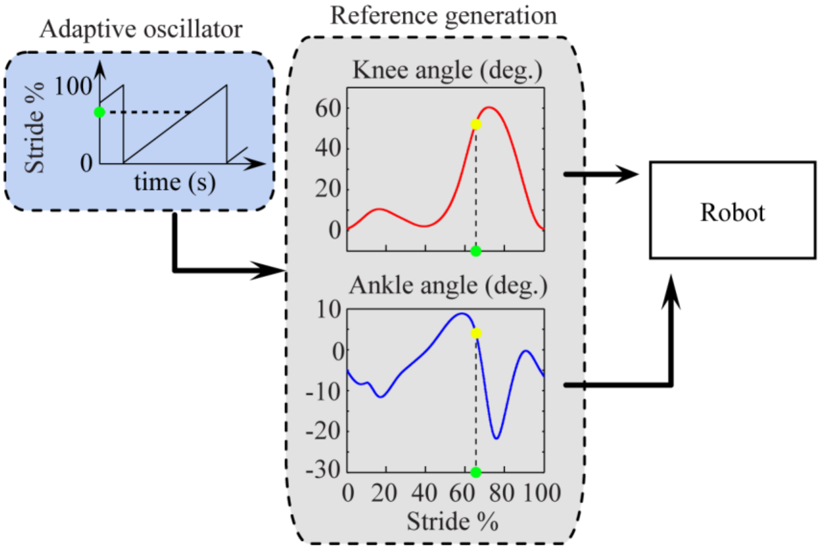

Figure 5-5. The reference trajectory for the robot is generated with a LUT based on the estimated stride percentage from the adaptive oscillator. Reference trajectories for multiple robotic joints can be generated from the same stride percentage.

2.3 Assistive control strategy for gait rehabilitation

Based on the reference trajectory that is synchronous to the human gait, an assistive walking method is implemented in our exoskeleton robot. This method is also applicable for rehabilitation robot with n joints to provide assistance during overground walking (Figure 5-6).

The gait event information is transmitted to the adaptive oscillator (Figure 5-6, green arrow) to achieve synchronization between the robot and the human walking. The robot starts in zero-assistive control mode and switches to impedance control mode after five steps (Figure 5-6, red arrow). The number of steps is counted with the gait event of IC. Furthermore, with regard to potential safety issues, if human–robot synchronization is not guaranteed, i.e. the phase difference between the trajectory and the actual human gait is large; the robot switches to the zero-assistive mode, so that no assistance is given. The impedance controller is implemented in the robot to determine the assistive torque based on the reference trajectory, which is described as

$$\boldsymbol{\tau}_I = \mathbf{K}_V(\boldsymbol{\theta}-\boldsymbol{\theta}_0) \tag{5-11}$$

where $\boldsymbol{\theta}=[\theta_1,\cdots,\theta_n]\in\mathbb{R}^n$ is the angles of n joints, $\boldsymbol{\theta}_0\in\mathbb{R}^n$ is the joint angle reference, $\mathbf{K}_V = diag(k_{v1},\cdots,k_{vn})\in\mathbb{R}^{n\times n}$ is a virtual stiffness matrix, where $k_{vi}\in\mathbb{R}$ is the virtual stiffness of the controller for the ith joint, and $\boldsymbol{\tau}_I\in\mathbb{R}^n$ is the desired assistive torque from the controller.

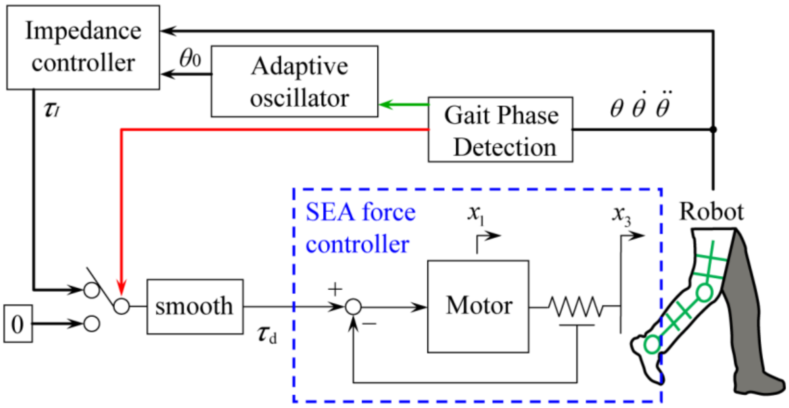

Figure 5-6. Control diagram of the exoskeleton robot, where $\theta,\dot{\theta},\ddot{\theta}$ represent the kinematics of the knee and ankle joints; θ_0 is the reference trajectory from the adaptive oscillator; τ_I is the output of the

impedance controller; τ_d is the desired assistive torque; the blue dashed box represents the inner force control loop of the SEA, in which x_1, x_3 are the motor position and robot position.

To avoid a sudden change of assistive torque, the assistive torque is smoothed using an exponential function [155]:

$$\boldsymbol{\tau}_{dt} = \mathbf{A}\boldsymbol{\tau}_{It} + (\mathbf{I} - \mathbf{A})\boldsymbol{\tau}_{d(t-1)} \tag{5-12}$$

where $\boldsymbol{\tau}_{It} \in \mathbb{R}^n$ is the desired torque $\boldsymbol{\tau}_I$ at time point *t*, $\boldsymbol{\tau}_{dt} \in \mathbb{R}^n$ is the smoothed desired torque, and $\mathbf{A} = diag(\alpha_1, \cdots, \alpha_n) \in \mathbb{R}^{n \times n}$ is a smoothing factor matrix, where $0 < \alpha_i < 1$ is the smoothing factor for the *i*th joint (shown in Figure 5-6 as the box labeled “smooth”).

The force controller that has been presented in Chapter 4 is implemented as the inner loop to control the interaction torque, which is shown in the blue dashed box in Figure 5-6. This controller can provide an accurate assistive torque during overground walking. With this setup, a gait rehabilitation control strategy is implemented in the robot.

3. *Experimental protocol*

Experiments are conducted to evaluate the effectiveness of the control strategy for gait rehabilitation, especially the synchronization method. Different gait events are used for synchronization to prove the flexibility of the proposed method. The dominating parameters of the adaptive oscillator are also discussed with the results of trials with different configurations.

3.1 Experimental setup

The proposed control strategy is tested with our portable, exoskeleton robot. As a prototype, we put the controller and power supply on a trolley for overground walking test (Figure 5-7). An experimenter pushes the trolley to follow the subjects.

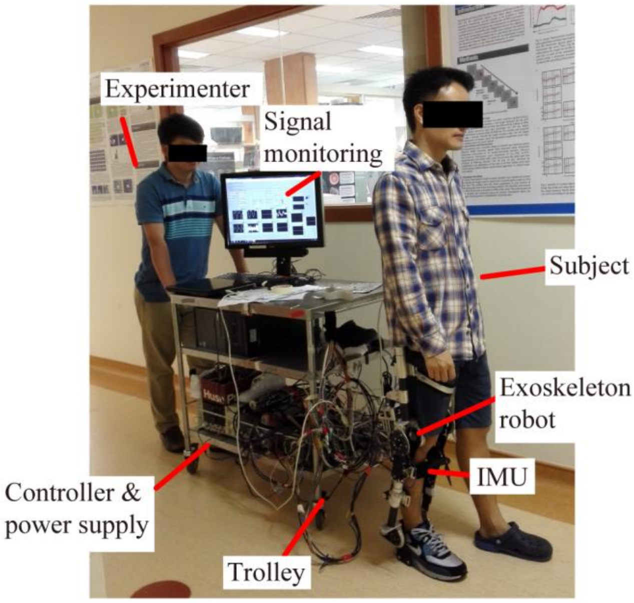

Figure 5-7. Experiment setup for overground walking experiment.

In our experiment, an abnormal gait pattern is simulated to resemble common pathological conditions of stroke patients, such as the stiff-knee gait [156]. An elastic bandage is wrapped around the knee and ankle joints of the exoskeleton to increase the joint impedance. Flexion motion of the knee joint, and both dorsiflexion and plantar flexion of the ankle joint, are hindered. The experiment aims to investigate the robustness of the synchronization method when an abnormal gait pattern is involved. It also aims to test the feasibility of the robotic gait training application, i.e. the robot provides assistance to improve the gait pattern.

3.2 Experimental protocol

The experiment is tested on 15 healthy male subjects (25.5±5.3 years old, 174.9±6.1 cm in height, 70.2±10.7 kg in weight) to evaluate the effectiveness of the gait-event-based synchronization method. The subjects were informed of the protocol of the experiment and signed a consent form, which was approved by the IRB of National University of Singapore.

The subjects were required to wear the exoskeleton on their right leg, except in the "Free walking" condition, which is explained below. The subjects were also asked to wear the IMU sensors on both legs in all conditions. Several trials served as practice before the collection of data to make the subjects familiar with the exoskeleton and the test scenario. At the beginning of each test, the subjects were asked to stand upright. After the experimenter started the robot, the participants could start walking at any time. The subjects were then asked to perform overground walking in a straight line at a preferred speed for about 30 m and stop in standing-up posture. There are five types of scenario, which are as follows.

Free walking (FW): subjects perform walking with the IMU sensors but without the robot. The average trajectories of the knee and ankle joints are recorded as the robot reference for each subject, and will be used in other conditions.

Zero-assistive walking (ZA): subjects wear the robot on their right leg. The robot functions in zero-assistive mode and tries to be transparent to the subjects.

Simulated abnormal walking (SAW): the subjects wear the robot on the right leg, which functions in zero-assistive mode. Elastic bandages are involved to provide resistive torque on the knee and ankle joints (as described in the experimental setup).

Walking with low assistance (ASL): the subjects wear the robot on the right leg, with elastic bandages on the joints. The impedance controller is implemented in both knee and ankle joints to provide assistance. The gait events of OI and TV are used for synchronization. A set of parameters were selected for the adaptive oscillator: $\omega_{\min} = 0.2$, $\omega_{\max} = 2$, $\varepsilon = 0.02$, $P = 11$. The impedance controller as described in (5-11) with $k_v = 0.2$ Nm/deg. was implemented in the knee and ankle joints to provide assistance. The smoothing factor in equation (5-12) was chosen to be $\alpha = 0.04$.

Walking with high assistance (ASH): this scenario is similar to the ASL scenario, except with $k_v = 0.4$ Nm/deg. for the impedance controller to provide higher assistive torque during walking.

3.3 Data analysis

The kinematics of the knee and ankle joints and the results of online gait-phase detection were recorded. Knee and ankle joint angles of ten gait cycles, which were segmented by the gait event IC, were taken and averaged in each condition. The corresponding assistive torque was also collected and segmented. The statistical significance of the changes in different conditions was evaluated with repeated measures ANOVA. When a significant effect was found, Tukey's post hoc test was performed to contrast differences among the experimental conditions, with a p factor of 0.05.

To enable better understanding, the phase error is normalized from $[0, 2\pi)$ to $[-\pi, \pi)$. Hence, a negative phase error represents a delay of the reference trajectory, and vice versa.

In order to quantitatively evaluate how fast the adaption is, we define a value of ±0.5 rad. When a step is reached after which the phase errors in the following five cycles are below this value, the number of this step is recorded. This number can be further compared among different experimental conditions to evaluate the robustness of the proposed method.

4. Experimental results

4.1 Evaluation of synchronization

In this sub-section, experimental results of a representative subject are given to show the details of the synchronization process, including the reference and actual gait trajectories, the adaptation of the frequency and the estimated phase error. The efficiency and flexibility of the proposed method is investigated with different configurations and synchronization using different gait events. The reliability and feasibility of rehabilitation robot application is also evaluated with various experimental conditions.

(A) FW test.

Figure 5-8 shows the experimental results of the FW test, in which the gait event of IC ($\Phi = 0\%$) is used for synchronization. The results include knee and ankle joint angles (Figure 5-8(a) and (b)), the phase difference between the adaptive oscillator and the actual gait (Figure 5-8(c)), the frequency of the adaptive oscillator and the estimated frequency of the actual gait (Figure 5-8(d)), and the phase angle of the adaptive oscillator (Figure 5-8(e)). It should be noted that in this configuration, where IC is used for synchronization, the phase angle of the adaptive oscillator equals the phase difference between the adaptive oscillator and the actual gait when IC is detected (Figure 5-8(c) and (e)).

It can be seen that the test began with the subjects standing still. No gait event occurred; hence the synchronization procedure was not triggered. The subjects started walking at a random time point. The gait frequency is around 0.7 Hz (Figure 5-8(d)). The gait event of IC was detected in real time (orange circle in Figure 5-8(b)), and the phase error between the oscillator and the actual gait was detected (Figure 5-8(c)). The frequency of the adaptive oscillator was adapted according to Equation (5-5) (Figure 5-8(d)) and the phase angle grows according to the frequency (Figure 5-8(e)). The phase error between the adaptive oscillator and the actual gait was reduced gradually (Figure 5-8(c)). The figure shows that the reference trajectory was synchronized with human motion ($|\Delta\phi| < 0.5$ rad; gray bar in Figure 5-8(c)) at the fourth step and onwards. In the last six steps in this figure, the averaged phase error is -0.053 rad, which is less than 2% error.

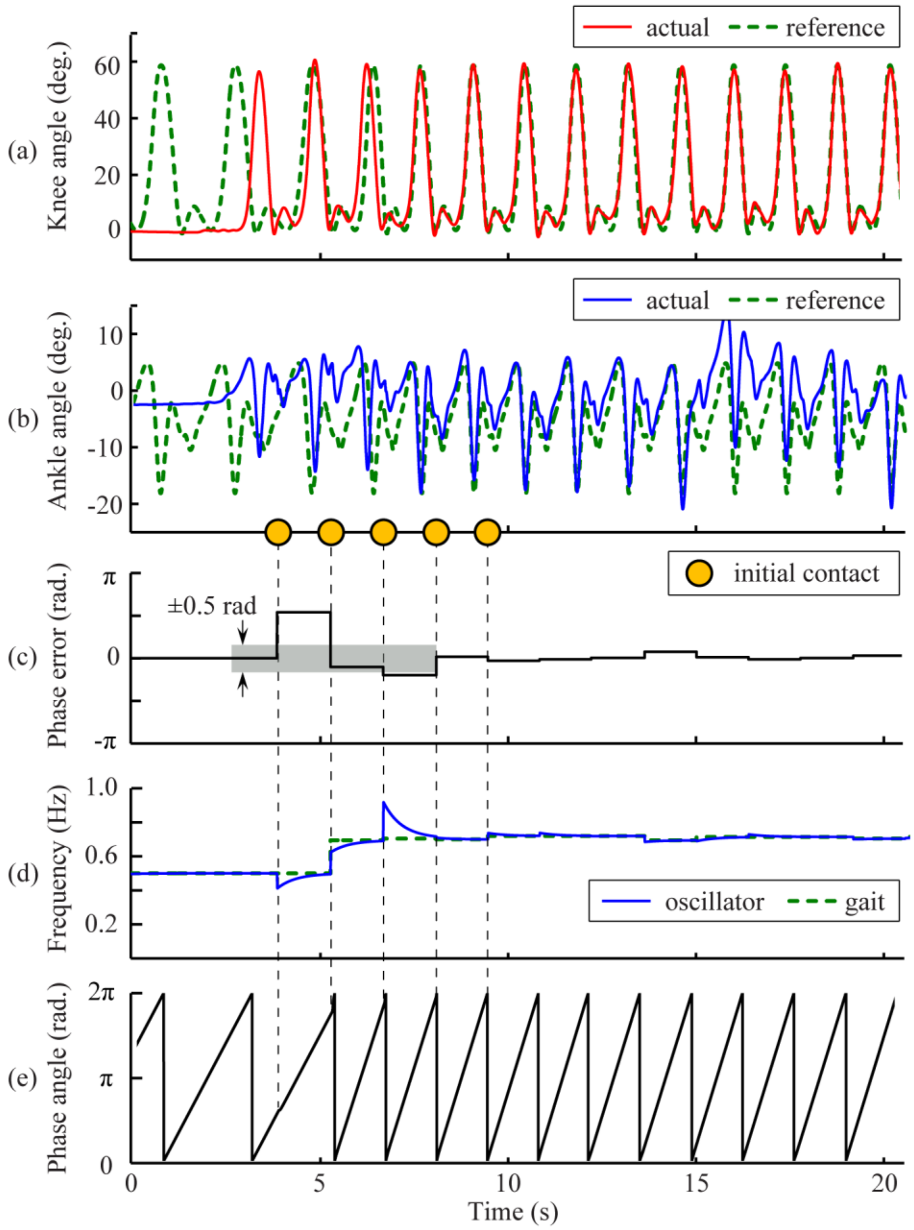

Figure 5-8. Experiment results of free walking using IC for synchronization, including (a) knee and (b) ankle joint angles; (c) phase error between the estimated phase and actual phase of gait; gray bar denotes the steps with phase error larger than 0.5 rad; (d) frequency of the adaptive oscillator and estimated frequency of the actual gait; (e) phase angle of the adaptive oscillator.

(B) ZA test.

This part describes the results of ZA mode to show the performance of the proposed algorithm with different gait events and experimental conditions. Without loss of generality, two gait events, OI ($\Phi_1 = 50\%$) and TV ($\Phi_2 = 87\%$), are used for synchronization.

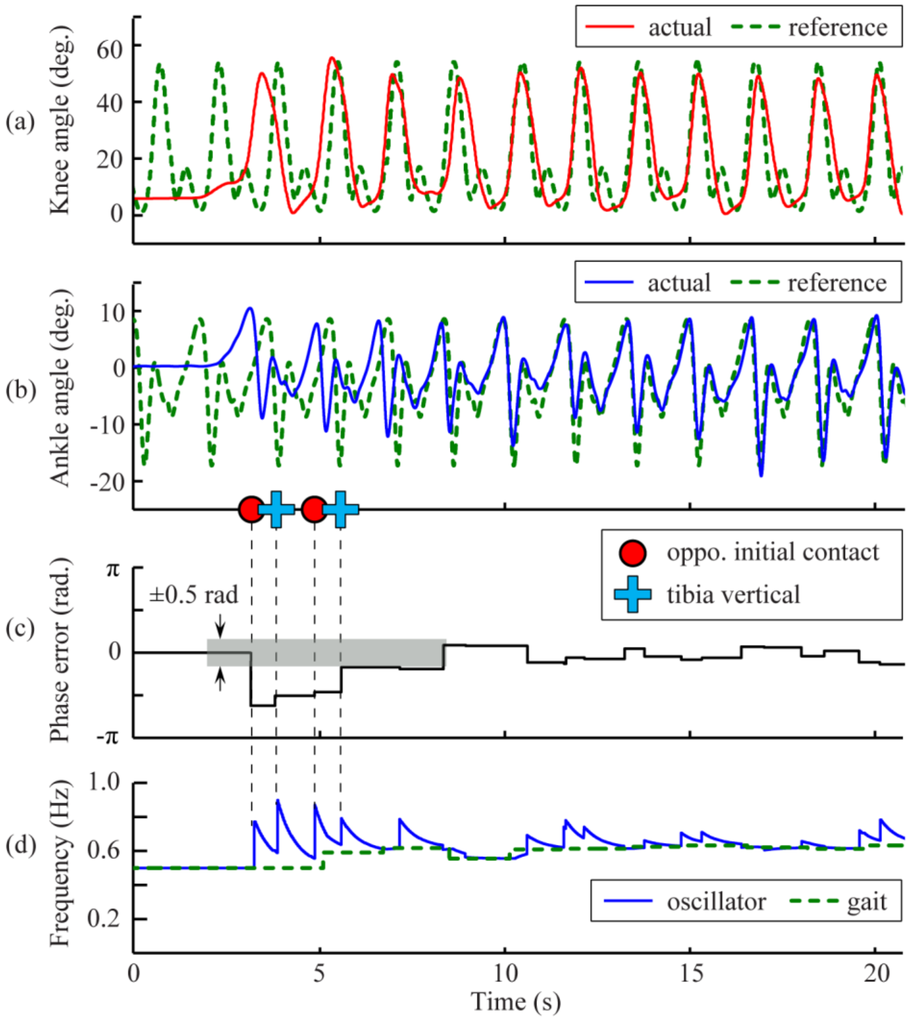

Figure 5-9. Experimental results of zero-assistive walking using OI and TV for synchronization, including (a) knee and (b) ankle joint angles; (c) phase error between the estimated phase and actual phase of gait; gray bar denotes the steps with phase error larger than 0.5 rad; (d) frequency of the adaptive oscillator and estimated frequency of the actual gait.

The results of the ZA test are shown in Figure 5-9. It is observed that the joint angles of the knee and ankle were slightly altered compared to those in the FW test (Figure 5-8(a) and (b)). The first peak in the knee joint angle was suppressed and the plantar flexion of the ankle joint was slightly reduced. This could be explained with the weight of the robot, which affects the subject's gait. However, the gait events were accurately detected in this condition (red circle and blue cross in Figure 5-9(c)) and synchronization was achieved with the proposed method.

In addition, the figure indicates that with the same parameters, when compared to the FW test, the phase error adaptation was faster with more gait events detected (Figure 5-9(c)). The synchronization was achieved after the third step, which was faster than the test where only one gait event was used for synchronization. The average phase error in the last six steps is 0.049 rad.

(C) SAW test.

Another SAW test was conducted to evaluate the reliability of the proposed strategy. Another two different gait events, HR ($\Phi_1 = 48\%$) and FA ($\Phi_2 = 77\%$), were used for synchronization.

Under this condition, the gait patterns of the knee and ankle joints were seriously altered (Figure 5-10(a) and (b)). The first peak of the knee joint angles was suppressed and the range of knee motion was significantly reduced; the plantar flexion of the ankle during push-off was also limited. However, the gait events could still be detected reliably, as shown in Figure 5-10(c) (green circle and orange triangle). Synchronization was achieved at the third step (Figure 5-10(c) shaded bar).

The average phase error in the last six steps in this figure is around 0.037 rad. This result indicates the robustness of the proposed synchronization method, since the gait events are the only information used for synchronization, which minimizes the influence of the abnormality in the gait pattern. The trajectory thus could be employed in the robot for reference.

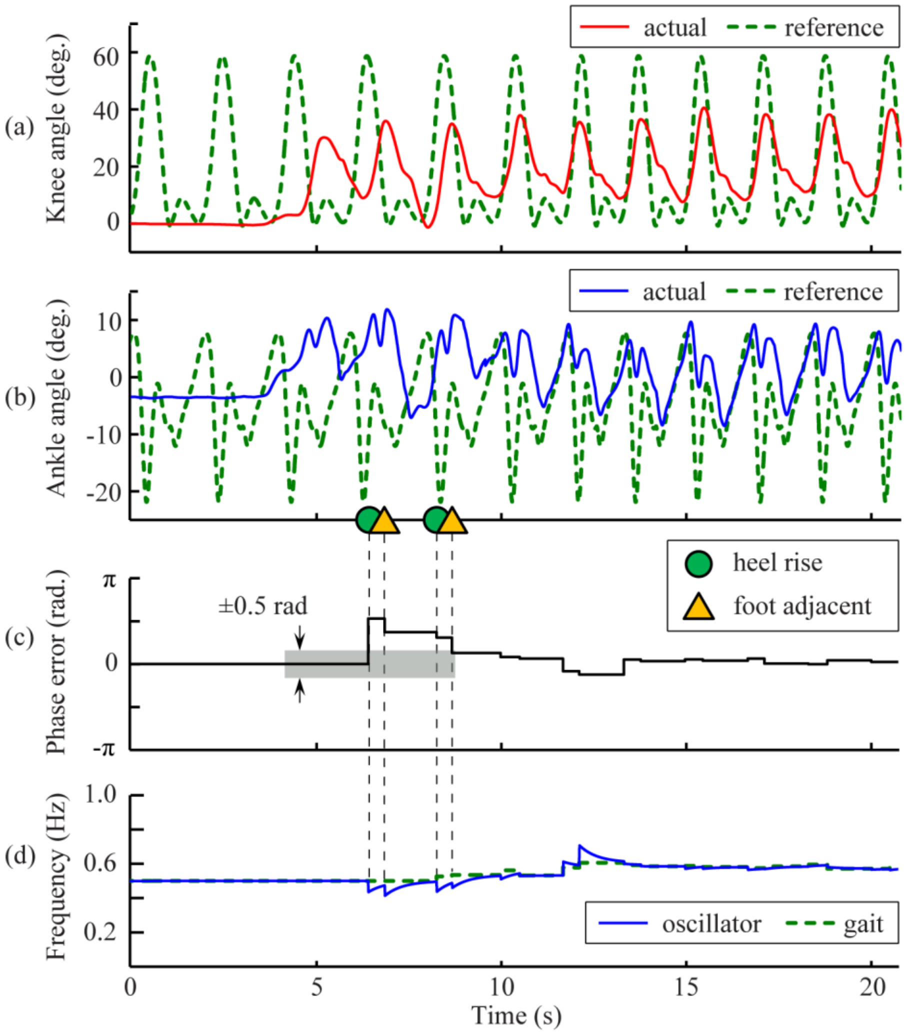

Figure 5-10. Experimental results of simulated abnormal walking using HR and FA for synchronization, including (a) knee and (b) ankle joint angles; (c) phase error between the estimated phase and actual phase of gait; gray bar denotes the steps with phase error larger than 0.5 rad; (d) frequency of the adaptive oscillator and estimated frequency of the actual gait.

4.2 Efficiency of the adaptive oscillator

Statistical results of experiments involving 15 subjects are presented in this section. Figure 5-11 and Table 5-2 show the mean and standard deviation of the steps needed to achieve human–robot synchronization ($|\Delta\phi| < 0.5$ rad) among all experiment conditions. From these results, it can be seen that the synchronization was achieved in less than four steps in all experiment conditions. The adaptation process was not elongated when an abnormal gait pattern was involved and repeated measures ANOVA failed to reach significance ($F(4,56) = 0.078, P = 0.99$). This was because the gait event was the only information needed to achieve synchronization and it minimized the influence of the abnormality on the gait pattern. This result demonstrated that the proposed control strategy was efficient and robust in achieving human–robot synchronization.

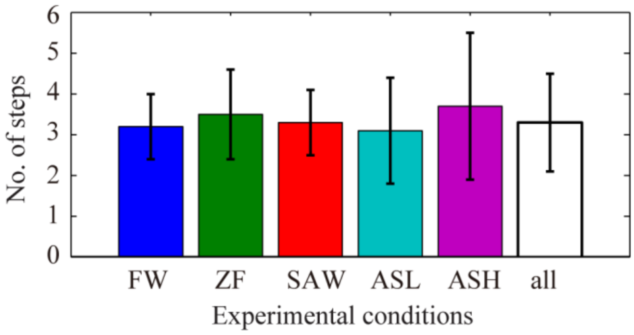

Figure 5-11. Number of steps needed to achieve human-robot synchronization in different experimental conditions.

4.3 Evidence of assistance

In this subsection, experimental results of the robot-assisted walking are shown. We first provide results of a representative subject to illustrate the performance; then provide statistical results across all the subjects.

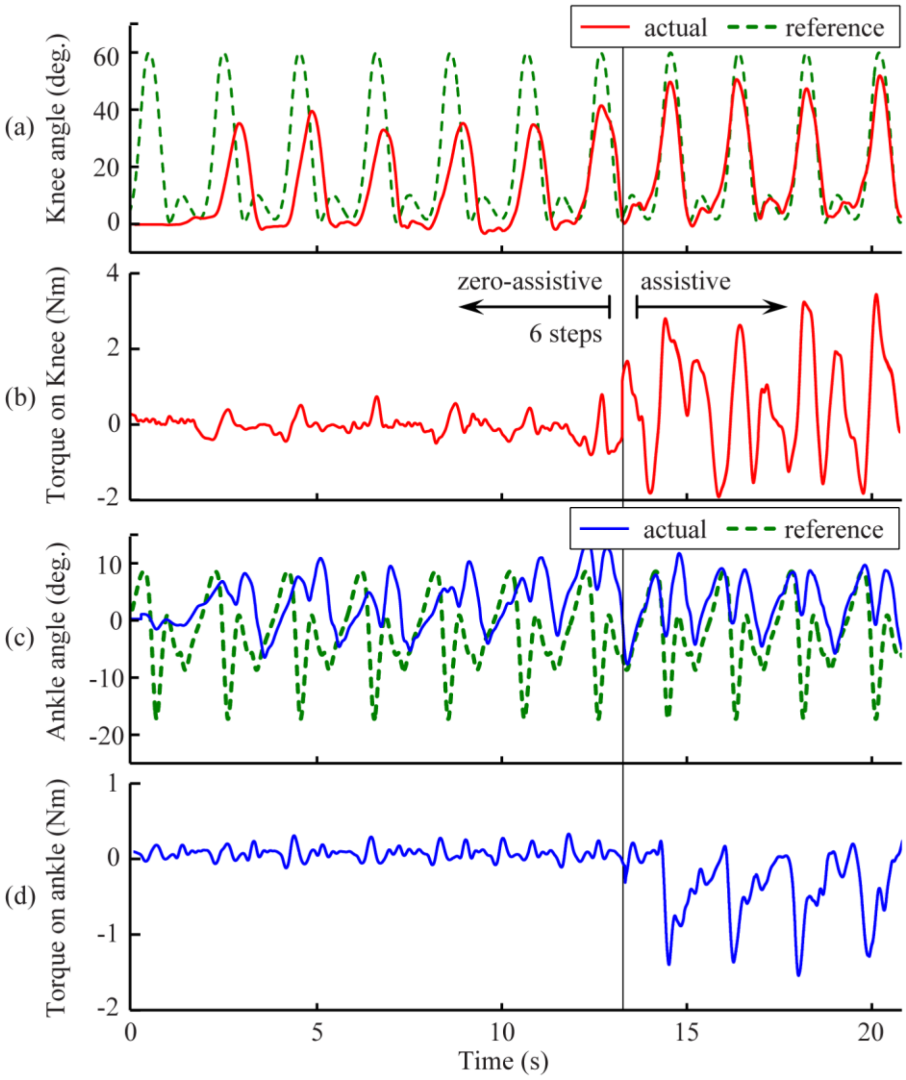

Figure 5-12. Experimental results of ASH, including the actual knee (a) and ankle (c) joint angles, and their corresponding oscillating reference trajectory; robotic assistive torque profiles on the knee (b) and ankle (d) joints.

The results of the ASH test on one representative subject are shown in Figure 5-12 as an example. According to the protocol, the robot worked in zero-assistive mode in the first six steps in order to achieve human-robot synchronization. In these steps, the gait patterns of the knee and ankle joints were seriously altered as in the SAW condition (Figure 5-10(a) and (c)). The desired assistive torque was zero and the robot tried to minimize the interaction torque (Figure 5-12(b) and (c)). Starting from the seventh step, the robot provided assistive torque during walking. It can be found that the human-robot synchronization has been achieved and the assistive torque was provided based on the deviation of the actual gait and the reference trajectories. The robotic assistive torque improved the gait pattern and pushed the actual gait pattern closer to the reference.

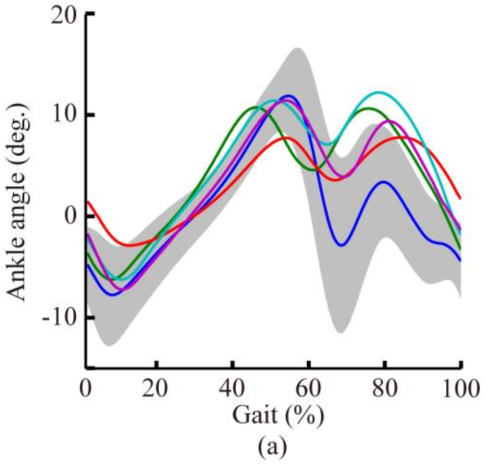

(a) (b)

Figure 5-13. Joint angles of (a) knee and (b) ankle in different experiment conditions. The gray shaded bar is the standard deviation of the joint angles in FW condition.

The averaged angles of the knee and ankle joints of all subjects in different experimental conditions are shown in Figure 5-13. The movement ranges of the ankle and knee joints are shown in Table 5-2. It can be seen that the kinematics of both ankle and knee were similar in FW (blue curve) and ZA (green curve). The range of motion for both knee and ankle joints were reduced in the SAW condition.

The gait pattern of the knee and ankle was improved with the assistance of the exoskeletal robot. The ankle angles in ASL and ASH were closer to that in FW, which was the reference trajectory of the robot. The motion range of the knee was extended compared to the SAW scenario. The peak knee angle was about 45° in ASL and 52° in ASH, which were significantly larger than that in the SAW condition. Repeated measures ANOVA reached significance, with a post hoc test establishing a significant difference among the two assisted conditions and the abnormal condition ($F(4,56) > 18.0$, $P < 0.0001$).

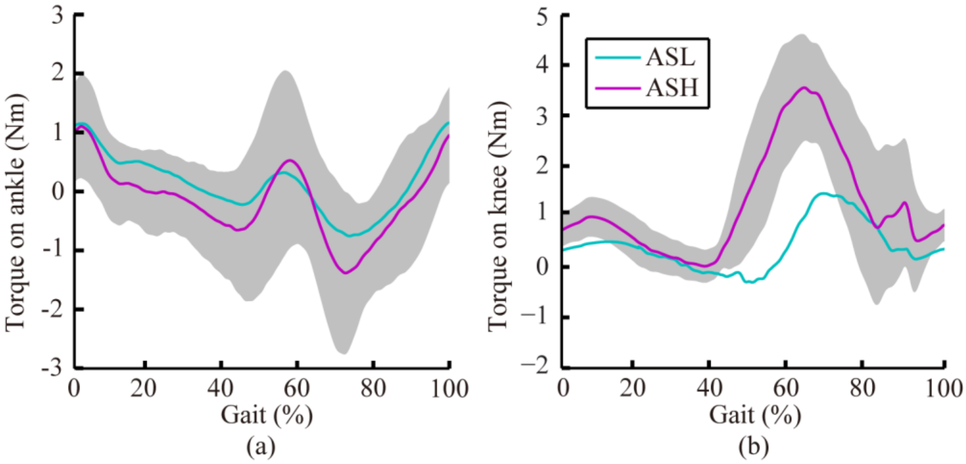

(a)

(b)

Figure 5-14. Assistive torque of knee and ankle in ASL and ASH conditions; the gray shaded bar is the standard deviation of the torque in ASH condition.

The averaged assistive torque profile across all subjects on the knee and ankle provided by the robot in ASL and ASH is shown in Figure 5-14. The standard deviation of the torque profile in ASH is also shown in the figure (gray-shaded bar). It can be seen that assistive torque was provided by the robot, which was based on the deviation of the actual knee and ankle positions from the reference trajectory. The assistive torque in ASH was relatively larger in amplitude than that in ASL, which resulted in a more improved gait pattern. This result indicated that the robot, by employing the proposed control strategy, was able to synchronize with the human gait and provide assistive torque to improve the gait pattern during overground walking.

Table 5-2. Relevant variables with different conditions

Variable	FW	ZA	SAW	ASL	ASH
Ankle movement range (deg.)	21.9±5.6	20.8±4.0	12.7±1.9	20.3±2.8	21.4±3.5
Knee movement range (deg.)	55.4±2.7	52.7±5.2	32.4±3.0	44.1±5.4	49.8±3.2

5. *Discussion*

This study provides a new solution for achieving human–robot synchronization in gait rehabilitation robotics. The principle of the proposed method is to achieve synchronization by estimating the stride percentage based on the gait-event information. The synchronization method can be applied to a wide range of control strategies, such as identifying the stance and swing phase [52, 157, 158], or applying FES synchronously [133, 134]. With the estimated stride percentage, reference trajectories can be easily generated for the robots with a LUT. In actual rehabilitation applications for patients with abnormal gait patterns, the LUT can be built with the trajectories recorded from healthy subjects [108], or clinical gait analysis (CGA) data

[159] and torque trajectory [145]. It should be noted that the reference trajectory for different joints can be generated with the same adaptive oscillator, instead of employing multiple oscillators [137].

The performance of the adaptive oscillator is determined by the parameters ε and P: ε decides how fast the frequency of the oscillator returns to the gait frequency, and ε and P collectively determine how quickly human–robot synchronization can be achieved. Generally, a relatively small ε should be employed to have gentle adaptation, which leads to a smooth reference trajectory. However, if ε is too small, the frequency of the oscillator cannot return to the gait frequency. In this condition, the frequency of the oscillator cannot converge and the adaptive oscillator cannot function stably. Instead, a relatively large P should be selected for the application so that the phase error can be decreased rapidly. A proper P that makes the system converge within four steps is suggested for application.

Figure 5-15 shows another experimental result in the FW test. The same gait event (IC) was employed for synchronization. The parameters of the oscillator were selected to be $\varepsilon = 0.02$ and $P = 5$. Compared to the FW result in Figure 5-8, a small P was selected in this test. It is observed that synchronization can be achieved with this configuration. However, phase error is reduced less in one gait cycle, and it takes more cycles (seven steps) to achieve synchronization.

Figure 5-16 shows the result of the third trial with the same gait event of IC used for synchronization. The parameters of the oscillator were selected to be $\varepsilon = 0.06$ and $P = 11$. Compared to the FW result in Figure 5-8, a large ε was employed in this test. From the result, it can be seen that the frequency of the oscillator returned to the estimated gait frequency faster, and the adaptation of the oscillator finished in a short period of time (Figure 5-16(b)), which could result in a sharp change in the reference trajectory.

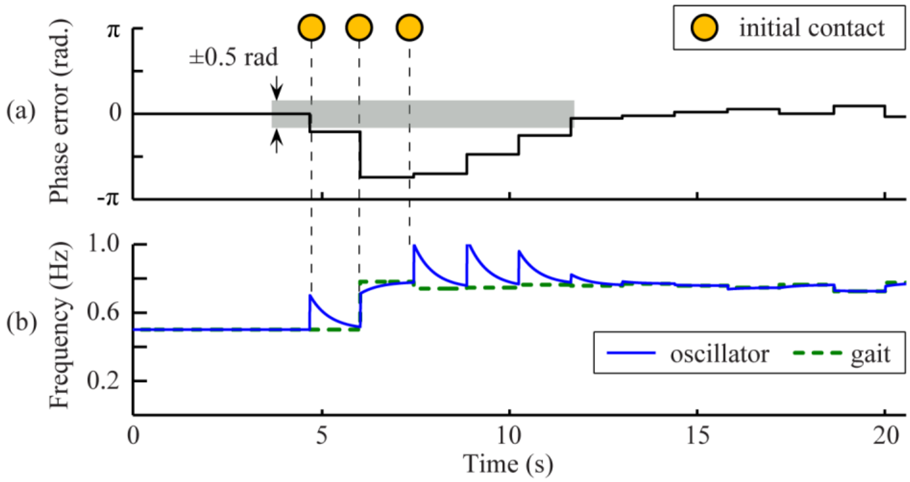

Figure 5-15. Experiment results of human–robot synchronization using IC, including (a) the phase error between the estimated phase and actual phase of the gait; gray bar denotes the steps with phase error larger than 0.5 rad; (b) the frequency of the adaptive oscillator and the estimated frequency of the actual gait. The parameters of the oscillator were selected to be $\varepsilon = 0.02$, $P = 5$.

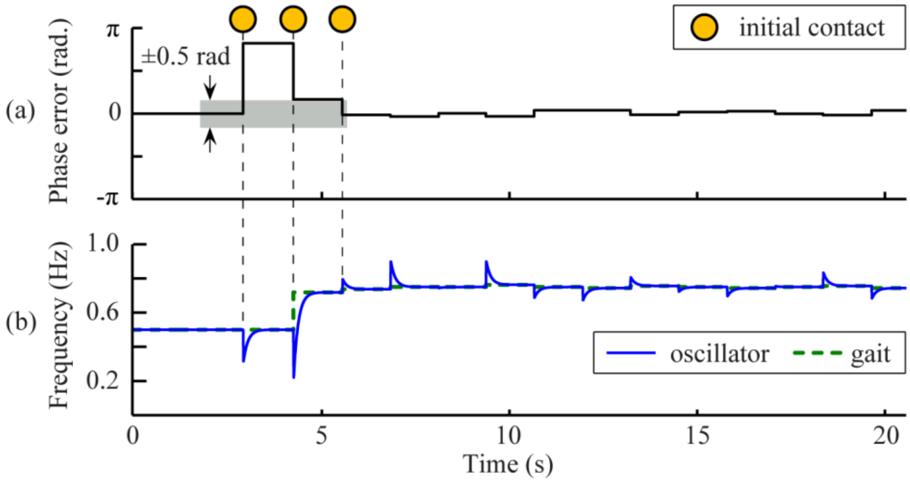

Figure 5-16. Experimental results of human–robot synchronization using IC, including (a) phase error between the estimated phase and the actual phase of the gait; gray bar denotes the steps with phase error larger than 0.5 rad; (b) the frequency of the adaptive oscillator and the estimated frequency of the actual gait. The parameters of the oscillator were selected to be $\varepsilon = 0.06$, $P = 11$.

The focus of this work is on the gait-event-based synchronization method. In order to evaluate the feasibility of the robotic application, we implemented the method in a rehabilitation exoskeletal robot. To further investigate the reliability of the synchronization method when interaction torque between the robot and the human is involved, we designed the impedance-based assistive control strategy for the robot. However, we found that there was very little robotic assistance during the assistive walking tests if the elastic band was not wrapped around the joints. That is because the experiment was conducted on healthy subjects whose gait trajectories were close to the synchronous reference, thus resulting in a small robotic assistive torque. This was confirmed by the kinematics result (Figure 5-9, ZA condition). Hence, we designed the SAW condition so the gait pattern was seriously altered and greater assistive torque could be induced. In the proposed method, the frequency of the gait is estimated using the duration between successive gait events. If the detection of a gait event is delayed or lost, the frequency estimation will be less accurate, which deteriorates the performance of the synchronization. The reliability of the adaptive oscillator can be further improved with a more robust estimator of the gait frequency, such as the aforementioned adaptive oscillator, which can extract the frequency information through gait kinematics [145].

In the experiment, we set up an abnormal walking condition in healthy subjects to simulate the abnormal gait pattern of stroke patients. Significant decrease in the range of motion of both the knee and ankle joints was observed and human–robot synchronization was still achieved. However, the pathological conditions in clinical practice can be more complicated. The feasibility and robustness of the proposed synchronization method should be further investigated with clinical experiments. The potential solution is to find the available gait events in several pre-training trials and employ one or more gait events for synchronization.

6. Summary

In this chapter, a novel method to achieve human–robot synchronization has been proposed for robot-aided gait training. This method is inspired by the phenomenon of the synchronous flashing of fireflies, which implies that synchronization can be achieved based on compulsive signals – the gait events in our work. The gait events are detected in real time during overground walking based on HMM. An adaptive oscillator has been developed to estimate the stride percentage of the human gait based on the gait events. Reference trajectories synchronous to the human gait are then generated according to the estimated phase.

Based on this synchronous reference trajectory, an impedance-based assistive control strategy is implemented on our portable exoskeleton robot for gait training. Experiments have been conducted on 15 healthy subjects, which show that 1) the adaptive oscillator has a simple structure and is easy to implement; 2) the proposed algorithm is effective at achieving synchronization with the gait events; 3) our method is efficient in adaptation (in less than four steps); 4) this method is robust in synchronization with abnormal gait patterns so it is applicable to clinical application; and 5) the implementation into rehabilitation robots is feasible and robotic assistance can be effectively delivered to the subjects based on the synchronous reference trajectories.

Chapter 6

Conclusion and Recommended Future Work

Conclusion of this thesis and recommended future work are summarized in this chapter.

1. Conclusion

In this project, we have developed a robotic exoskeleton system that can provide overground gait rehabilitation training to stroke patients. The main contributions of this thesis are presented in Chapter 3, Chapter 4 and Chapter 5.

Chapter 3 presents the mechanical design and experimental evaluation of a compact, portable, wearable exoskeleton robot. A novel SEA utilizes two springs in series with different stiffness to achieve back-drivability, large force range and low output impedance for safe human robot interaction. The SEA design is proposed as a solution to overcome the limitation of conventional SEA design. The mechanism for the joint motion was designed and optimized based on gait biomechanics. The actuator modeling and force controller design are presented; and an excellent force tracking performance is achieved. Overground walking trials on healthy subjects demonstrated accurate force tracking performance of the novel actuators. Muscle activation was reduced gradually with increased levels of assistance, demonstrating that the robot can provide stable and effective assistive forces during gait cycles.

Chapter 4 presented a human-robot interaction controller based on the SEA model. By combining joint motion compensation, friction compensation, a disturbance observer and feedback control, this controller can implement human-robot interaction control ranging from human-in-charge mode to assistive mode. Theoretical analysis for the proposed controller has proven that it can guarantee the stability of the human-robot interaction. Experimental results have confirmed that the proposed controller can achieve stable force control with good performance in different modes for the rehabilitation ankle robot.

Chapter 5 presents a control strategy for rehabilitation robot to provide assistive overground gait training. The major novelty in this control strategy is the development of a human–robot synchronization method using gait events information. The gait events are detected in real time during overground walking based on HMM. An adaptive oscillator has been developed to estimate the stride percentage of the human gait based on the detected gait events. Reference trajectories synchronous to the human gait are then generated according to the estimated phase. An impedance-based assistive control strategy is implemented to provide gait training according to the synchronous reference trajectory. Experimental results show that 1) the adaptive oscillator has a simple structure and is easy to implement; 2) the proposed algorithm is effective at achieving synchronization with the gait-event information; 3) our method is efficient in adaptation (in less than four steps); 4) this method is robust in synchronization with abnormal gait patterns so it is applicable to clinical application; and 5) the implementation into rehabilitation robots is feasible and robotic assistance can be effectively delivered to the subjects.

The major limitation of this project is: due to the constrained availability of clinical trials with stroke patients, we have only conducted healthy subjects experiment to evaluate this robotic system. Although decent experimental results have been achieved, the proposed robotic system should be further tested with stroke patients. Varieties of symptoms can be found in the patients, which are interesting topics to be investigated.

2. Recommended future work

In this thesis, we developed a prototype of a portable exoskeleton robotic system for gait rehabilitation, which shows some promise in the rehabilitation application. The following points present possible directions in our future developments.

In our current prototype, we implemented actuated joints for the knee and ankle of the right leg. Considering more general applications, a full exoskeleton that can provide assistance to the hip, knee and ankle joints for both legs can be developed. Multiple DoFs in the hip and ankle joints should also be considered to facilitate a natural gait. Fortunately, we employed modular design in our robot, which can be easily extended to the other joints.

In Chapter 5, a human-robot synchronization method is developed. This method can be applied into a wide range of gait rehabilitation applications. In the next stage, we will develop advanced intelligent control strategies based on the synchronous reference trajectory. For example, we intended to provide assistance within certain gait phases instead of the whole gait cycles. Impedance control with varying adaptive impedance configuration will be implemented.

In this thesis, the design of the robot and the control strategies are evaluated with experiment on healthy subjects. In the next stage, we will conduct clinical experiments to evaluate the effectiveness of our system and try to achieve good rehabilitation progress in patients.

BIBLIOGRAPHY

[1] D. Mozaffarian, E. J. Benjamin, A. S. Go, D. K. Arnett, M. J. Blaha, M. Cushman, S. de Ferranti, J.-P. Després, H. J. Fullerton, and V. J. Howard, "Heart Disease and Stroke Statistics—2015 Update A Report From the American Heart Association," *Circulation,* vol. 131, pp. e29-e322, 2015.

[2] A. S. Go, D. Mozaffarian, V. L. Roger, E. J. Benjamin, J. D. Berry, W. B. Borden, D. M. Bravata, S. Dai, E. S. Ford, and C. S. Fox, "Heart disease and stroke statistics--2013 update: a report from the American Heart Association," *Circulation*, vol. 127, p. e6, 2013.

[3] C. R. Gross, D. Shinar, J. P. Mohr, D. B. Hier, L. R. Caplan, T. R. Price, P. A. Wolf, C. S. Kase, I. G. Fishman, and S. Calingo, "Interobserver agreement in the diagnosis of stroke type," *Archives of Neurology,* vol. 43, pp. 893-898, 1986.

[4] N. Khodaparast, S. A. Hays, A. M. Sloan, D. R. Hulsey, A. Ruiz, M. Pantoja, R. L. Rennaker, 2nd, and M. P. Kilgard, "Vagus nerve stimulation during rehabilitative training improves forelimb strength following ischemic stroke," *Neurobiol Dis,* vol. 60, pp. 80-8, Dec 2013.

[5] P. A. Goldie, T. A. Matyas, and O. M. Evans, "Deficit and change in gait velocity during rehabilitation after stroke," *Archives of Physical Medicine and Rehabilitation,* vol. 77, pp. 1074-1082, 10// 1996.

[6] S. J. Olney and C. Richards, "Hemiparetic gait following stroke. Part I: Characteristics," *Gait & Posture,* vol. 4, pp. 136-148, 4// 1996.

[7] A. Pennycott, D. Wyss, H. Vallery, V. Klamroth-Marganska, and R. Riener, "Towards more effective robotic gait training for stroke rehabilitation: a review," *J Neuroeng Rehabil,* vol. 9, p. 65, 2012.

[8] J. M. Potter, A. L. Evans, and G. Duncan, "Gait speed and activities of daily living function in geriatric patients," *Archives of physical medicine and rehabilitation,* vol. 76, pp. 997-999, 1995.

[9] C. M. Mumma, "Perceived Losses Following Stroke," *Rehabilitation Nursing,* vol. 11, pp. 19-24, 1986.

[10] E. Dietrichs, "[Brain plasticity after stroke--implications for post-stroke rehabilitation]," *Tidsskrift for den Norske laegeforening: tidsskrift for praktisk medicin, ny raekke,* vol. 127, pp. 1228-1231, 2007.

[11] B. B. Johansson, "Brain plasticity and stroke rehabilitation The Willis lecture," *Stroke,* vol. 31, pp. 223-230, 2000.

[12] B. Langhammer and J. K. Stanghelle, "Bobath or motor relearning programme? A comparison of two different approaches of physiotherapy in stroke rehabilitation: a randomized controlled study," *Clinical Rehabilitation,* vol. 14, pp. 361-9, Aug 2000.

[13] R. Dickstein, "Rehabilitation of gait speed after stroke: a critical review of intervention approaches," *Neurorehabilitation and Neural Repair,* 2008.

[14] S. Hesse, C. Bertelt, A. Schaffrin, M. Malezic, and K.-H. Mauritz, "Restoration of gait in nonambulatory hemiparetic patients by treadmill training with partial body-weight support," *Archives of physical medicine and rehabilitation,* vol. 75, pp. 1087-1093, 1994.

[15] B. H. Dobkin, "An overview of treadmill locomotor training with partial body weight support: a neurophysiologically sound approach whose time has come for randomized clinical trials," *Neurorehabilitation and neural repair,* vol. 13, pp. 157-165, 1999.

[16] C. Werner, S. Von Frankenberg, T. Treig, M. Konrad, and S. Hesse, "Treadmill Training With Partial Body Weight Support and an Electromechanical Gait Trainer for Restoration of Gait in Subacute Stroke Patients A Randomized Crossover Study," *Stroke,* vol. 33, pp. 2895-2901, 2002.

[17] R. Riener, L. Lunenburger, S. Jezernik, M. Anderschitz, G. Colombo, and V. Dietz, "Patient-cooperative strategies for robot-aided treadmill training: First experimental results," *Ieee Transactions on Neural Systems and Rehabilitation Engineering,* vol. 13, pp. 380-394, Sep 2005.

[18] M. Wirz, D. H. Zemon, R. Rupp, A. Scheel, G. Colombo, V. Dietz, and T. G. Hornby, "Effectiveness of automated locomotor training in patients with chronic incomplete spinal cord injury: A multicenter trial," *Archives of Physical Medicine and Rehabilitation,* vol. 86, pp. 672-680, Apr 2005.

[19] D. J. Reinkensmeyer, J. L. Emken, and S. C. Cramer, "Robotics, motor learning, and neurologic recovery," *Annual Review of Biomedical Engineering,* vol. 6, pp. 497-525, 2004.

[20] J. Hidler, D. Nichols, M. Pelliccio, and K. Brady, "Advances in the understanding and treatment of stroke impairment using robotic devices," *Topics in stroke rehabilitation,* vol. 12, pp. 22-35, 2005.

[21] A. M. Dollar and H. Herr, "Lower extremity exoskeletons and active orthoses: Challenges and state-of-the-art," *Ieee Transactions on Robotics,* vol. 24, pp. 144-158, Feb 2008.

[22] G. Chen, C. K. Chan, Z. Guo, and H. Yu, "A review of lower extremity assistive robotic exoskeletons in rehabilitation therapy," *Critical Reviews™ in Biomedical Engineering,* vol. 41, 2013.

[23] M. M. Zhang, T. C. Davies, and S. N. Xie, "Effectiveness of robot-assisted therapy on ankle rehabilitation - a systematic review," *Journal of Neuroengineering and Rehabilitation,* vol. 10, Mar 21 2013.

[24] A. Pennycott, D. Wyss, H. Vallery, V. Klamroth-Marganska, and R. Riener, "Towards more effective robotic gait training for stroke rehabilitation: a review," *Journal of Neuroengineering and Rehabilitation,* vol. 9, p. 65, 2012.

[25] J. Cao, S. Q. Xie, R. Das, and G. L. Zhu, "Control strategies for effective robot assisted gait rehabilitation: The state of art and future prospects," *Medical Engineering & Physics,* vol. 36, pp. 1555-1566, 2014.

[26] M. F. Ng, R. K. Tong, and L. S. Li, "A pilot study of randomized clinical controlled trial of gait training in subacute stroke patients with partial body-

weight support electromechanical gait trainer and functional electrical stimulation six-month follow-up," *Stroke,* vol. 39, pp. 154-160, 2008.

[27] W. H. Chang, M. S. Kim, J. P. Huh, P. K. Lee, and Y.-H. Kim, "Effects of Robot-Assisted Gait Training on Cardiopulmonary Fitness in Subacute Stroke Patients A Randomized Controlled Study," *Neurorehabilitation and Neural Repair,* vol. 26, pp. 318-324, 2012.

[28] M. Pohl, C. Werner, M. Holzgraefe, G. Kroczek, I. Wingendorf, G. Hoölig, R. Koch, and S. Hesse, "Repetitive locomotor training and physiotherapy improve walking and basic activities of daily living after stroke: a single-blind, randomized multicentre trial (DEutsche GAngtrainerStudie, DEGAS)," *Clinical Rehabilitation,* vol. 21, pp. 17-27, 2007.

[29] S. Fisher, L. Lucas, and T. Adam Thrasher, "Robot-assisted gait training for patients with hemiparesis due to stroke," *Topics in Stroke Rehabilitation,* vol. 18, pp. 269-276, 2011.

[30] B. Husemann, F. Müller, C. Krewer, S. Heller, and E. Koenig, "Effects of locomotion training with assistance of a robot-driven gait orthosis in hemiparetic patients after stroke a randomized controlled pilot study," *Stroke,* vol. 38, pp. 349-354, 2007.

[31] J. Hidler, D. Nichols, M. Pelliccio, K. Brady, D. D. Campbell, J. H. Kahn, and T. G. Hornby, "Multicenter randomized clinical trial evaluating the effectiveness of the Lokomat in subacute stroke," *Neurorehabilitation and Neural Repair,* vol. 23, pp. 5-13, 2009.

[32] S. Morrison, "Financial feasibility of robotics in neurorehabilitation," *Topics in spinal cord injury rehabilitation,* vol. 17, pp. 77-81, 2011.

[33] R. G. Burdett, D. Borello-France, C. Blatchly, and C. Potter, "Gait comparison of subjects with hemiplegia walking unbraced, with ankle-foot orthosis, and with Air-Stirrup® brace," *Physical Therapy,* vol. 68, pp. 1197-1203, 1988.

[34] D. Wade, V. Wood, A. Heller, J. Maggs, and H. R. Langton, "Walking after stroke. Measurement and recovery over the first 3 months," *Scandinavian Journal of Rehabilitation Medicine,* vol. 19, pp. 25-30, 1986.

[35] M. Grun, R. Muller, and U. Konigorski, "Model Based Control of Series Elastic Actuators," *2012 4th Ieee Ras & Embs International Conference on Biomedical Robotics and Biomechatronics (Biorob),* pp. 538-543, 2012.

[36] K. Kong, J. Bae, and M. Tomizuka, "Control of Rotary Series Elastic Actuator for Ideal Force-Mode Actuation in Human-Robot Interaction Applications," *Ieee-Asme Transactions on Mechatronics,* vol. 14, pp. 105-118, Feb 2009.

[37] H. Sadeghian, M. Keshmiri, L. Villani, and B. Siciliano, "Null-space impedance control with disturbance observer," in *Intelligent Robots and Systems (IROS), 2012 IEEE/RSJ International Conference on,* 2012, pp. 2795-2800.

[38] M. Pietrusinski, I. Cajigas, Y. Mizikacioglu, M. Goldsmith, P. Bonato, and C. Mavroidis, "Gait Rehabilitation therapy using robot generated force fields applied at the pelvis," in *Haptics Symposium, 2010 IEEE,* 2010, pp. 401-407.

[39] G. Colombo, M. Joerg, R. Schreier, and V. Dietz, "Treadmill training of paraplegic patients using a robotic orthosis," *Journal of Rehabilitation Research and Development*, vol. 37, pp. 693-700, Nov-Dec 2000.

[40] "http://www.motorika.com/?categoryId=65108."

[41] P. C. Kao, S. Srivastava, S. K. Agrawal, and J. P. Scholz, "Effect of robotic performance-based error-augmentation versus error-reduction training on the gait of healthy individuals," *Gait & Posture*, vol. 37, pp. 113-120, Jan 2013.

[42] J. F. Veneman, R. Kruidhof, E. E. G. Hekman, R. Ekkelenkamp, E. H. F. Van Asseldonk, and H. van der Kooij, "Design and evaluation of the LOPES exoskeleton robot for interactive gait rehabilitation," *Ieee Transactions on Neural Systems and Rehabilitation Engineering*, vol. 15, pp. 379-386, Sep 2007.

[43] S. Hussain, S. Q. Xie, P. K. Jamwal, and J. Parsons, "An intrinsically compliant robotic orthosis for treadmill training," *Medical Engineering & Physics*, vol. 34, pp. 1448-1453, Dec 2012.

[44] D. J. Reinkensmeyer, D. Aoyagi, J. L. Emken, J. A. Galvez, W. Ichinose, G. Kerdanyan, S. Maneekobkunwong, K. Minakata, J. A. Nessler, R. Weber, R. R. Roy, R. de Leon, J. E. Bobrow, S. J. Harkema, and V. R. Edgerton, "Tools for understanding and optimizing robotic gait training," *Journal of Rehabilitation Research and Development*, vol. 43, pp. 657-670, Aug-Sep 2006.

[45] S. Hesse and D. Uhlenbrock, "A mechanized gait trainer for restoration of gait," *Journal of Rehabilitation Research and Development*, vol. 37, pp. 701-708, 2000.

[46] S. Freivogel, J. Mehrholz, T. Husak-Sotomayor, and D. Schmalohr, "Gait training with the newly developed'LokoHelp'-system is feasible for non-ambulatory patients after stroke, spinal cord and brain injury. A feasibility study," *Brain Injury*, vol. 22, pp. 625-632, 2008.

[47] "https://www.hocoma.com/usa/us/products/erigo/."

[48] C. Schmitt, P. Métrailler, A. Al-Khodairy, R. Brodard, J. Fournier, M. Bouri, and R. Clavel, "The Motion Maker™: a Rehabilitation System Combining an Orthosis with Closed-Loop Electrical Muscle Stimulation," in *Proceedings of the 8th Vienna International Workshop in Functional Electrical Stimulation*, 2004, pp. 117-20.

[49] M. Bouri, B. Le Gall, and R. Clavel, "A new concept of parallel robot for rehabilitation and fitness: the Lambda," in *Robotics and Biomimetics (ROBIO), 2009 IEEE International Conference on*, 2009, pp. 2503-2508.

[50] W. Wang, Z.-G. Hou, L. Tong, F. Zhang, Y. Chen, and M. Tan, "A novel leg orthosis for lower limb rehabilitation robots of the sitting/lying type," *Mechanism and Machine Theory*, vol. 74, pp. 337-353, 2014.

[51] A. Roy, H. I. Krebs, D. J. Williams, C. T. Bever, L. W. Forrester, R. M. Macko, and N. Hogan, "Robot-Aided Neurorehabilitation: A Novel Robot for Ankle Rehabilitation," *Ieee Transactions on Robotics*, vol. 25, pp. 569-582, Jun 2009.

[52] J. A. Blaya and H. Herr, "Adaptive control of a variable-impedance ankle-foot orthosis to assist drop-foot gait," *Ieee Transactions on Neural Systems and Rehabilitation Engineering,* vol. 12, pp. 24-31, Mar 2004.

[53] D. P. Ferris, J. M. Czerniecki, and B. Hannaford, "An ankle-foot orthosis powered by artificial pneumatic muscles," *Journal of Applied Biomechanics,* vol. 21, pp. 189-197, May 2005.

[54] A. C. Satici, A. Erdogan, and V. Patoglu, "Design of a reconfigurable ankle rehabilitation robot and its use for the estimation of the ankle impedance," in *Rehabilitation Robotics, 2009. ICORR 2009. IEEE International Conference on*, 2009, pp. 257-264.

[55] G. Zeilig, H. Weingarden, M. Zwecker, I. Dudkiewicz, A. Bloch, and A. Esquenazi, "Safety and tolerance of the ReWalk (TM) exoskeleton suit for ambulation by people with complete spinal cord injury: A pilot study," *Journal of Spinal Cord Medicine,* vol. 35, pp. 96-101, Mar 2012.

[56] "http://eksobionics.com/."

[57] G. S. Sawicki and D. P. Ferris, "A pneumatically powered knee-ankle-foot orthosis (KAFO) with myoelectric activation and inhibition," *Journal of Neuroengineering and Rehabilitation,* vol. 6, Jun 23 2009.

[58] H. Kawamoto and Y. Sankai, "Comfortable power assist control method for walking aid by HAL-3," in *Systems, Man and Cybernetics, 2002 IEEE International Conference on*, 2002, p. 6 pp. vol. 4.

[59] B. J. Ruthenberg, N. A. Wasylewski, and J. E. Beard, "An experimental device for investigating the force and power requirements of a powered gait orthosis," *Journal of Rehabilitation Research and Development,* vol. 34, pp. 203-214, 1997.

[60] S. Murray, K. H. Ha, C. Hartigan, and M. Goldfarb, "An Assistive Control Approach for a Lower-Limb Exoskeleton to Facilitate Recovery of Walking following Stroke," 2015.

[61] "https://www.hocoma.com/usa/us/products/andago/."

[62] J. Patton, D. A. Brown, M. Peshkin, J. J. Santos-Munne, A. Makhlin, E. Lewis, J. E. Colgate, and D. Schwandt, "KineAssist: Design and development of a robotic overground gait and balance therapy device," *Topics in Stroke Rehabilitation,* vol. 15, pp. 131-139, Mar-Apr 2008.

[63] K.-R. Mun, Z. Guo, and H. Yu, "Development and evaluation of a novel overground robotic walker for pelvic motion support," in *Rehabilitation Robotics (ICORR), 2015 IEEE International Conference on*, 2015, pp. 95-100.

[64] Y. Stauffer, Y. Allemand, M. Bouri, J. Fournier, R. Clavel, P. Metrailler, R. Brodard, and F. Reynard, "The WalkTrainer—a new generation of walking reeducation device combining orthoses and muscle stimulation," *Neural Systems and Rehabilitation Engineering, IEEE Transactions on,* vol. 17, pp. 38-45, 2009.

[65] K. C. Kong and D. Jeon, "Design and control of an exoskeleton for the elderly and patients," *Ieee-Asme Transactions on Mechatronics,* vol. 11, pp. 428-432, Aug 2006.

[66] Z. Guo, Y. Fan, J. Zhang, H. Yu, and Y. Yin, "A new 4m model-based human-machine interface for lower extremity exoskeleton robot," in *Intelligent Robotics and Applications*, ed: Springer, 2012, pp. 545-554.

[67] T. P. Luu, H. Lim, X. Qu, and K. Low, "Pelvic motion assistance of NaTUre-gaits with adaptive body weight support," in *Control Conference (ASCC), 2011 8th Asian*, 2011, pp. 950-955.

[68] G. R. West, "Powered gait orhtosis and method of utilizing same," 6689075, 2004.

[69] S. K. Banala, S. K. Agrawal, and J. P. Scholz, "Active Leg Exoskeleton (ALEX) for gait rehabilitation of motor-impaired patients," *2007 Ieee 10th International Conference on Rehabilitation Robotics, Vols 1 and 2*, pp. 401-407, 2007.

[70] K. N. Winfree, P. Stegall, and S. K. Agrawal, "Design of a Minimally Constraining, Passively Supported Gait Training Exoskeleton: ALEX II," *2011 Ieee International Conference on Rehabilitation Robotics (Icorr)*, 2011.

[71] D. Zanotto, P. Stegall, and S. K. Agrawal, "ALEX III: A novel robotic platform with 12 DOFs for human gait training," in *Robotics and Automation (ICRA), 2013 IEEE International Conference on*, 2013, pp. 3914-3919.

[72] R. van den Brand, J. Heutschi, Q. Barraud, J. DiGiovanna, K. Bartholdi, M. Huerlimann, L. Friedli, I. Vollenweider, E. M. Moraud, S. Duis, N. Dominici, S. Micera, P. Musienko, and G. Courtine, "Restoring Voluntary Control of Locomotion after Paralyzing Spinal Cord Injury," *Science*, vol. 336, pp. 1182-1185, Jun 1 2012.

[73] S. J. Lee and J. Hidler, "Biomechanics of overground vs. treadmill walking in healthy individuals," *Journal of Applied Physiology*, vol. 104, pp. 747-755, Mar 2008.

[74] K. Kong, H. Moon, B. Hwang, D. Jeon, and M. Tomizuka, "Impedance Compensation of SUBAR for Back-Drivable Force-Mode Actuation," *Ieee Transactions on Robotics*, vol. 25, pp. 512-521, Jun 2009.

[75] P. Wang, K. H. Low, A. Tow, and P. H. Lim, "Initial System Evaluation of an Overground Rehabilitation Gait Training Robot (NaTUre-gaits)," *Advanced Robotics*, vol. 25, pp. 1927-1948, 2011.

[76] A. Esquenazi, M. Talaty, A. Packel, and M. Saulino, "The ReWalk Powered Exoskeleton to Restore Ambulatory Function to Individuals with Thoracic-Level Motor-Complete Spinal Cord Injury," *American Journal of Physical Medicine & Rehabilitation*, vol. 91, pp. 911-921, Nov 2012.

[77] S. Wang, L. Wang, C. Meijneke, E. van Asseldonk, T. Hoellinger, G. Cheron, Y. Ivanenko, V. La Scaleia, F. Sylos-Labini, and M. Molinari, "Design and Control of the MINDWALKER Exoskeleton," *Neural Systems and Rehabilitation Engineering, IEEE Transactions on*, vol. 23, pp. 277-286, 2015.

[78] J. Ghan, R. Steger, and H. Kazerooni, "Control and system identification for the Berkeley lower extremity exoskeleton (BLEEX)," *Advanced Robotics*, vol. 20, pp. 989-1014, 2006.

[79] K. Amundson, J. Raade, N. Harding, and H. Kazerooni, "Development of hybrid hydraulic-electric power units for field and service robots," *Advanced Robotics*, vol. 20, pp. 1015-1034, 2006.

[80] S. Hussain, S. Q. Xie, and P. K. Jamwal, "Robust Nonlinear Control of an Intrinsically Compliant Robotic Gait Training Orthosis."

[81] R. v. Ham, T. Sugar, B. Vanderborght, K. Hollander, and D. Lefeber, "Compliant actuator designs," *Robotics & Automation Magazine, IEEE,* vol. 16, pp. 81-94, 2009.

[82] R. Schiavi, G. Grioli, S. Sen, and A. Bicchi, "VSA-II: A novel prototype of variable stiffness actuator for safe and performing robots interacting with humans," *2008 Ieee International Conference on Robotics and Automation, Vols 1-9*, pp. 2171-2176, 2008.

[83] S. Wolf and G. Hirzinger, "A new variable stiffness design: Matching requirements of the next robot generation," in *Robotics and Automation, 2008. ICRA 2008. IEEE International Conference on*, 2008, pp. 1741-1746.

[84] G. A. Pratt and M. M. Williamson, "Series elastic actuators," in *Intelligent Robots and Systems 95.'Human Robot Interaction and Cooperative Robots', Proceedings. 1995 IEEE/RSJ International Conference on*, 1995, pp. 399-406.

[85] T. G. Sugar, "A novel selective compliant actuator," *Mechatronics,* vol. 12, pp. 1157-1171, 2002.

[86] D. W. Robinson, J. E. Pratt, D. J. Paluska, and G. A. Pratt, "Series elastic actuator development for a biomimetic walking robot," in *Advanced Intelligent Mechatronics, 1999. Proceedings. 1999 IEEE/ASME International Conference on*, 1999, pp. 561-568.

[87] D. W. Robinson, "Design and analysis of series elasticity in closed-loop actuator force control," Massachusetts Institute of Technology, 2000.

[88] M. M. Williamson, "Series elastic actuators," 1995.

[89] H. Yu, S. Huang, G. Chen, S.-L. Toh, M. S. Cruz, Y. Ghorbel, C. Zhu, and Y. Yin, "Design and analysis of a novel compact compliant actuator with variable impedance," in *Robotics and Biomimetics (ROBIO), 2012 IEEE International Conference on*, 2012, pp. 1188-1193.

[90] H. Vallery, J. Veneman, E. Van Asseldonk, R. Ekkelenkamp, M. Buss, and H. Van der Kooij, "Compliant actuation of rehabilitation robots - Benefits and limitations of series elastic actuators," *Ieee Robotics & Automation Magazine,* vol. 15, pp. 60-69, Sep 2008.

[91] C. Yang, G. Ganesh, S. Haddadin, S. Parusel, A. Albu-Schaeffer, and E. Burdet, "Human-like adaptation of force and impedance in stable and unstable interactions," *Robotics, IEEE Transactions on,* vol. 27, pp. 918-930, 2011.

[92] J. Pratt, B. Krupp, and C. Morse, "Series elastic actuators for high fidelity force control," *Industrial Robot,* vol. 29, pp. 234-241, 2002.

[93] J. E. Pratt, B. T. Krupp, C. J. Morse, and S. H. Collins, "The RoboKnee: an exoskeleton for enhancing strength and endurance during walking," in *Robotics and Automation, 2004. Proceedings. ICRA'04. 2004 IEEE International Conference on*, 2004, pp. 2430-2435.

[94] F. Sergi, D. Accoto, G. Carpino, N. L. Tagliamonte, and E. Guglielmelli, "Design and characterization of a compact rotary Series Elastic Actuator for knee assistance during overground walking," in *Biomedical Robotics and Biomechatronics (BioRob), 2012 4th IEEE RAS & EMBS International Conference on*, 2012, pp. 1931-1936.

[95] J. F. Veneman, R. Ekkelenkamp, R. Kruidhof, F. C. T. van der Helm, and H. van der Kooij, "A series elastic- and Bowden-cable-based actuation system for use as torque actuator in exoskeleton-type robots," *International Journal of Robotics Research,* vol. 25, pp. 261-281, Mar 2006.

[96] T. Lenzi, S. M. M. De Rossi, N. Vitiello, and M. C. Carrozza, "Intention-Based EMG Control for Powered Exoskeletons," *Ieee Transactions on Biomedical Engineering,* vol. 59, pp. 2180-2190, Aug 2012.

[97] S. M. Cain, K. E. Gordon, and D. P. Ferris, "Locomotor adaptation to a powered ankle-foot orthosis depends on control method," *Journal of Neuroengineering and Rehabilitation,* vol. 4, Dec 21 2007.

[98] G. Cheron, M. Duvinage, C. De Saedeleer, T. Castermans, A. Bengoetxea, M. Petieau, K. Seetharaman, T. Hoellinger, B. Dan, T. Dutoit, F. S. Labini, F. Lacquaniti, and Y. Ivanenko, "From Spinal Central Pattern Generators to Cortical Network: Integrated BCI for Walking Rehabilitation," *Neural Plasticity,* 2012.

[99] J. T. Gwin, K. Gramann, S. Makeig, and D. P. Ferris, "Electrocortical activity is coupled to gait cycle phase during treadmill walking," *Neuroimage,* vol. 54, pp. 1289-1296, Jan 15 2011.

[100] J. T. Gwin, K. Gramann, S. Makeig, and D. P. Ferris, "Removal of Movement Artifact From High-Density EEG Recorded During Walking and Running," *Journal of Neurophysiology,* vol. 103, pp. 3526-3534, Jun 2010.

[101] T. H. Petersen, M. Willerslev - Olsen, B. A. Conway, and J. B. Nielsen, "The motor cortex drives the muscles during walking in human subjects," *J Physiol,* vol. 590, pp. 2443-2452, 2012.

[102] J. T. Gwin and D. P. Ferris, "An EEG-based study of discrete isometric and isotonic human lower limb muscle contractions," *J. Neuroeng. Rehabil,* vol. 9, pp. 1-13, 2012.

[103] H. A. Quintero, R. J. Farris, C. Hartigan, I. Clesson, and M. Goldfarb, "A Powered Lower Limb Orthosis for Providing Legged Mobility in Paraplegic Individuals," *Topics in spinal cord injury rehabilitation,* vol. 17, pp. 25-33, 2011.

[104] Y. H. Yin, Y. J. Fan, and L. D. Xu, "EMG and EPP-Integrated Human–Machine Interface Between the Paralyzed and Rehabilitation Exoskeleton," *Information Technology in Biomedicine, IEEE Transactions on,* vol. 16, pp. 542-549, 2012.

[105] M. Lotze, C. Braun, N. Birbaumer, S. Anders, and L. G. Cohen, "Motor learning elicited by voluntary drive," *Brain,* vol. 126, pp. 866-872, Apr 2003.

[106] R. A. Schmidt and R. A. Bjork, "New conceptualizations of practice: Common principles in three paradigms suggest new concepts for training," *Psychological science,* vol. 3, pp. 207-217, 1992.

[107] N. Hogan, "Impedance control: An approach to manipulation: Part II—Implementation," *Journal of dynamic systems, measurement, and control*, vol. 107, pp. 8-16, 1985.

[108] S. K. Banala, S. H. Kim, S. K. Agrawal, and J. P. Scholz, "Robot Assisted Gait Training With Active Leg Exoskeleton (ALEX)," *Ieee Transactions on Neural Systems and Rehabilitation Engineering*, vol. 17, pp. 2-8, Feb 2009.

[109] R. Ekkelenkamp, J. Veneman, and H. van der Kooij, "LOPES : Selective control of gait functions during the gait rehabilitation of CVA patients.," *2005 Ieee 9th International Conference on Rehabilitation Robotics*, pp. 361-364, 2005.

[110] A. Duschau-Wicke, J. von Zitzewitz, A. Caprez, L. Lunenburger, and R. Riener, "Path Control: A Method for Patient-Cooperative Robot-Aided Gait Rehabilitation," *Ieee Transactions on Neural Systems and Rehabilitation Engineering*, vol. 18, pp. 38-48, Feb 2010.

[111] D. Aoyagi, W. Ichinose, S. Harkema, D. Reinkensmeyer, and J. Bobrow, "An assistive robotic device that can synchronize to the pelvic motion during human gait training," in *Rehabilitation Robotics, 2005. ICORR 2005. 9th International Conference on*, 2005, pp. 565-568.

[112] D. Aoyagi, W. E. Ichinose, S. J. Harkema, D. J. Reinkensmeyer, and J. E. Bobrow, "A robot and control algorithm that can synchronously assist in naturalistic motion during body-weight-supported gait training following neurologic injury," *Neural Systems and Rehabilitation Engineering, IEEE Transactions on*, vol. 15, pp. 387-400, 2007.

[113] J. M. Potter, A. L. Evans, and G. Duncan, "Gait speed and activities of daily living function in geriatric patients," *Arch Phys Med Rehabil*, vol. 76, pp. 997-9, Nov 1995.

[114] A. L. Behmran and S. J. Harkema, "Locomotor training after human spinal cord injury: A series of case studies," *Physical Therapy*, vol. 80, pp. 688-700, Jul 2000.

[115] R. W. Horst, "A bio-robotic leg orthosis for rehabilitation and mobility enhancement," *Conf Proc IEEE Eng Med Biol Soc*, vol. 2009, pp. 5030-3, 2009.

[116] TOYOTA, "http://www.toyota-global.com/innovation/partner_robot/family_2.html."

[117] K. Shamaei, P. C. Napolitano, and A. M. Dollar, "Design and functional evaluation of a quasi-passive compliant stance control knee-ankle-foot orthosis," *IEEE Trans Neural Syst Rehabil Eng*, vol. 22, pp. 258-68, Mar 2014.

[118] B. I. Prilutsky, L. N. Petrova, and L. M. Raitsin, "Comparison of mechanical energy expenditure of joint moments and muscle forces during human locomotion," *Journal of Biomechanics*, vol. 29, pp. 405-415, 1996.

[119] "http://www.clinicalgaitanalysis.com/data/index.html."

[120] X. Li, Y. Pan, G. Chen, and H. Yu, "Continuous Tracking Control for A Compliant Actuator with Two-Stage Variable Stiffness," *IEEE Transactions on Automation Science and Engineering*, 2015, (submitted).

[121] E. Criswell, *Cram's introduction to surface electromyography*: Jones & Bartlett Publishers, 2010.

[122] M. Halaki and K. Ginn, "Normalization of EMG Signals: To Normalize or Not to Normalize and What to Normalize to?," 2012.

[123] D. W. Robinson and G. A. Pratt, "Force controllable hydro-elastic actuator," in *Robotics and Automation, 2000. Proceedings. ICRA'00. IEEE International Conference on*, 2000, pp. 1321-1327.

[124] G. Wyeth, "Control issues for velocity sourced series elastic actuators," in *Proceedings of the Australasian Conference on Robotics and Automation 2006*, 2006.

[125] H. Vallery, R. Ekkelenkamp, H. Van Der Kooij, and M. Buss, "Passive and accurate torque control of series elastic actuators," in *Intelligent Robots and Systems, 2007. IROS 2007. IEEE/RSJ International Conference on*, 2007, pp. 3534-3538.

[126] F. Sergi, D. Accoto, G. Carpino, N. L. Tagliamonte, and E. Guglielmelli, "Design and Characterization of a Compact Rotary Series Elastic Actuator for Knee Assistance During Overground Walking," *2012 4th Ieee Ras & Embs International Conference on Biomedical Robotics and Biomechatronics (Biorob)*, pp. 1931-1936, 2012.

[127] W. S. Levine, *The control handbook*: CRC press, 1996.

[128] S. Hussain, S. Q. Xie, and P. K. Jamwal, "Adaptive Impedance Control of a Robotic Orthosis for Gait Rehabilitation," 2012.

[129] B. Armstrong-Helouvry, "Stick slip and control in low-speed motion," *Automatic Control, IEEE Transactions on*, vol. 38, pp. 1483-1496, 1993.

[130] H. Olsson, "Control systems with friction," Lund University, 1996.

[131] F. Blanchini, "Ultimate boundedness control for uncertain discrete-time systems via set-induced Lyapunov functions," in *Decision and Control, 1991., Proceedings of the 30th IEEE Conference on*, 1991, pp. 1755-1760.

[132] H. Yu, S. Huang, G. Chen, and N. Thakor, "Control design of a novel compliant actuator for rehabilitation robots," *Mechatronics*, vol. 23, pp. 1072-1083, 2013.

[133] M. Goldfarb, K. Korkowski, B. Harrold, and W. Durfee, "Preliminary evaluation of a controlled-brake orthosis for FES-aided gait," *Neural Systems and Rehabilitation Engineering, IEEE Transactions on*, vol. 11, pp. 241-248, 2003.

[134] S. Gharooni, B. Heller, and M. Tokhi, "A new hybrid spring brake orthosis for controlling hip and knee flexion in the swing phase," *Neural Systems and Rehabilitation Engineering, IEEE Transactions on*, vol. 9, pp. 106-107, 2001.

[135] S. Jezernik, G. Colombo, and M. Morari, "Automatic gait-pattern adaptation algorithms for rehabilitation with a 4-DOF robotic orthosis," *Ieee Transactions on Robotics and Automation*, vol. 20, pp. 574-582, Jun 2004.

[136] J. L. Emken, S. J. Harkema, J. A. Beres-Jones, C. K. Ferreira, and D. J. Reinkensmeyer, "Feasibility of manual teach-and-replay and continuous impedance shaping for robotic locomotor training following spinal cord

injury," *Biomedical Engineering, IEEE Transactions on,* vol. 55, pp. 322-334, 2008.

[137] R. Ronsse, T. Lenzi, N. Vitiello, B. Koopman, E. van Asseldonk, S. M. M. De Rossi, J. van den Kieboom, H. van der Kooij, M. C. Carrozza, and A. J. Ijspeert, "Oscillator-based assistance of cyclical movements: model-based and model-free approaches," *Medical & Biological Engineering & Computing,* vol. 49, pp. 1173-1185, Oct 2011.

[138] R. Ronsse, N. Vitiello, T. Lenzi, J. van den Kieboom, M. C. Carrozza, and A. J. Ijspeert, "Human-Robot Synchrony: Flexible Assistance Using Adaptive Oscillators," *Ieee Transactions on Biomedical Engineering,* vol. 58, pp. 1001-1012, Apr 2011.

[139] L. Righetti, J. Buchli, and A. J. Ijspeert, "Dynamic hebbian learning in adaptive frequency oscillators," *Physica D: Nonlinear Phenomena,* vol. 216, pp. 269-281, 2006.

[140] A. Gams, T. Petric, T. Debevec, and J. Babic, "Effects of robotic knee exoskeleton on human energy expenditure," *IEEE Trans. Biomed. Engineering,* vol. 60, pp. 1636-1644, 2013.

[141] T. Petrič, A. Gams, A. J. Ijspeert, and L. Žlajpah, "On-line frequency adaptation and movement imitation for rhythmic robotic tasks," *The International Journal of Robotics Research,* vol. 30, pp. 1775-1788, 2011.

[142] A. Gams, A. J. Ijspeert, S. Schaal, and J. Lenarčič, "On-line learning and modulation of periodic movements with nonlinear dynamical systems," *Autonomous Robots,* vol. 27, pp. 3-23, 2009.

[143] R. Ronsse, B. Koopman, N. Vitiello, T. Lenzi, S. M. M. De Rossi, J. van den Kieboom, E. Van Asseldonk, M. C. Carrozza, H. van der Kooij, and A. J. Ijspeert, "Oscillator-based walking assistance: A model-free approach," in *Rehabilitation Robotics (ICORR), 2011 IEEE International Conference on,* 2011, pp. 1-6.

[144] R. Ronsse, S. M. De Rossi, N. Vitiello, T. Lenzi, B. Koopman, H. van der Kooij, M. C. Carrozza, and A. J. Ijspeert, "Real-time estimate of period derivatives using adaptive oscillators: Application to impedance-based walking assistance," in *Intelligent Robots and Systems (IROS), 2012 IEEE/RSJ International Conference on,* 2012, pp. 3362-3368.

[145] T. Lenzi, M. C. Carrozza, and S. K. Agrawal, "Powered hip exoskeletons can reduce the user's hip and ankle muscle activations during walking," *Neural Systems and Rehabilitation Engineering, IEEE Transactions on,* vol. 21, pp. 938-948, 2013.

[146] J. B. Buck, "Synchronous rhythmic flashing of fireflies," *The Quarterly Review of Biology,* vol. 13, pp. 301-314, 1938.

[147] M. W. Whittle, *Gait analysis: an introduction,* 2003.

[148] J. Perry and J. R. Davids, "Gait analysis: normal and pathological function," *Journal of Pediatric Orthopaedics,* vol. 12, p. 815, 1992.

[149] A. M. Sabatini, C. Martelloni, S. Scapellato, and F. Cavallo, "Assessment of walking features from foot inertial sensing," *Biomedical Engineering, IEEE Transactions on,* vol. 52, pp. 486-494, 2005.

[150] C. M. Senanayake and S. A. Senanayake, "Computational intelligent gait-phase detection system to identify pathological gait," *Information Technology in Biomedicine, IEEE Transactions on,* vol. 14, pp. 1173-1179, 2010.

[151] X. Meng, H. Yu, and M. P. Tham, "Gait phase detection in able-bodied subjects and dementia patients," *Conf Proc IEEE Eng Med Biol Soc,* vol. 2013, pp. 4907-10, 2013.

[152] L. Rabiner, "A tutorial on hidden Markov models and selected applications in speech recognition," *Proceedings of the Ieee,* vol. 77, pp. 257-286, 1989.

[153] A. Seward, "Low-latency incremental speech transcription in the synface project," in *INTERSPEECH*, 2003.

[154] M. Ryynanen and A. Klapuri, "Automatic bass line transcription from streaming polyphonic audio," in *Acoustics, Speech and Signal Processing, 2007. ICASSP 2007. IEEE International Conference on*, 2007, pp. IV-1437-IV-1440.

[155] G. Chen, V. Salim, and H. Yu, "A novel gait phase-based control strategy for a portable knee-ankle-foot robot," in *Rehabilitation Robotics (ICORR), 2015 IEEE International Conference on*, 2015, pp. 571-576.

[156] B. Balaban and F. Tok, "Gait disturbances in patients with stroke," *Pm&R,* vol. 6, pp. 635-642, 2014.

[157] K. Shamaei, M. Cenciarini, A. A. Adams, K. N. Gregorczyk, J. M. Schiffman, and A. M. Dollar, "Design and evaluation of a quasi-passive knee exoskeleton for investigation of motor adaptation in lower extremity joints," *IEEE Trans Biomed Eng,* vol. 61, pp. 1809-21, Jun 2014.

[158] J. Bae, K. Kong, and M. Tomizuka, "Gait Phase-Based Control for a Rotary Series Elastic Actuator Assisting the Knee Joint," *Journal of Medical Devices-Transactions of the Asme*, vol. 5, Sep 2011.

[159] A. Zoss and H. Kazerooni, "Design of an electrically actuated lower extremity exoskeleton," *Advanced Robotics,* vol. 20, pp. 967-988, 2006.